The Dissertation Committee for Chun-Hsien Wu Certifies that this is the approved version of the following dissertation:

Magneto-Plasmonic Nanoparticle Platform for Detection of Rare Cells and Cell Therapy

Committee:

Konstantin Sokolov, Supervisor

Andrew Dunn

Stanislav Emelianov

Hsin-Chih Yeh

Tomasz Zal

Magneto-Plasmonic Nanoparticle Platform for Detection of Rare Cells and Cell Therapy

by

Chun-Hsien Wu, B.S.; M.S.

Dissertation

Presented to the Faculty of the Graduate School of

The University of Texas at Austin

in Partial Fulfillment

of the Requirements

for the Degree of

Doctor of Philosophy

The University of Texas at Austin

August 2014

Dedication

To my wife, Sabrina Chang,

for her unconditional support and love.

Acknowledgements

I would like to thank my graduate advisor, Dr. Konstantin Sokolov, for his guidance at UT Austin. I would also like to thank my committee members who were an aid during my graduate research career. I enjoyed spending a great deal of time with my collaborators whose support was crucial. Finally, I would like to thank my family for their encouragement.

Magneto-Plasmonic Nanoparticle Platform for Detection of Rare Cells and Cell Therapy

Chun-Hsien Wu, Ph.D.

The University of Texas at Austin, 2014

Supervisor: Konstantin Sokolov

Magnetic and plasmonic properties combined in a single nanostructure provide a synergy that is advantageous in a number of biomedical applications, such as contrast enhancement in multimodal imaging, simultaneous capture and detection of circulating tumor cells, and photothermal therapy of cancer. These applications have stimulated significant interest in development of magneto-plasmonic nanoparticles with optical absorbance in the near-infrared region and a strong magnetic moment. In this dissertation, we addressed this need to create a novel immunotargeted magneto-plasmonic nanoparticle platform. The nanostructures were synthetized by self-assembly of primary 6 nm iron oxide core-gold shell particles, resulting in densely packed spherical nanoclusters. The close proximity of the primary particles in the nanoclusters generates a greatly improved response to an external magnetic field and strong near-infrared plasmon resonances. A procedure for antibody conjugation and PEGylation to the hybrid nanoparticles was developed for biomedical applications which require molecular and biocompatible targeting. Furthermore, we presented two biomedical applications based on the immunotargeted hybrid nanoparticle platform, including circulating tumor cell (CTC) detection and cell-based immunotherapy of cancer. In the CTC detection assays, rare cancer cells were specifically targeted by antibody-conjugated nanoparticles and

efficiently separated from normal blood cells by a magnetic force in a microfluidic chamber. The experiments in whole blood showed capture efficiency greater than 90% for a variety of cancers. We also explored photoacoustic imaging to detect nanoparticle-labeled CTCs in whole blood. The results showed excellent sensitivity to delineate the distribution of hybrid nanoparticles on the cancer cells. Thus, these works paves the way for a novel CTC detection approach which utilizes immunotargeted magneto-plasmonic nanoclusters for a simultaneous magnetic capture and photoacoustic detection of CTCs. In another application, we introduced a novel approach to label cytotoxic T cells using the magnetic nanoparticles with an expectation to enhance T cell recruitment in tumor under external magnetic stimulus. A series of *in vitro* experiments demonstrated highly controllable manipulation of labeled T cells. Thus, these results highlight the promise of using our nanoparticle platform as a multifunctional probe to manipulate and track immune cells *in vivo* and further improve the efficacy of cell-based cancer immunotherapy.

Table of Contents

List of Figures

Chapter 1: Introduction

1.1 Background on Cancer Management

The increase of survival rates for cancer patients significantly reflects improvements in early diagnosis, effective treatment, and/or appropriate monitoring.[1-3] The use of screening tools to recognize possible warning signs of cancer leads to early diagnosis. Over the past decades, several techniques have revolutionized the practice of medicine. For example, mammography is an x-ray examination to detect abnormalities of the breasts that may be breast cancer. The Pap smear test is to detect cervical cancer by collection of exfoliating epithelial cells from the cervical squamolcolumnar junction. Screening the blood level of prostate-specific antigen yields predictive value for prostate cancer. By using these examination techniques, abnormalities can be detected well before they produce clinical signs or symptoms.

To date, there are many treatment options for patients who are diagnosed with cancer. Conventionally, surgery with radiation or chemotherapy have significantly reduced the morbidity and mortality associated with solid neoplasms.[4-6] However, high rates of unwanted side effects are still the primary concern for patients.[7, 8] Relapsing of advanced cancer may occur so that patients would be given lower doses of chemotherapy as maintenance therapy for a couple of years to keep the cancer from returning.[9] With the attempt to improve deficiencies from current standard therapy, development of molecular specific therapies targets several biomarkers of cancer, such as human epidermal receptor (HER) 1 and 2, vascular endothelial growth factor receptor, and prostate-specific membrane antigen.[10-13] More recently, an experimental anticancer therapy, called adoptive cell therapy (ACT), which attempts to enhance the natural cancer-fighting

ability of cytotoxic T cells has demonstrated high efficacy for the treatment of metastatic melanoma.[14]

Along with the development of novel therapeutics aiming at complex pathways and mode of actions, methods to monitor the treatment response and predict the therapeutic success have been expanded beyond conventional response criteria, i.e. anatomic changes. Thus, monitoring response to cancer therapy at molecular or single cell level has gained popularity in recent years. Innovative imaging approaches, such as positron emission tomography allows longitudinal assessment of specific biological processes rather than anatomic changes in tumor size.[15] Accurate quantitation of circulating cancer cells (CTC) in the bloodstream shows great potential to determine prognosis and predict the overall survival in metastatic breast cancer patients.[16, 17] Overall, all these advanced techniques paved the way to improve our understanding of the underlying molecular and cellular features of cancers, thus contributing to better diagnosis, management and treatment of cancers.

1.2 The Demand of Hybrid Magneto-Plasmonic Nanoparticles

The field of nanotechnology provides opportunities for development of novel hybrid nanomaterials which enable new approaches and methods in various biomedical applications including molecular imaging and therapy.[18, 19] During the past few years, the combination of magnetic and plasmonic properties on nanoscale have drawn particular interest due to unique characteristics of each material.[20, 21] Indeed, gold-based nanoparticles exhibit strong localized surface plasmon resonances in visible and near-infrared (NIR) spectral regions; this property has been explored in a plethora of exciting applications ranging from molecular dark-field, reflectance and photoacoustic imaging to photothermal therapy and drug release.[22-25] Similarly, superparamagnetic nanoparticles

are of great interest because of their applications in various cell and molecular separation assays; magneto-motive optical and ultrasound imaging; magnetic resonance imaging (MRI); and hyperthermia cancer treatment.[26-29]

Recent reports have demonstrated a synergistic potential of combining plasmonic and superparamagnetic nanoparticles. For example, spherical gold shell/iron oxide core nanoparticles were used for molecular imaging of cancer cells overexpressing epidermal growth factor receptor (EGFR).[30] Furthermore, cancer cells labeled with these nanoparticles were destructed by a 700 nm laser irradiation with a very high efficiency demonstrating theranostic capabilities of these agents. In another study, gold shell/iron oxide core nanoparticles were used in a highly sensitive magneto-motive dark-field optical imaging of cancer cells.[31] In this case, the combination of bright plasmon resonance scattering from the gold shell and modulation of the optical signal by an external magnetic field was used to significantly increase imaging contrast. The same approach was used for the detection of single stellated gold nanoparticles containing a magnetic iron oxide core, demonstrating high sensitivity of this imaging approach.[32] More recently, magneto-plasmonic nanoparticles were used in development of a new imaging approach - magneto-photoacoustic imaging.[27, 33] In this imaging method, a combination of plasmonic and magnetic properties of hybrid nanoparticles is used to greatly increase imaging contrast in cellular and molecular imaging at significant tissue depth.

One emerging applications of magneto-plasmonic nanomaterials is a simultaneous capture and detection of CTCs. In initial experiments, two separate functionalized nanoparticles were used - magnetic iron oxide particles for cell capture and gold-plated carbon nanotubes for photoacoustic (PA) detection of the captured CTCs.[34] These experiments showed the feasibility of capture and detection of breast cancer cells pre-

injected into a live mouse bloodstream *in vivo*. However, the use of two different nanoparticles for capture and detection of CTCs can significantly limit efficacy of this approach because of a limited number of specific biomarkers which are overexpressed in cancer and the associated problem in funding two different biomarkers for each cancer type. Therefore, the latest approaches in this field have utilized hybrid magneto-plasmonic nanoparticles.[35, 36] Silica-coated gold nanorods adorned with iron-oxide nanoparticles and conjugated with folic acid molecules were used to demonstrate the feasibility of capture and PA detection of HeLa cancer cells under flow conditions.[36] HeLa cells were pre-labeled with the hybrid nanoparticles, fixed and, then, simultaneously captured and detected in flow at concentrations as low as one cell per mL. In another study, we synthesized immunotargeted 6 nm iron oxide shell/gold core nanoparticles for capture of cancer cells in whole blood.[35] Skin, breast, or colon cancer cells were mixed with whole human blood at concentrations ranging from 2 to 200 cells/mL, then, the immunotargeted nanoparticles were added to label cancer cells; the cells were captured in whole blood without any pre-processing steps using a permanent magnet and a flow chamber. Detection of the captured cells was carried out by taking advantage a strong scattering from the nanoparticles in dark-field optical imaging and by a standard fluorescent immunostaining. We showed the capture efficiency greater than 90% when a mixture of two nanoparticles targeted to two cancer biomarkers per cell type was used.

In sum, novel approaches to synthesize hybrid magneto-plasmonic nanoparticles with a high magnetic moment and strong plasmonic resonances in the red-NIR spectral region can lead to significant improvements in various biomedical applications, including sensitivity of multi-modal molecular imaging, specificity of targeted photothermal therapy, and capture efficacy of rare cells such as CTCs.

1.3 Roles of CTC detection in Cancer Management and Current Detection Technologies

The origin of CTCs in the peripheral blood has been considered the detachment from primary solid tumor. CTCs then travel in bloodstream, colonize a new distant tissue, and form therein a new tumor mass.[37] The process leads to the deadly aspect of cancer, metastasis, by compromising the functions of an organ, i.e. lung, brain, liver or bones. However, CTCs are thought very rare, estimated as one to few CTCs among millions of leukocytes and billions of erythrocytes.[16] The presence of five or more CTCs in 7.5 mL blood correlated with poor clinical outcomes than the case of less than five CTCs.[17] More recently, several studies have suggested that information provided by CTC count may be useful to stratify cancer stages and select therapeutics that could provide differential palliative benefit for patients.[38, 39] In addition, the presence of one or more CTCs in chemonaive patients with non-metastatic breast cancer may predict early recurrence and decreased overall survival. Thus, creating a sensitive assay to access metastatic tumor cells may be able to determine individual prognosis, stratify cancer patients at-risk for systemic adjuvant anticancer therapies, and monitor the efficacy of these therapies.

Currently, there are several assays described for the detection and enumeration of CTCs, relying on the physical properties, biomarker expression, or functional characteristics of CTCs.[40] One of the most effective methods is antibody-based capture technologies that are usually carried out with antibodies against common biomarkers. The isolation is realized using an antibody-mediated substrate which CTCs are specifically interacted with and directly or indirectly captured. One of the systems, CellSearch™, is the well-known and the first platform to gain FDA approval for prognosis in breast, prostate and colorectal cancer.[16] Basically, the CellSearch™ system utilizes ferrofluids consisting of magnetic nanoparticles embedded by a polymeric layer coated with

antibodies against epithelial cell adhesion molecules (EpCAM).[16, 17] After the positive selection of CTCs, the enriched cells are subsequently stained with fluorescent nuclear dye DAPI (4',6-diamidino-2-phenylindole), fluorescent antibody specific to CD45+ leukocytes (negative selection) and fluorescent antibodies to intracellular cytokeratins 8, 18 and 19, which are specific to epithelial cells. A semi-automated, four colored microscope is used to identify CTC as DAPI positive, cytokeratin positive, and CD45 negative.

Physical properties of cells, such as size, mechanical plasticity, density, and dielectric properties, can be exploited to isolate CTCs from the blood. Size-based isolation mainly relies on the larger size of CTCs in comparison with blood cells. Several substrates, including membrane filter and microfluidic chips, with size selection function have been demonstrated.[41, 42] Furthermore, the most sensitive CTC detection assay could be derived from nucleic acid-based approach which identifies specific DNA or mRNA molecules in the sample. The extracted substance from the enriched sample is employed in polymerase chain reaction to target CTC-specific genes correlated to either tissue-, organ-, or tumor-specific proteins or polypeptides.[43] Approaches based on mRNA molecule are considered more effective since mRNA molecule is unstable and rapidly degraded in the circulation. Thus, the presence of mRNA expression can be associated with the living CTCs in the blood sample.[44]

Despite these techniques show promise to provide desirable sensitivity of CTC detection, each of them could be a compromise. Highly sensitive methods may not be rapid or low-cost, whereas quicker tests are not necessarily effective. For example, several antibody-based capture assays have been realized to detect CTCs. Due to lack of a universal surface antigen for CTCs, a subpopulation of metastatic tumor cells could be potentially missed by using a single biomarker.[45, 46] Furthermore, enrichment methods

based on the differentiation of cell size address the problem to reduce dependency on antigen expression. Although the assays are simple and label-free, the accuracy may be sacrificed because of the non-uniformity size of CTCs.[47] In addition, microfluidic platform offers high CTC counts in cancer patients but slow flow rates lengthen the process to restrict clinical practice.[40] Nucleic acid-based techniques with impressive sensitivity gain attention, yet its specificity could dampen its usage. False-positive signals could easily be derived from the inflammation, invasive diagnostic biopsies, or during the tumor resection surgeries.[48] Thus, the best method for detection and isolation of CTCs still depends on the targeted application and resources.

1.4 Roles of Adoptive Cell Therapy in Cancer Treatment and Current Status

Adoptive cell therapy has emerged as the most effective treatment for patients with metastatic melanoma.[49] The basic concept of ACT is to generate large number of tumor-reactive T cells in patients with cancer, followed by transferring cultured tumor-reactive T cells expanded *in vitro* into a properly prepared recipient who allows manipulation of the host to minimize inhibitory factors to support the transferred T cells. Of patients with metastatic melanoma refractory to all other treatments, approximate half of the patients experienced an objective response *via* ACT and some of them showed complete responses.[50]

The high effectiveness of ACT on melanoma is due to that the natural course of tumor growth induces significant numbers of lymphocytes with anti-tumor activity.[51] These tumor infiltrating lymphocytes (TIL) can be isolated to provide a consistent source of T cells to expand in culture, thus enabling the identification of multiple melanoma associated antigen for immunotherapy. However, simply infusing large number of TILs along with Interleukin 2 only caused a third of patients to brief response.[52] The decisive

improvement in efficacy was greatly enhanced by introduction of an immunodepleting preparative regimen given before the ACT.[14] Lymphodepletion leads to elimination of T regulatory cells and other lymphocytes which compete homeostatic cytokines with the transferred cells. Thus, immunosuppressing the host immediately before ACT improves survival of transfer cells thus increases therapeutic efficacy.

Despite the success on melanoma patients whose TIL can be isolated and expanded, ACT still remains challenging for patients who cannot grow TIL or patients with non-melanoma tumors. Until recently, the ability to genetically engineer lymphocytes opened possibility for the extension of ACT to patients with a variety of cancer.[53] By modifying peripheral blood lymphocytes with new functions and specificity, such as classical major histocompatibility complex (MHC)-restricted T cell receptor or chimeric (antibody-based) antigen receptors (CARs), ACT showed improved antitumor effects and enhanced immune reconstitution on immunosuppressed cancer patients.[54]

There are several issues that need to be addressed before ACT becomes a clinical fit into current modes of oncological practice. ACT is a highly personalized treatment which is labor intensive and requires laboratory expertise. Each patient receives individualized reagents so it contradicts the production paradigm of pharmaceutical or biotech companies. In addition, several lines of evidence showed that the cell delivery is still a major concern for ACT. For example, persistence of the transferred cells *in vivo* was short with barely 0.01% of transferred cells in the circulation after receiving ACT for one week.[55] The homing efficiency of transferred T cells to tumor was disappointing for less than 1% migrating to the tumor, whereas the majority localized in the lung, liver, and spleen.[56, 57] Therefore, new approaches are required for time effective and highly targeted cell delivery to tumor.

1.5 Overall Research Goals

The overall goals of this dissertation are to develop a magneto-plasmonic nanoparticle platform, which can be applicable to the filed of cancer management including CTC detection and ACT for cancer. In Chapter 2, the build and characterization of an immunotargeted magneto-plasmonic nanoparticle platform is described. In Chapter 3, the CTC detection assays are introduced which are based on the immunotargeted nanoparticle platform. In Chapter 4, the feasibility of magnetically guided cell delivery for ACT is explored. Finally, Chapter 5 lists the overall conclusions and future directions.

1.6 References

1. Siegel, R.; Naishadham, D.; Jemal, A., Cancer statistics, 2012. *CA Cancer J Clin* **2012**, 62, 10-29.

2. Etzioni, R.; Tsodikov, A.; Mariotto, A.; Szabo, A.; Falcon, S.; Wegelin, J.; DiTommaso, D.; Karnofski, K.; Gulati, R.; Penson, D. F.; Feuer, E., Quantifying the role of PSA screening in the US prostate cancer mortality decline. *Cancer Causes Control* **2008**, 19, 175-181.

3. Berry, D. A.; Cronin, K. A.; Plevritis, S. K.; Fryback, D. G.; Clarke, L.; Zelen, M.; Mandelblatt, J. S.; Yakovlev, A. Y.; Habbema, J. D.; Feuer, E. J., Effect of screening and adjuvant therapy on mortality from breast cancer. *N Engl J Med* **2005**, 353, 1784-1792.

4. Figueras, J.; Torras, J.; Valls, C.; Llado, L.; Ramos, E.; Marti-Rague, J.; Serrano, T.; Fabregat, J., Surgical resection of colorectal liver metastases in patients with expanded indications: a single-center experience with 501 patients. *Dis Colon Rectum* **2007**, 50, 478-488.

5. Delaney, G.; Jacob, S.; Featherstone, C.; Barton, M., The role of radiotherapy in cancer treatment: estimating optimal utilization from a review of evidence-based clinical guidelines. *Cancer* **2005**, 104, 1129-1137.

6. Ohlsson, B.; Stenram, U.; Tranberg, K. G., Resection of colorectal liver metastases: 25-year experience. *World J Surg* **1998**, 22, 268-276; discussion 276-267.

7. Carelle, N.; Piotto, E.; Bellanger, A.; Germanaud, J.; Thuillier, A.; Khayat, D., Changing patient perceptions of the side effects of cancer chemotherapy. *Cancer* **2002**, 95, 155-163.

8. Partridge, A. H.; Burstein, H. J.; Winer, E. P., Side effects of chemotherapy and combined chemohormonal therapy in women with early-stage breast cancer. *J Natl Cancer Inst Monogr* **2001**, 135-142.

9. Gerber, D. E.; Schiller, J. H., Maintenance chemotherapy for advanced non-small-cell lung cancer: new life for an old idea. *J Clin Oncol* **2013**, 31, 1009-1020.

10. Kobayashi, S.; Boggon, T. J.; Dayaram, T.; Janne, P. A.; Kocher, O.; Meyerson, M.; Johnson, B. E.; Eck, M. J.; Tenen, D. G.; Halmos, B., EGFR mutation and resistance of non-small-cell lung cancer to gefitinib. *N Engl J Med* **2005**, 352, 786-792.

11. Slamon, D. J.; Leyland-Jones, B.; Shak, S.; Fuchs, H.; Paton, V.; Bajamonde, A.; Fleming, T.; Eiermann, W.; Wolter, J.; Pegram, M.; Baselga, J.; Norton, L., Use of chemotherapy plus a monoclonal antibody against HER2 for metastatic breast cancer that overexpresses HER2. *N Engl J Med* **2001**, 344, 783-792.

12. Casanovas, O.; Hicklin, D. J.; Bergers, G.; Hanahan, D., Drug resistance by evasion of antiangiogenic targeting of VEGF signaling in late-stage pancreatic islet tumors. *Cancer Cell* **2005**, 8, 299-309.

13. Henry, M. D.; Wen, S.; Silva, M. D.; Chandra, S.; Milton, M.; Worland, P. J., A prostate-specific membrane antigen-targeted monoclonal antibody-chemotherapeutic conjugate designed for the treatment of prostate cancer. *Cancer Res* **2004**, 64, 7995-8001.

14. Dudley, M. E.; Yang, J. C.; Sherry, R.; Hughes, M. S.; Royal, R.; Kammula, U.; Robbins, P. F.; Huang, J.; Citrin, D. E.; Leitman, S. F.; Wunderlich, J.; Restifo, N. P.; Thomasian, A.; Downey, S. G.; Smith, F. O.; Klapper, J.; Morton, K.; Laurencot, C.; White, D. E.; Rosenberg, S. A., Adoptive cell therapy for patients with metastatic melanoma: evaluation of intensive myeloablative chemoradiation preparative regimens. *J Clin Oncol* **2008**, 26, 5233-5239.

15. Malviya, G.; Nayak, T. K., PET imaging to monitor cancer therapy. *Curr Pharm Biotechnol* **2013**, 14, 669-682.

16. Cristofanilli, M.; Budd, G. T.; Ellis, M. J.; Stopeck, A.; Matera, J.; Miller, M. C.; Reuben, J. M.; Doyle, G. V.; Allard, W. J.; Terstappen, L. W.; Hayes, D. F., Circulating tumor cells, disease progression, and survival in metastatic breast cancer. *New England Journal of Medicine* **2004**, 351, 781-791.

17. Cristofanilli, M.; Hayes, D. F.; Budd, G. T.; Ellis, M. J.; Stopeck, A.; Reuben, J. M.; Doyle, G. V.; Matera, J.; Allard, W. J.; Miller, M. C.; Fritsche, H. A.; Hortobagyi, G. N.; Terstappen, L. W., Circulating tumor cells: a novel prognostic factor for newly diagnosed metastatic breast cancer. *Journal of Clinical Oncology* **2005**, 23, 1420-1430.

18. Bogart, L. K.; Pourroy, G.; Murphy, C. J.; Puntes, V.; Pellegrino, T.; Rosenblum, D.; Peer, D.; Levy, R., Nanoparticles for imaging, sensing, and therapeutic intervention. *ACS Nano* **2014**, 8, 3107-3122.

19. Doane, T. L.; Burda, C., The unique role of nanoparticles in nanomedicine: imaging, drug delivery and therapy. *Chem Soc Rev* **2012**, 41, 2885-2911.

20. Dreaden, E. C.; Alkilany, A. M.; Huang, X.; Murphy, C. J.; El-Sayed, M. A., The golden age: gold nanoparticles for biomedicine. *Chem Soc Rev* **2012**, 41, 2740-2779.

21. Colombo, M.; Carregal-Romero, S.; Casula, M. F.; Gutierrez, L.; Morales, M. P.; Bohm, I. B.; Heverhagen, J. T.; Prosperi, D.; Parak, W. J., Biological applications of magnetic nanoparticles. *Chem Soc Rev* **2012**, 41, 4306-4334.

22. Sokolov, K.; Follen, M.; Aaron, J.; Pavlova, I.; Malpica, A.; Lotan, R.; Richards-Kortum, R., Real-time vital optical imaging of precancer using anti-epidermal growth factor receptor antibodies conjugated to gold nanoparticles. *Cancer Res* **2003**, 63, 1999-2004.

23. Mallidi, S.; Larson, T.; Aaron, J.; Sokolov, K.; Emelianov, S., Molecular specific optoacoustic imaging with plasmonic nanoparticles. *Opt Express* **2007**, 15, 6583-6588.

24. Jain, P. K.; Huang, X.; El-Sayed, I. H.; El-Sayed, M. A., Noble metals on the nanoscale: optical and photothermal properties and some applications in imaging, sensing, biology, and medicine. *Acc Chem Res* **2008**, 41, 1578-1586.

25. Hirsch, L. R.; Stafford, R. J.; Bankson, J. A.; Sershen, S. R.; Rivera, B.; Price, R. E.; Hazle, J. D.; Halas, N. J.; West, J. L., Nanoshell-mediated near-infrared thermal therapy of tumors under magnetic resonance guidance. *Proc Natl Acad Sci U S A* **2003**, 100, 13549-13554.

26. Jing, Y.; Moore, L. R.; Williams, P. S.; Chalmers, J. J.; Farag, S. S.; Bolwell, B.; Zborowski, M., Blood progenitor cell separation from clinical leukapheresis product by magnetic nanoparticle binding and magnetophoresis. *Biotechnol Bioeng* **2007**, 96, 1139-1154.

27. Qu, M.; Mallidi, S.; Mehrmohammadi, M.; Truby, R.; Homan, K.; Joshi, P.; Chen, Y.-S.; Sokolov, K.; Emelianov, S., Magneto-photo-acoustic imaging. *Biomedical optics express* **2011**, 2, 385-396.

28. Sun, C.; Lee, J. S.; Zhang, M., Magnetic nanoparticles in MR imaging and drug delivery. *Adv Drug Deliv Rev* **2008**, 60, 1252-1265.

29. Ito, A.; Kuga, Y.; Honda, H.; Kikkawa, H.; Horiuchi, A.; Watanabe, Y.; Kobayashi, T., Magnetite nanoparticle-loaded anti-HER2 immunoliposomes for combination of antibody therapy with hyperthermia. *Cancer Lett* **2004**, 212, 167-175.

30. Larson, T. A.; Bankson, J.; Aaron, J.; Sokolov, K., Hybrid plasmonic magnetic nanoparticles as molecular specific agents for MRI/optical imaging and photothermal therapy of cancer cells. *Nanotechnology* **2007**, 18, 325101.

31. Aaron, J. S.; Oh, J.; Larson, T. A.; Kumar, S.; Milner, T. E.; Sokolov, K. V., Increased optical contrast in imaging of epidermal growth factor receptor using magnetically actuated hybrid gold/iron oxide nanoparticles. *Optics express* **2006**, 14, 12930-12943.

32. Song, H.-M.; Wei, Q.; Ong, Q. K.; Wei, A., Plasmon-resonant nanoparticles and nanostars with magnetic cores: synthesis and magnetomotive imaging. *ACS nano* **2010**, 4, 5163-5173.

33. Jin, Y.; Jia, C.; Huang, S.-W.; O'Donnell, M.; Gao, X., Multifunctional nanoparticles as coupled contrast agents. *Nat Commun* **2010**, 1, 41.

34. Galanzha, E. I.; Shashkov, E. V.; Kelly, T.; Kim, J.-W.; Yang, L.; Zharov, V. P., In vivo magnetic enrichment and multiplex photoacoustic detection of circulating tumour cells. *Nature nanotechnology* **2009**, 4, 855-860.

35. Wu, C.-H.; Huang, Y.-Y.; Chen, P.; Hoshino, K.; Liu, H.; Frenkel, E. P.; Zhang, J. X. J.; Sokolov, K. V., Versatile Immunomagnetic Nanocarrier Platform for Capturing Cancer Cells. *ACS nano* **2013**, 7, 8816-8823.

36. Hu, X.; Wei, C. W.; Xia, J.; Pelivanov, I.; O'Donnell, M.; Gao, X., Trapping and Photoacoustic Detection of CTCs at the Single Cell per Milliliter Level with Magneto–Optical Coupled Nanoparticles. *Small* **2013**, 9, 2046-2052.

37. Hanahan, D.; Weinberg, R. A., Hallmarks of cancer: the next generation. *Cell* **2011**, 144, 646-674.

38. Giuliano, M.; Giordano, A.; Jackson, S.; Hess, K. R.; De Giorgi, U.; Mego, M.; Handy, B. C.; Ueno, N. T.; Alvarez, R. H.; De Laurentiis, M.; De Placido, S.; Valero, V.; Hortobagyi, G. N.; Reuben, J. M.; Cristofanilli, M., Circulating tumor cells as prognostic and predictive markers in metastatic breast cancer patients receiving first-line systemic treatment. *Breast Cancer Res* **2011**, 13, R67.

39. Zhang, L.; Riethdorf, S.; Wu, G.; Wang, T.; Yang, K.; Peng, G.; Liu, J.; Pantel, K., Meta-analysis of the prognostic value of circulating tumor cells in breast cancer. *Clin Cancer Res* **2012**, 18, 5701-5710.

40. Esmaeilsabzali, H.; Beischlag, T. V.; Cox, M. E.; Parameswaran, A. M.; Park, E. J., Detection and isolation of circulating tumor cells: Principles and methods. *Biotechnol Adv* **2013**, 31, 1063-1084.

41. Desitter, I.; Guerrouahen, B. S.; Benali-Furet, N.; Wechsler, J.; Janne, P. A.; Kuang, Y.; Yanagita, M.; Wang, L.; Berkowitz, J. A.; Distel, R. J.; Cayre, Y. E., A new device for rapid isolation by size and characterization of rare circulating tumor cells. *Anticancer Res* **2011**, 31, 427-441.

42. Zheng, X.; Cheung, L. S.; Schroeder, J. A.; Jiang, L.; Zohar, Y., A high-performance microsystem for isolating circulating tumor cells. *Lab Chip* **2011**, 11, 3269-3276.

43. Riethdorf, S.; Wikman, H.; Pantel, K., Review: Biological relevance of disseminated tumor cells in cancer patients. *Int J Cancer* **2008**, 123, 1991-2006.

44. Gerges, N.; Rak, J.; Jabado, N., New technologies for the detection of circulating tumour cells. *Br Med Bull* **2010**, 94, 49-64.

45. Sieuwerts, A. M.; Kraan, J.; Bolt, J.; van der Spoel, P.; Elstrodt, F.; Schutte, M.; Martens, J. W.; Gratama, J. W.; Sleijfer, S.; Foekens, J. A., Anti-epithelial cell adhesion molecule antibodies and the detection of circulating normal-like breast tumor cells. *Journal of the National Cancer Institute (1988)* **2009**, 101, 61-66.

46. Mostert, B.; Kraan, J.; Bolt-de Vries, J.; van der Spoel, P.; Sieuwerts, A. M.; Schutte, M.; Timmermans, A. M.; Foekens, R.; Martens, J. W.; Gratama, J. W.; Foekens, J. A.; Sleijfer, S., Detection of circulating tumor cells in breast cancer may improve through enrichment with anti-CD146. *Breast Cancer Research and Treatment* **2011**, 127, 33-41.

47. Allard, W. J.; Matera, J.; Miller, M. C.; Repollet, M.; Connelly, M. C.; Rao, C.; Tibbe, A. G.; Uhr, J. W.; Terstappen, L. W., Tumor cells circulate in the peripheral blood of all major carcinomas but not in healthy subjects or patients with nonmalignant diseases. *Clin Cancer Res* **2004**, 10, 6897-6904.

48. Crisan, D.; Ruark, D. S.; Decker, D. A.; Drevon, A. M.; Dicarlo, R. G., Detection of circulating epithelial cells after surgery for benign breast disease. *Mol Diagn* **2000**, 5, 33-38.

49. Rosenberg, S. A.; Restifo, N. P.; Yang, J. C.; Morgan, R. A.; Dudley, M. E., Adoptive cell transfer: a clinical path to effective cancer immunotherapy. *Nat Rev Cancer* **2008**, 8, 299-308.

50. Dudley, M. E.; Wunderlich, J. R.; Yang, J. C.; Sherry, R. M.; Topalian, S. L.; Restifo, N. P.; Royal, R. E.; Kammula, U.; White, D. E.; Mavroukakis, S. A.; Rogers, L. J.; Gracia, G. J.; Jones, S. A.; Mangiameli, D. P.; Pelletier, M. M.; Gea-Banacloche, J.; Robinson, M. R.; Berman, D. M.; Filie, A. C.; Abati, A.; Rosenberg, S. A., Adoptive cell transfer therapy following non-myeloablative but lymphodepleting chemotherapy for the treatment of patients with refractory metastatic melanoma. *J Clin Oncol* **2005**, 23, 2346-2357.

51. Muul, L. M.; Spiess, P. J.; Director, E. P.; Rosenberg, S. A., Identification of specific cytolytic immune responses against autologous tumor in humans bearing malignant melanoma. *J Immunol* **1987**, 138, 989-995.

52. Rosenberg, S. A.; Dudley, M. E., Adoptive cell therapy for the treatment of patients with metastatic melanoma. *Curr Opin Immunol* **2009**, 21, 233-240.

53. June, C. H., Principles of adoptive T cell cancer therapy. *J Clin Invest* **2007**, 117, 1204-1212.

54. June, C. H., Adoptive T cell therapy for cancer in the clinic. *J Clin Invest* **2007**, 117, 1466-1476.

55. Rosenberg, S. A.; Aebersold, P.; Cornetta, K.; Kasid, A.; Morgan, R. A.; Moen, R.; Karson, E. M.; Lotze, M. T.; Yang, J. C.; Topalian, S. L.; et al., Gene transfer into humans--immunotherapy of patients with advanced melanoma, using tumor-infiltrating lymphocytes modified by retroviral gene transduction. *N Engl J Med* **1990**, 323, 570-578.

56. Fisher, B.; Packard, B. S.; Read, E. J.; Carrasquillo, J. A.; Carter, C. S.; Topalian, S. L.; Yang, J. C.; Yolles, P.; Larson, S. M.; Rosenberg, S. A., Tumor localization of adoptively transferred indium-111 labeled tumor infiltrating lymphocytes in patients with metastatic melanoma. *J Clin Oncol* **1989**, 7, 250-261.

57. Bobisse, S.; Rondina, M.; Merlo, A.; Tisato, V.; Mandruzzato, S.; Amendola, M.; Naldini, L.; Willemsen, R. A.; Debets, R.; Zanovello, P.; Rosato, A., Reprogramming T lymphocytes for melanoma adoptive immunotherapy by T-cell receptor gene transfer with lentiviral vectors. *Cancer Res* **2009**, 69, 9385-9394.

Chapter 2: Development of an Immunotargeted Magneto-Plasmonic Nanoparticle Platform

2.1 INTRODUCTION

Hybrid nanoparticles consisting of different materials with distinct physico-chemical properties can open new opportunities in biomedical applications including multimodal molecular imaging, therapy delivery and monitoring, new screening and diagnostic assays.[1-3] The combination of plasmonic and magnetic properties in a single nanoparticle is of particular interest because it provides a very strong light scattering and absorption cross-sections associated with plasmon resonances that are coupled with responsiveness to a magnetic field. For example, magneto-plasmonic nanoparticles were used to increase contrast in dark-field imaging of labeled cells by applying a temporal signal modulation *via* an external electromagnet.[3-5] More recently, a similar principle was applied to development of a new imaging modality – magneto-photoacoustic imaging where magneto-plasmonic nanoparticles enable great improvement of contrast.[6, 7] It was also shown that the hybrid nanoparticles can be used for simultaneous capture and detection of circulating tumor cells in whole blood and *in vivo*.[8, 9] Furthermore, magneto-plasmonic nanoparticles are promising theranostic agents which can be used for molecular specific optical and MR imaging combined with photothermal therapy of cancer cells.[10]

Several approaches were explored for synthesis of magneto-plasmonic nanoparticles. For example, Yu et al. utilized decomposition and oxidation of $Fe(CO)_5$ on the gold nanoparticles to form dumbbell-like bifunctional $Au–Fe_3O_4$ nanoparticles.[11] Wang et al. have synthesized gold-coated iron oxide nanoparticle by using thermal decomposition method.[12] Some other approaches rely on coating polymer or amine functional molecules onto magnetic core nanoparticles followed by deposition of a gold

shell onto the polymer surface to create the hybrid particles.[7, 13] In addition, iron-oxide nanoparticles were attached to gold nanorods *via* electrostatic interactions or a chemical reaction.[14, 15] Although these approaches yield magneto-plasmonic nanostructures, they compromise to some extent properties of the magneto-plasmonic combination such as optical absorbance in the near-infrared (NIR) window or a strong magnetic moment, both of which are highly desirable in biomedical applications. For example, the dumbbell Au–Fe_3O_4 nanoparticles have a plasmon resonance peak at 520 nm which limits their utility *in vivo* due to high tissue turbidity in this spectral range. Furthermore, the multi-step synthesis involving polymer coating for gold deposition is not facile. Uneven or low polymer coverage on the magnetic core can compromise the deposition of a gold shell. This approach is also limited to a single superparamagnetic moiety per a magneto-plasmonic nanoparticle. In general, iron oxide nanoparticles exhibit superparamagnetic behavior in sizes up to about 20 to 30 nm in diameter, above which the particles become ferromagnetic that puts a limit on the magnetic moment of superparamagnetic nanoparticles which are based on a single iron oxide core. In addition, the magneto-plasmonic nanoparticles produced by the current protocols are limited to just one[11] or a few (less than 10)[14, 15] superparamagnetic moieties (e.g., iron oxide nanoparticles) that is significantly less than those could be achieved in a densely packed nanostructure. The use of gold nanorods as a template for the deposition of iron oxide nanoparticles further requires careful optimization to ensure colloidal stability and there is significant variability in the number of iron oxide moieties per hybrid nanoparticle because of limited nanorod surface area. Therefore, there is great room for improving magnetic properties of the hybrid nanoparticles. Moreover, some of the protocols are relatively complex and require careful optimization in order to avoid aggregation of the particles during synthesis.[14, 15]

Novel approaches to synthesize hybrid nanoparticles with a high magnetic moment and strong absorbance in the red-NIR spectral region can lead to significant improvements in various biomedical applications including sensitivity of multi-modal molecular imaging, image guidance of photothermal therapy, and CTC assays. In this chapter, we describe a method for synthesis of magneto-plasmonic nanoparticles with a strong magnetic moment and a strong NIR absorbance that addresses major limitations of the current art (Figure 2.1). The synthesis has its origins in oil-in-water microemulsion method.[16] It is based on assembly of nanoparticles of a desired size from a much smaller primary particles. This approach has been successfully used to produce nanostructures from a single material such as gold, iron oxide and semiconductor primary particles.[16] We extended it to synthesis of magneto-plasmonic nanoparticles by, first, making 6 nm diameter gold shell/iron oxide core particles and, then, assembling the primary hybrid particles into the final spherical nanostructure. Assembling primary particles into nanoclusters not only allows enhancing the properties of constituent nanoparticles, such as achieving a stronger magnetic moment while preserving superparamagnetic properties, but also takes advantage of the interactions between individual nanoparticles which creates new characteristics absent from the constituent nanoparticles, such as strong optical absorbance in the NIR window. Furthermore, we also developed an antibody conjugation procedure to the hybrid nanoparticles for various biomedical applications which require molecular specific targeting. Antibodies are attached through the Fc moiety leaving the Fab portion that is responsible for antigen binding available for targeting. The contents of this chapter have been published in the journal ACS Nano[8], accepted in Journal of Visualized Experiments and Advanced Functional Materials.

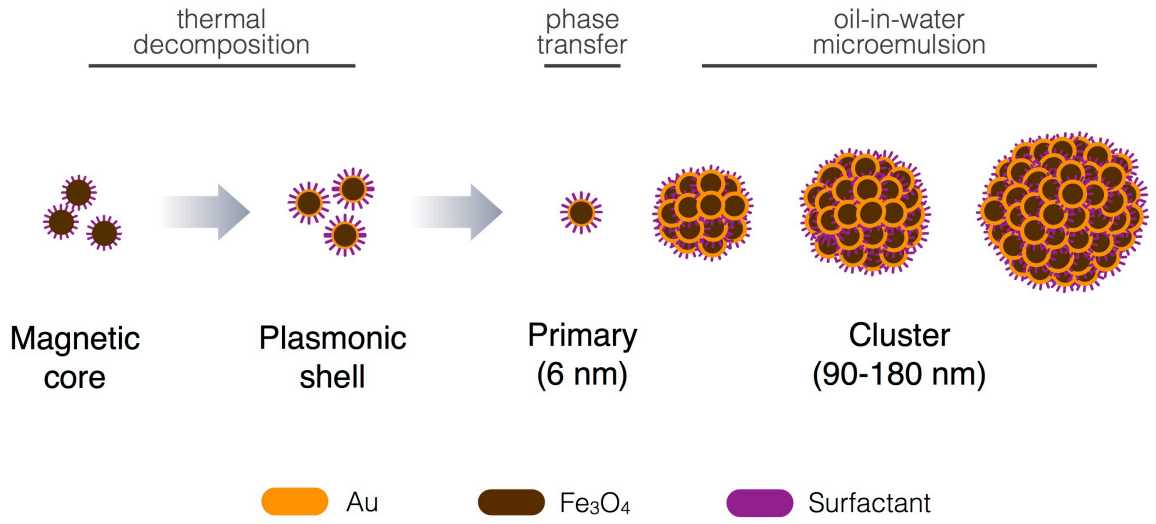

Figure 2.1 Synthetic scheme of magneto-plasmonic nanoparticles.

2.2 PRIMARY AU SHELL/Fe_3O_4 CORE NANOPARTICLES

2.2.1 Materials and Methods

Synthesis and characterization of gold shell/iron oxide core nanoparticles

The gold-coated iron oxide nanoparticles were prepared according to a previously published protocol with a number of modifications.[17] Briefly, 1 mM iron(III) acetylacetonate was mixed in 10 mL phenyl ether, followed by adding 3 mM oleic acid, 2 mM oleylamine, and 3 mM 1,2-hexadecanediol (Fisher Scientific). The mixture was stirred vigorously, heated to 260 °C, and refluxed for 1 h yielding a suspension of highly uniform 5.1 nm Fe_3O_4 nanoparticles. Five mL of the Fe_3O_4 nanoparticle suspension was cooled to room temperature followed by addition of 1.1 mM gold acetate, 0.75 mM oleic acid, 3 mM oleylamine, 3 mM 1,2-hexadecanediol, and 15 mL phenyl ether (Fisher Scientific) under vigorous stirring. The reaction mixture was heated to 180 °C and was refluxed for 1 h. Then, a dark purple precipitate was formed after addition of ethanol and centrifugation. The recovered gold-coated iron oxide nanoparticles were dispersed in hexane. To render gold-coated iron oxide nanoparticles hydrophilic, the transfer of the

nanoparticles from organic to aqueous phase was modified as previously described.[18] Nanoparticles in hexane at *ca*. 0.6 mg nanoparticle/mL and equal volume of 5 mM α-cyclodextrin (α-CD, Fisher Scientific) were mixed and stirred overnight at room temperature. Then, the nanoparticles were recovered by centrifugation, and the supernatant was discarded. The precipitate was resuspended in 0.2 mM sodium citrate using 10 min sonication.

Transmission election microscopy (TEM) images were obtained using a FEI TECNAI G2 F20 X-TWIN TEM at 80 keV. The samples were prepared by depositing 10 μL of a nanoparticle suspension onto a carbon-coated copper TEM grid for observation. UV-Vis spectra were collected with a BioTek Synergy HT micro-titer plate spectrometer. Magnetic properties of the core/shell nanoparticles were characterized using SQUID magnetometry upon cycling the field between -50 K Oe to 50 K Oe at 300 k.

Conjugation of monoclonal antibodies to nanoparticles

Anti-Epithelial Cell Adhesion Molecule (EpCAM), anti-HER2, anti-EGFR, and anti-Cytokeratin (CK) antibodies (Sigma Aldrich) were attached to the gold shell/magnetic core nanoparticles *via* a heterofunctional PEG linker with hydrazide and dithiol moieties - dithiolaromatic PEG6-CONHNH2 (SensoPath Technologies). Antibody solution (100 μL, 1 mg/mL) in 4 mM HEPES was incubated in the dark with 10 μL 100 mM $NaIO_4$ for 30 min at room temperature, followed by quenching the reaction with 500 μL phosphate buffered saline (PBS). Then, 2 μL of 46.5 mM linker solution was added to the antibody solution and shaken gently for 1 h. The excess linker was removed by filtration in a 10,000 MWCO centrifuge filter (Millipore) at 2,000*g*, 8 °C for 16 min. The retained antibodies were resuspended in PBS to a concentration of 1 mg/mL. The modified antibodies were mixed with gold shell/magnetic core nanoparticles in 4 mM HEPES for 1 h at room temperature. Then, 10^{-5} M 10 kD PEG-thiol (SensoPath

Technologies) was added to passivate the remaining nanoparticles surface. The functionalized nanoparticles were recovered by centrifugation at 2,000*g* for 5 min and were resuspended in 2 % w/v 10 kD PEG in PBS.

Cell labeling specificity assays

COLO 205, SK-BR-3, and A-431 cells (ATCC) were used as cancer cell models to demonstrate molecular specific cellular imaging. Cells were cultured in Dulbecco's Modified Eagle Medium (DMEM, Life Technologies) supplemented with 5 % fetal bovine serum (FBS, Hyclone), and harvested at ~90% confluence with trypsin. Cell suspensions containing ~3×10^5 cells were resuspended in complete media. Then, approximately 6×10^{12} immunotargeted nanocarriers conjugated with either anti-HER2, anti-EGFR, or anti-EpCAM antibodies were added to a cell suspension for 2 h at room temperature under mild mixing. To target the intracellular cytokeratins, cells were fixed with 4% formaldehyde for 10 min followed by permeabilized with 1% Triton X-100 (Sigma Aldrich) for 15 min before incubating with immunotargeted nanocarriers against anti-CK. After incubation with nanocarriers, cells were washed in PBS and were spun down to remove any unbound nanoparticles followed by imaging using 20×, 0.5-NA dark-field objective under Leica DM6000 upright microscope.

2.2.2 Results and Discussion

Gold shell/iron oxide core nanoparticles

Parameters of an optimal immunomagnetic nanocarrier include monodispersity, high-stability in aqueous phase, and ease of conjugation with targeting antibodies. Here, highly uniform Au shell/Fe_3O_4 core nanoparticles were synthesized *via* thermal decomposition of iron(III) acetylacetonate in a mixture of oleylamine and oleic acid followed by reduction of gold acetate in the presence of the iron oxide seeds.[17] TEM of

both Fe_3O_4 and Au shell/Fe_3O_4 core nanoparticles dispersed in organic solvent shows spherical, uniform nanocrystals (Figure 2.2a and 2.2b). The core/shell nanoparticles were transferred into aqueous phase by mixing the particles in hexane with alpha-cyclodextrin molecules dissolved in water. α-CD is cyclic oligosaccharides containing six glucopyranose units whose hydrophobic cavities can form complexes with organic molecules and hydroxyl groups on rims provide hydrophilic properties.[18] Therefore, the interaction between α-CD and oleic acid on nanoparticle surface stabilizes nanoparticles during phase transfer. The α-CD modified core/shell nanoparticles were readily dispersed in water with no detectable aggregation (Figure 2.2c). The core/shell nanoparticles in water phase had a narrow size distribution with the mean diameter of 6.2 ± 0.8 nm that was determined from TEM measurements of more than 200 particles (Figure 2.2d).

The uniform gold coating is evident from the darker appearance of the core/shell nanoparticles as compared to the Fe_3O_4 precursors in TEM images (Figure 2.2a and 2.2b). In addition, the UV-Vis absorption spectrum of Au shell/Fe_3O_4 core nanoparticles shows a distinctive absorption band at 533 nm that is associated with the surface plasmon resonance of the gold shell (Figure 2.2e); this plasmon resonance determines red color of the core/shell nanoparticle suspension. Size comparison of Fe_3O_4 and Fe_3O_4/Au core/shell nanoparticles using TEM images showed that the thickness of the gold layer is approximately 1.1 nm. Magnetic properties of the core/shell nanoparticles were characterized using SQUID magnetometry upon cycling the field between -50 K Oe to 50 K Oe at 300 k. The maximum magnetization value is 16.13 emu/g, and neither coercivity nor remanence was observed indicating superparamagnetic property of the nanoparticles (Figure 2.2f). The nanoparticles can be quickly separated from a colloidal suspension using a magnetic field gradient created by a simple permanent magnet as can be seen in the insert in Figure 2.2f.

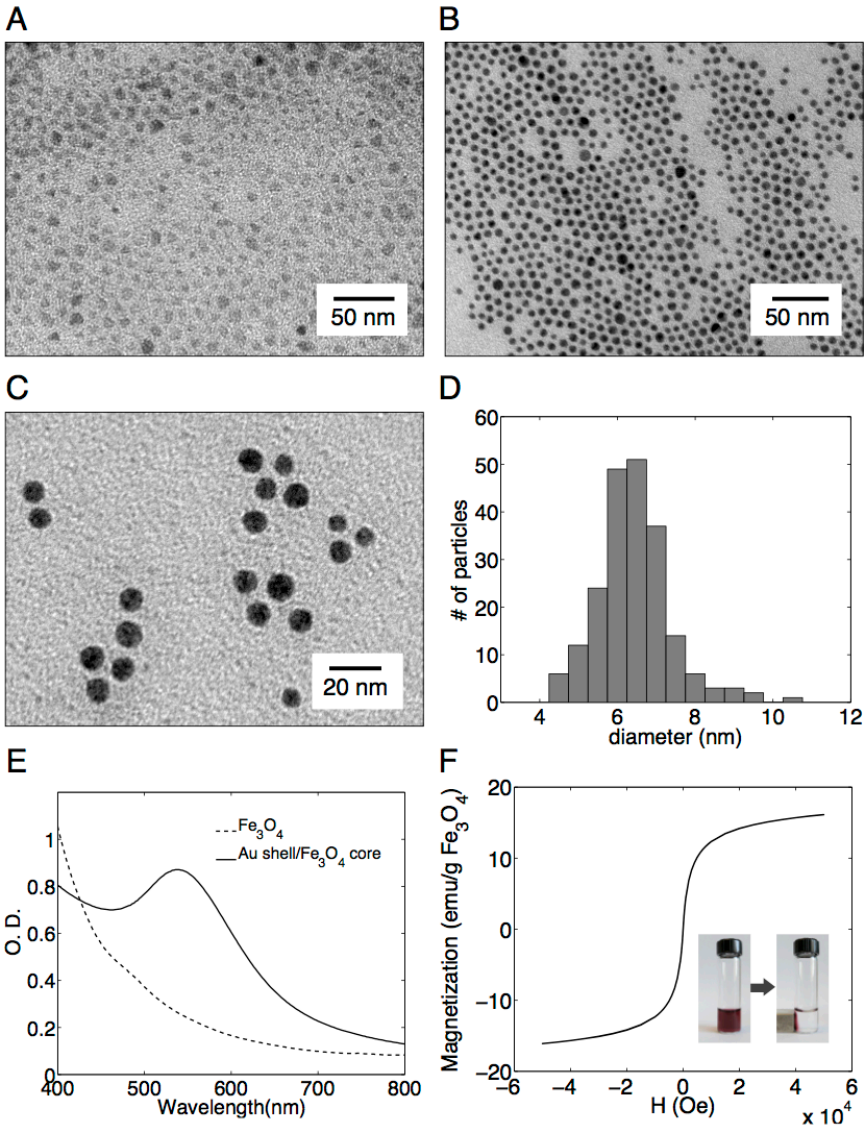

Figure 2.2 Characterization of magnetic core/shell nanocarriers. TEM images of Fe_3O_4 nanoparticles in hexane before (A) and after (B) coating with gold shell; gold shell/magnetic core nanoparticles after transferring into aqueous phase (C). Gold shell/Fe_3O_4 core nanoparticle size distribution (6.2 ± 0.8 nm) as determined from TEM image analysis of more than 200 particles (D). UV-Vis spectrum of oleic acid and oleylamine stabilized Fe_3O_4 nanoparticles (dashed) and gold shell/magnetic core particles in hexane (solid) (E). Magnetization hysteresis at 300 K of gold shell/magnetic core nanoparticles (F); the insert: separation of nanoparticles from a colloidal suspension using a magnetic field gradient created by a simple permanent magnet.

Molecular targeted nanoparticles

For molecular specific targeting of cancer biomarkers the core/shell nanoparticles were conjugated with monoclonal antibodies. Monoclonal antibodies are widely utilized probes due to their high binding constants and availability for a large number of established biomarkers.[19] Our conjugation strategy relies on directional covalent attachment of antibodies to gold nanoparticles through Fc moiety with the antigen binding sites on the Fab portion directed outward from the gold surface, and therefore available for targeting.[20, 21] The conjugation is carried out using a heterobifunctional PEG linker terminated at one end by a hydrazide moiety, and by a di-thiol group at the other end. First, the carbohydrate moiety on the antibody' Fc region is oxidized to an aldehyde group using sodium periodate; thereby allowing for preferential oxidation of orthodiols through a dehydration reaction. Although tyrosine and serine amino acids contain hydroxyl groups, they are not on the nearest neighbor carbons and therefore cannot be oxidized by sodium periodate.[22, 23] Then, the oxidized antibodies interact with hydrazide-PEG-thiol linkers in a reaction where the hydrazide portion of the linker reacts with the aldehyde formed during the oxidation reaction of antibody carbohydrate to form a stable linkage (Figure 2.3). The linker modified antibodies interact with gold surface of core/shell nanoparticles through the linker's thiol groups. Subsequently, methyl-PEG-thiol molecules are added to passivate any remaining bare gold surfaces thereby increasing the biocompatibility and reducing potential nonspecific interactions (Figure 2.3). Attachment of antibodies through the Fc region can be expected to diminish non-specific interactions between nanoparticle conjugates and Fc receptors of blood cells such as macrophages.

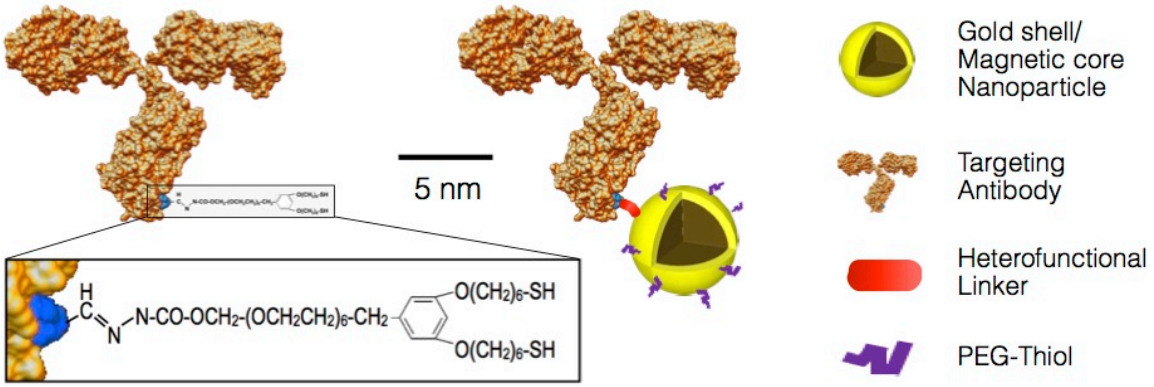

Figure 2.3 Schematic of an antibody molecule modified using a hetero-functional linker (left) and an immunomagnetic nanocarrier (right).

Molecular specificity of immunotargeted nanoparticles

The molecular specificity was demonstrated in three cell lines with known phenotypes: (1) COLO 205 – a model of colorectal cancer which expresses a high level of epithelial cell adhesion molecules (EpCAM), is positive for cytokeratin (CK) expression and is negative for both epidermal growth factor receptor-2 (HER2) and epidermal growth factor receptor-1 (EGFR); (2) SK-BR-3 – a breast cancer model which is EpCAM+/HER2+/EGFR–/CK+; and (3) A-431 – a model of skin cancer with the following expression profile EpCAM+/HER2–/EGFR+/CK+.[24, 25] Each cancer cell line was labeled with immunomagnetic nanocarriers targeted to either EpCAM, HER2, EGFR, or CK. The specificity of labeling was characterized by comparing the binding of the immunotargeted nanoparticles to cells with varying biomarker expression using dark-field microscopy (Figure 2.4).

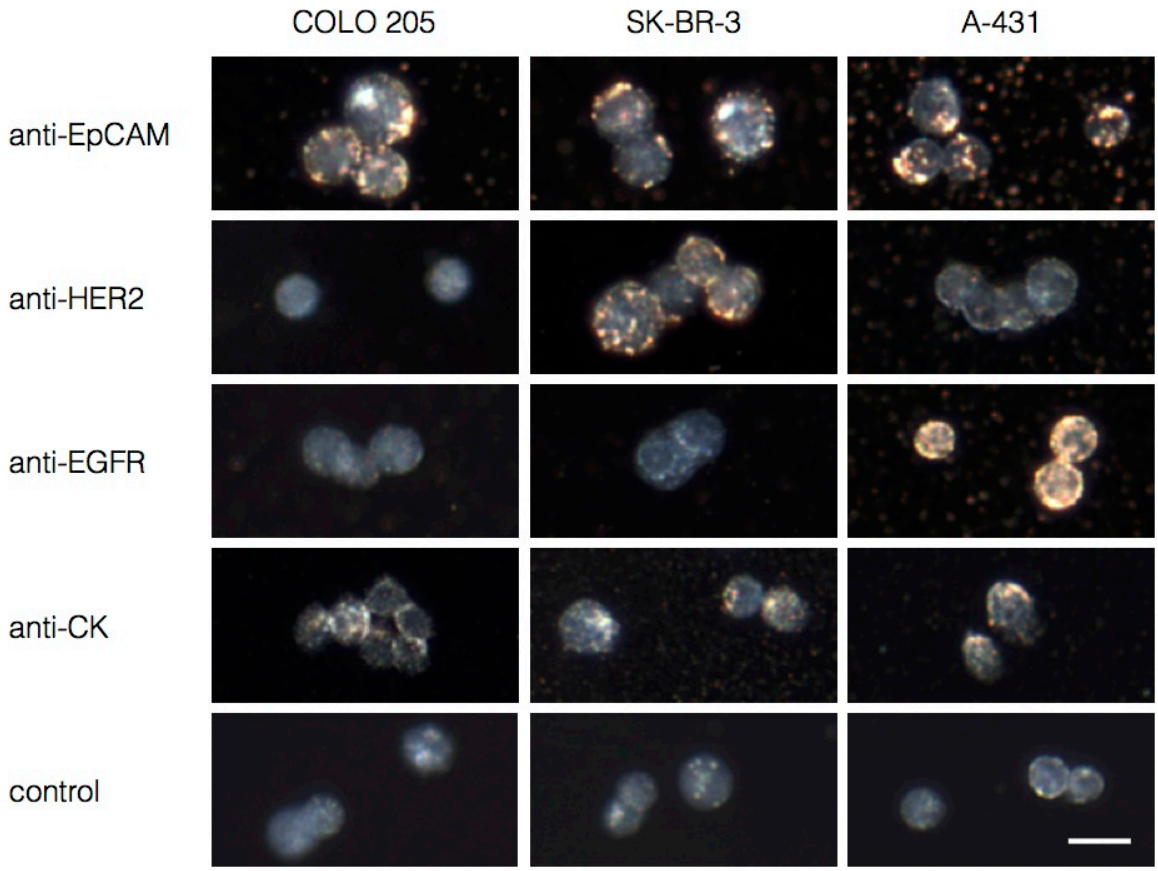

Figure 2.4 Dark-field reflectance images of cancer cells labeled with immunomagnetic nanocarriers. Columns correspond to cancer cells with the following expression profiles: COLO 205 (EpCAM+/HER2–/EGFR–/CK+), SK-BR-3 (EpCAM+/HER2+/EGFR–/CK+), and A-431 (EpCAM+/HER2–/EGFR+/CK+). Rows show labeling results obtained with (from top to bottom): anti-EpCAM, anti-HER2, anti-EGFR, anti-CK and no nanocarriers. The yellow-orange color in the darkfield images is associated with binding of the nanocarriers; unlabeled cells have a grey-bluish appearance.

In dark-field images, a yellow-orange color indicates specific binding of the nanoparticles to cancer cells whereas a grey-bluish color corresponds to the endogenous scattering of unlabeled cells.[26-30] As can be seen in Figure 2.4 the labeling pattern of cancer cells correlates very well with their known expression profiles demonstrating molecular specificity of the immunomagnetic nanocarriers. Indeed, all cells showed good

labeling with anti-EpCAM nanoparticles while only HER2+ SK-BR-3 cells and EGFR+ A-431 cells were labeled with anti-HER2 and anti-EGFR nanoparticles, respectively. Unbound nanocarries can be seen in some of the images; this is due to residual nanoparticles after a washing step. In addition to labeling of cytoplasmic membrane proteins – HER2, EGFR and EpCAM, we also demonstrated successful targeting of cytokeratin that is an intracellular biomarker of epithelial cells (Figure 2.4). The intracellular labeling is facilitated by the small size of the immunomagnetic nanoparticles. In addition, the cells were permeabilized using a procedure that is common in immunostaining of intracellular proteins. The ultra-small immunotargeted nanoparticles permitted passage through the permeabilized cell membrane and specific interactions with intracellular molecules. The ability to target a variety of intracellular molecular biomarkers opens new opportunities for the capture of CTCs since prevalent and universal biomarkers inside the cells reduce the variability that results from the heterogeneous levels of surface antigen expression.[24, 31]

2.3 Self-Assembly Hybrid Nanoclusters from Primary Nanoparticles

The 6 nm diameter core/shell nanoparticles have demonstrated versatility in labeling phenotypically different cancer cells, targeting both surface receptor molecules and intracellular biomarkers of epithelial-derived cancer cells. However, they also have identified limitations, such as a relatively small magnetic moment and exhibition of the plasmon resonance at *ca*. 520 nm where whole blood has a strong absorbance.[8] The latter limitation is overcome when spherical plasmonic nanoparticles are targeted to an overexpressed cancer biomarker or when they undergo an endosomal uptake by cancer cells; in this case, the effect of plasmon resonance coupling between closely spaced nanoparticles results in a strong broadband absorbance that extends to the NIR. However,

the effect of surface plasmon resonance coupling is not likely to be observed for all cancer biomarkers of interest. Here, we address these shortcomings by development of a new type of hybrid magneto-plasmonic nanostructures using oil-in-water microemulsion method.[16, 32] The nanostructures are synthetized from hybrid primary 6 nm iron oxide core-gold shell nanoparticles which self-assemble in highly dense spherical nanoclusters. The use of hybrid primary particles ensures consistent ratio of magnetic (iron oxide) and plasmonic (gold) moieties of the resulting nanoclusters. The dense packing of hybrid primary particles does not change their superparamagnetic properties and, therefore, the overall magnetic moment of the nanoclusters is not limited by the size transition of iron oxide from superparamagnetism to ferrimagnetism. Furthermore, close packing of the primary particles also results in strong red-NIR plasmon resonances that are not present in the primary particles.

2.3.1 Materials and Methods

Synthesis and characterization of hybrid nanoclusters

Oleic acid-capped Au shell/ iron oxide core primary nanoparticles were synthesized according to a previously published method.[33] Briefly, 1 mmol iron(III) acetylacetonate was mixed in 10 mL of phenyl ether, followed by addition of 2 mmol oleic acid, 2 mmol oleylamine, and 5 mmol 1,2-hexadecanediol. The mixture was stirred and heated to 260°C for 1 h under reflux. Then, 5 mL of as synthetized Fe_3O_4 nanoparticles was mixed with 1.1 mmol gold acetate, 0.75 mmol oleic acid, 3 mmol oleylamine, 3 mmol 1,2-hexadecanediol, and 15 mL of phenyl ether under vigorous stirring. The reaction mixture was heated to 180°C for 1 h under reflux. A dark purple precipitate was formed after addition of ethanol and centrifugation. The synthesis resulted

in primary magneto-plasmonic particles with *ca*. 6 nm diameter that were dispersed in hexane.

To make nanoclusters, one volume of a suspension of the primary particles (5 mg/mL by total weight) in hexane was mixed with ten volumes of deionized water containing an anionic surfactant – sodium dodecyl sulfate (SDS, Sigma Aldrich) at 2.8 mg/mL.[16] The mixture was placed in a sonicator bath (Model 1510, Branson) for 2 h. After starting the sonication, the solution was shaken by hand gently to facilitate mixing between the phase containing primary hybrid nanoparticles and the bottom aqueous phase. The solution was heated in a water bath at 80 °C for 10 min to remove hexane. The synthetized nanoclusters at this point had a wide size distribution. Nanoclusters with various sizes were separated using the following sequence of centrifugation steps: first, nanoclusters with sizes *ca*. 180 nm were collected by centrifugation at 100 ×g for 30 min; then, *ca*. 130 nm size was separated from the residual suspension applying the force of 400 ×g for 30 min; and *ca*. 90 nm size was recovered using 1500 ×g for 30 min.

The size and morphology of nanoclusters were examined using a FEI TECNAI G2 F20 X-TWIN TEM at 80 keV, and FEI Quanta 650 SEM. Ultraviolet-visible-NIR (UV-Vis-NIR) absorbance spectra were collected with a BioTek Synergy HT micro-titer plate spectrophotometer. Magnetization curves were analyzed using SQUID magnetometry upon cycling the magnetic field from – 10 K Oe to 10 K Oe at 300 K. A DelsaNano (Beckman Coulter) was used to determine zeta potentials of the nanoparticles. The response of the bare particles to a magnetic field as a function of time was characterized by placing a cubic magnet (1 × 1 × 1 cm, NdFeB, K&J Magnetics) next to one side of a 1 cm cuvette loaded with nanoparticles, followed by measurements of UV-Vis-NIR spectra from the colloidal suspension over time.

Conjugation of monoclonal antibodies to hybrid nanoclusters

The carbohydrate moiety on the Fc portion of monoclonal IgG antibodies – anti-Epidermal Growth Factor Receptor 2 (HER2) antibody (E2777, Sigma Aldrich) and anti-Epidermal Growth Factor Receptor 1 (EGFR) antibody (E2156, Sigma Aldrich) – were thiolated following our previously published protocol.[34] Briefly, 10 μL of 100 mM $NaIO_4$ was added to 100 μL of monoclonal antibody solution (1 mg/mL) in pH 7.2 HEPES for 30 min under dark conditions. The reaction was quenched with 500 μL of 1x PBS. Then, 2 μL of 46.5 mM heterobifunctional polyethylene glycol linker solution (dithiolaromatic PEG6-CONHNH2, SensoPath Inc.) was mixed with the antibody solution for 1 h at room temperature. The linker modified antibodies were purified using a 10k MWCO centrifuge filter at 3,250 ×g for 20 min at 8 °C. Then, the modified antibodies (1 μL at 1 mg/mL) were mixed with the nanoclusters (100 μL at O.D. 1) for 2 h at room temperature. Finally, 10 μL of 10^{-3} M 5 kDa methyl-PEG-SH (SensoPath Technologies) was added to the mixture to replace any residual SDS molecules from the surface of nanoclusters. The functionalized nanoclusters were recovered by centrifugation at 830 ×g for 3 min, and were resuspended in 100 uL 2 % w/v 5 kDa PEG in PBS.

Cell labeling specificity assays

Cancer cells SK-BR-3 and A-431 (ATCC) were cultured in Dulbecco's Modified Eagle Medium (DMEM, Gibco) supplemented with 5 % fetal bovine serum (FBS, Hyclone). Before labeling with nanoclusters, cells were harvested at ~90% confluence using trypsin and resuspended in 1 mL complete media containing *ca*. 5×10^5 cells. Nanoclusters (0.05 nM) conjugated with either anti-HER2 or anti-EGFR antibodies were mixed with a cell suspension for 2 h at room temperature under mild shaking. After incubation with nanoclusters, cells were washed from any unbound particles *via* centrifugation at 182 ×g for 3 min and were resuspended in a phosphate buffered saline.

Then, dark field images of the cells were obtained under Leica DM6000 upright microscope using 20×, 0.5-NA dark field objective and a Xe-lamp illumination.

Hyperspectral images were acquired in bright-field transmittance mode under Leica DM600 upright microscope equipped with a PARISS spectral imager (Lightform) using a 20×, 0.5-NA objective and a 100 W halogen light source. The wavelength calibration was carried out using a standard low pressure Hg wavelength calibration lamp (Lightform). The hyperspectral images of cells were normalized by a spectrum obtained from a region without cells.

Cell viability assay

Three groups of A-431 cells (5×10^3 cells) were incubated with SDS-capped clusters, CTAB (Cetyltrimethylammonium Bromide)-capped clusters, and PEG-capped clusters (particle concentration – 0.05 nM, sterilized by passing through 0.45 μm filter) in a phenol-free DMEM cell culture media supplemented with 5% FBS for 8 hours at 37°C. The cells incubated with nanoclusters and the untreated cell control were then washed twice with PBS and mixed with 100 μL MTS reagent, a mixture of MTS (3-(4,5-dimethylthiazol-2-yl)-5-(3-carboxymethoxyphenyl)-2-(4-sulfophenyl)-2H-tetrazolium) (0.32 mg/mL, Promega) and PMS (phenazine methosulfate) (7.3 μg/mL, Sigma Aldrich) in cell culture media. Absorbance at 490 nm was taken 3 h after the addition of the MTS reagent using a BioTek Synergy HT micro-titer plate spectrophotometer; the absorbance is proportional to the number of metabolically active live cells in a sample.

2.3.2 Results and Discussion

Hybrid magneto-plasmonic nanoclusters

Oil-in-water microemulsion has been demonstrated as a versatile method to prepare single material nanoclusters with high colloidal stability. Size, composition, and

surface charge of the nanoclusters are controllable and tunable by choosing primary metal nanoparticles and surfactants.[32] Several types of nanoclusters have been successfully synthesized and characterized by using magnetic (Fe_3O_4), plasmonic (Au), or semiconductor (CdS) primary nanoparticles.[16] Here, we extended this microemulsion approach to the synthesis of novel hybrid nanostructures with dual magneto-plasmonic properties (Figure 2.5). Nanocluster formation requires amphiphilic surfactants with a hydrophobic moiety to hold together the primary particles inside the cluster, through hydrophobic van der Waals interactions, and a polar group to provide aqueous solubility. There are many surfactants that can be used for this purpose such as cationic surfactants (e.g. cetyltrimethylammonium bromide (CTAB)), anionic surfactants (e.g. sodium dodecyl sulfate (SDS)), nonionic surfactants (e.g. Triton X-100), and polymers (e.g. polyethyleneimine). The surfactant choice depends on the application. In our case, we chose anionic SDS molecules because they result in nanoclusters with enhanced biocompatibility and can be easily replaced with methyl-PEG-thiol (mPEG-SH) molecules, as shown below.

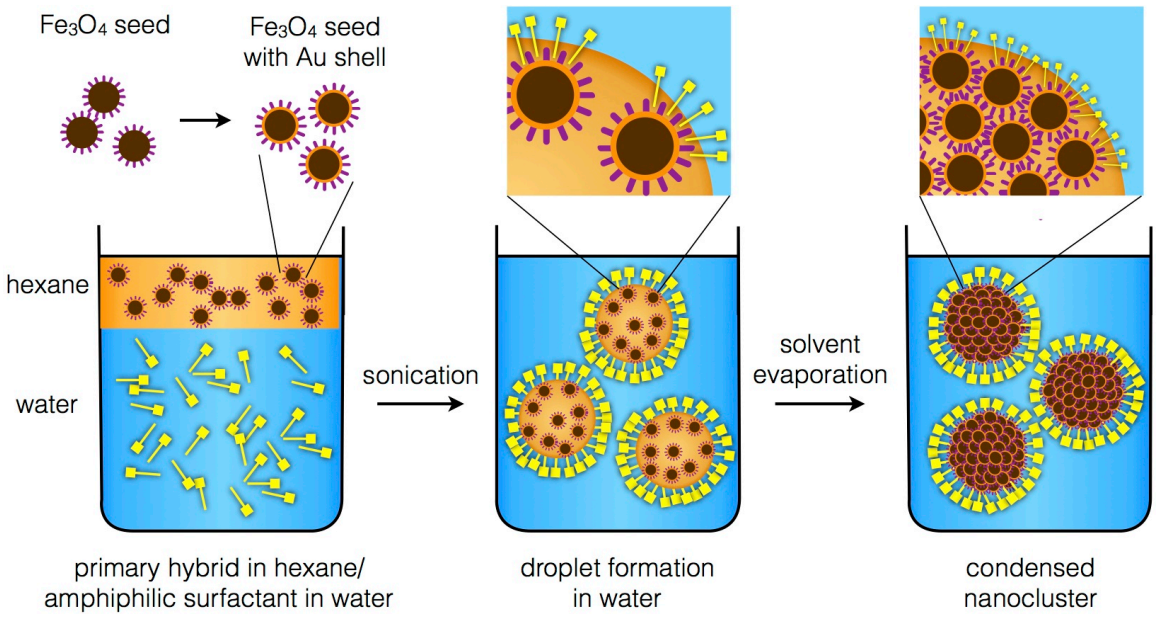

Figure 2.5 The synthesis scheme of the magneto-plasmonic nanoclusters by utilizing an oil-in-water microemulsion method.

Critical steps in successful synthesis of magneto–plasmonic nanoclusters include making highly monodispersed primary gold shell/iron oxide core nanoparticles and directing self-assembly of the primary particles into nanoclusters. A molar ratio between the primary particles and surfactants play an important role in determining size distribution of the nanoclusters. Non-uniform size distribution of primary nanoparticles may cause formation of big aggregates during assembly of magneto-plasmonic nanoclusters. In addition, the microemulsion method of nanocluster formation relies on amphiphilic surfactants: hydrophobic tail groups hold primary nanoparticles together and hydrophilic head groups stabilize nanoclusters in an aqueous solution. Concentration of surfactants determines nanocluster assembly: a high concentration would lead to formation of smaller nanoclusters or individual primary particles and a low concentration would result in particle aggregation.

First, primary iron oxide core/gold shell nanoparticles were prepared *via* the thermal decomposition method.[35] The resultant oleic acid-capped core/shell nanoparticles show high monodispersity with a 6.2 ± 0.8 nm diameter and are readily dispersed in hexane (Figure 2.6A). In a typical nanocluster synthesis, a suspension of the core/shell primary nanoparticles in hexane were carefully added to an aqueous solution containing anionic SDS surfactants with a hexane-to-water ratio of 1:10 by volume. The nanoclusters are formed under ultrasound treatment at the interfacial layer between the two immiscible phases. During this process the amphiphilic SDS surfactants from the aqueous phase undergo hydrophobic van der Waals interactions with the hydrocarbon tail of oleic acids, which stabilize the primary nanoparticles in hexane. Meanwhile, the hydrophilic head groups of SDS molecules interact with the aqueous phase acting as stabilizing agents and preventing aggregation of the forming nanoclusters (Figure 2.5). Subsequent heating of the reaction mixture above the boiling temperature of hexane results in hexane evaporation, and final formation of magneto-plasmonic nanoclusters with densely packed primary particles (Figure 2.6B).

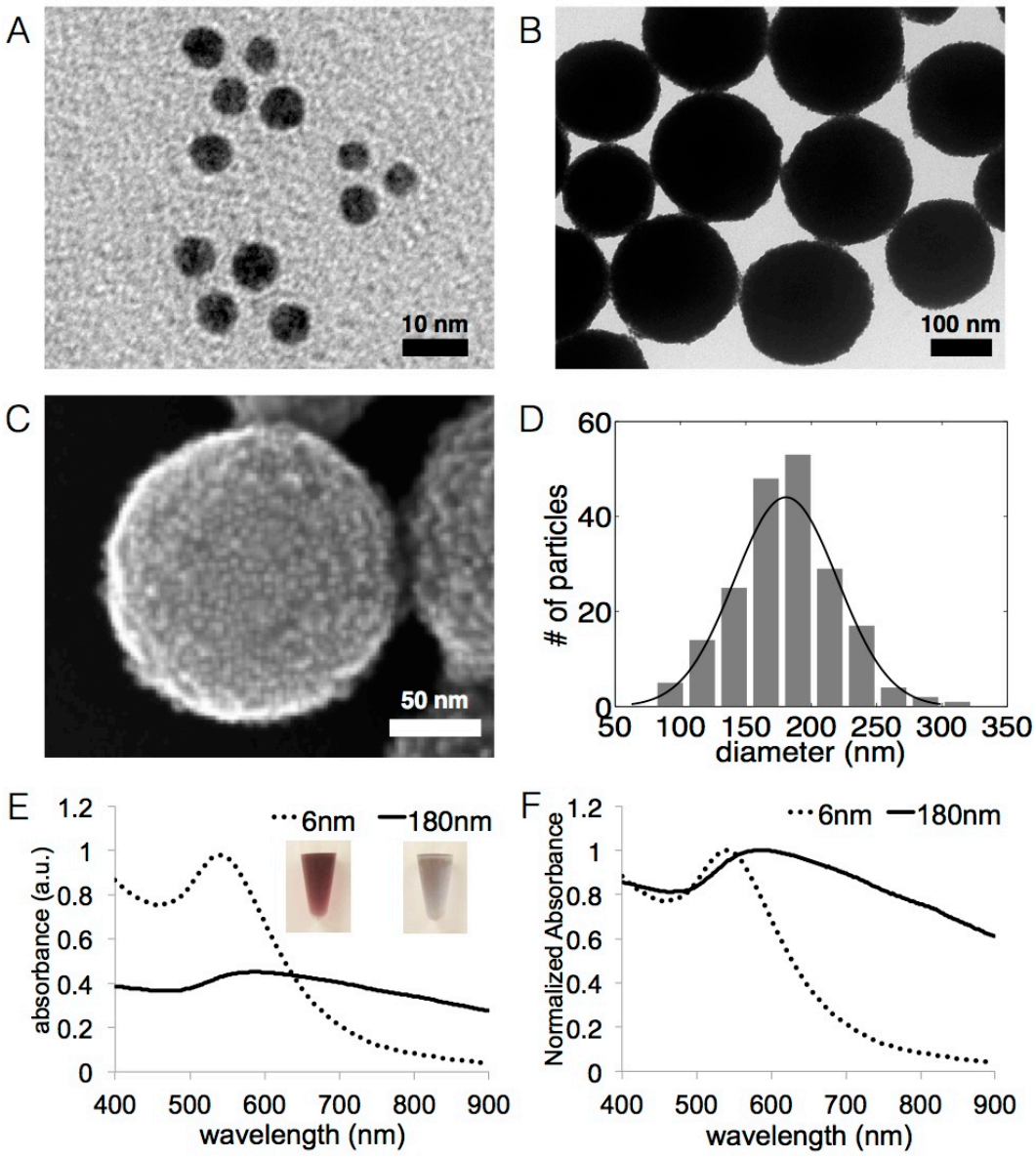

Figure 2.6 Characterization of magneto-plasmonic nanoclusters. (A) TEM image of primary gold shell/Fe_3O_4 core nanoparticles. (B - D) TEM image, SEM image and size distribution of *ca*. 180 nm diameter magneto-plasmonic nanoclusters, respectively; the size distribution was determined from TEM image analysis by counting more than 200 particles. (E and F) UV-Vis spectra of primary particles (dotted line) and nanoclusters (solid line) with the same mass of Au before and after normalization, respectively; the insert in (E) shows changes in colloid color from red for primary particles to purple-grey for nanoclusters.

Scanning electron microscopy (SEM) indicates that primary particles retain individual character and serve as building blocks in nanocluster formation (Figure 2.6C). As-synthesized nanoclusters have a wide size distribution from several nanometers to ~300 nm that requires an additional separation step. Various size fractions were separated by a gradient centrifugation (Figure 2.7). Figure 2.6D shows size distribution of nanoclusters with sizes 180 ± 39 nm as determined from TEM measurements of about 200 particles. Finer separation to produce narrower distributions should be possible by using a size-exclusion chromatography. This nanocluster size was selected, after thorough evaluation, because it exhibits significantly stronger NIR absorbance as compared to smaller nanoclusters (Figure 2.7). There are pronounced differences in the absorbance spectra of nanoclusters and primary nanoparticles (Figure 2.6E); the spectra were obtained for suspensions with the same mass of Au as determined by ICP-MS. Purple colloidal suspension of primary core/shell nanoparticles indicates a distinctive absorbance peak at 538 nm, which is characteristic of isolated core/shell spheres. The grey nanocluster dispersion has a broad absorbance in the NIR region (Figure 2.6F), which can be attributed to a plasmon resonance coupling between the closely spaced primary particles. The inter-particle gaps are a fraction of the primary particle diameter, thereby resulting in broadening and a red-NIR shift in the absorbance of the nanoclusters.[16, 21, 36, 37] However, It is interesting to note that there is a gradual increase in the NIR absorbance with increase in nanocluster sizes (Figure 2.7). Previously, it has been shown that asymmetrical clusters made from *ca*. 5 nm diameter gold nanoparticles with sizes as small as *ca*. 25 nm have a strong and broad NIR absorbance.[38] A pronounced increase in the NIR absorbance for the larger nanoclusters was associated with a significant difference in optical properties of primary particles that are located on the surface versus particles located in the inner nanocluster core, which becomes more

pronounced as size increases.[39,40] However, a thorough theoretical analysis would need to be carried out in order to get a better understanding of the optical behavior of these composite nanoclusters that is outside the scope of this study.

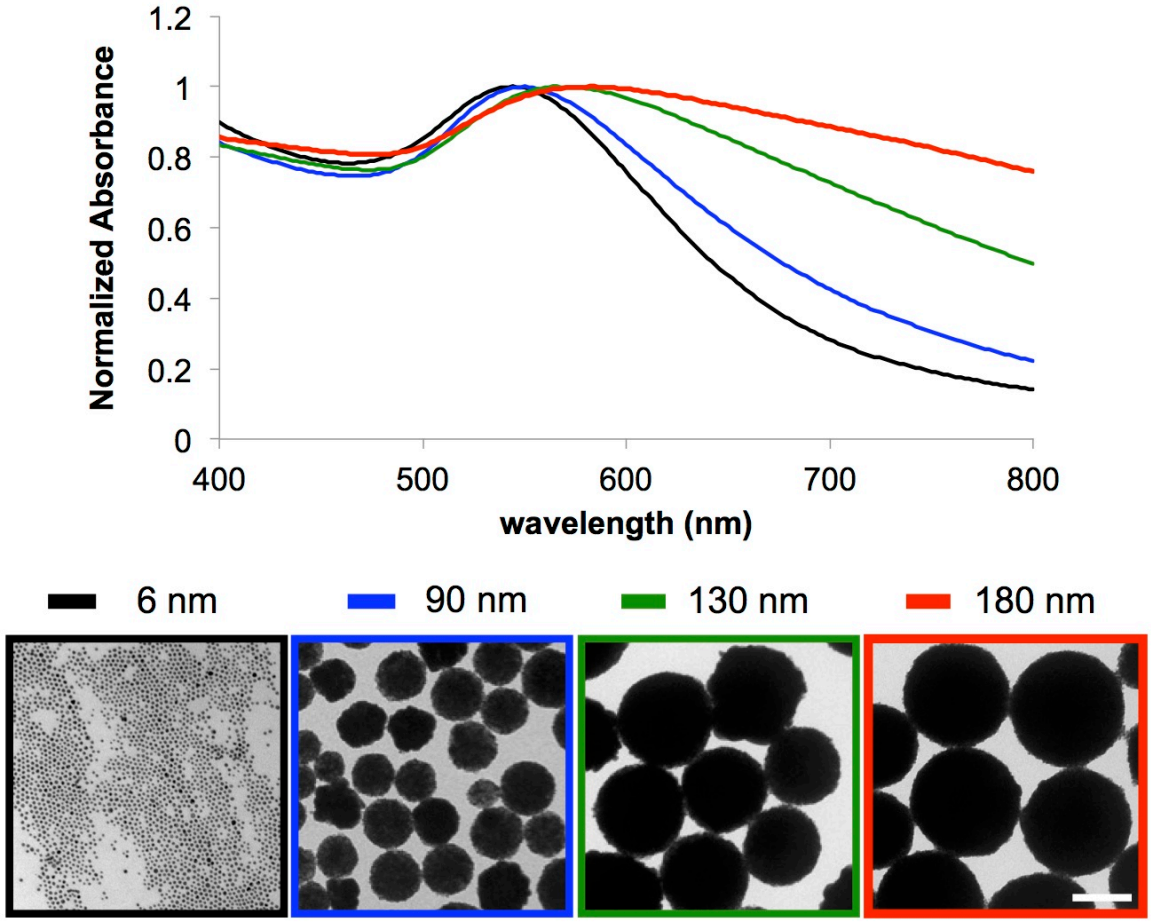

Figure 2.7 Size selection of as-synthesized nanoclusters (90, 130, and 180 nm) and comparison of UV-Vis spectra of primary particles (6 nm) and nanoclusters with various sizes.

Magnetic properties of nanoclusters were characterized using SQUID (superconducting quantum interference device) magnetometry by cycling the field

magnetic field between +10 and −10 K Oe at 300 K. Neither coercivity nor remanence was observed, indicating superparamagnetism with both the primary particles and the nanoclusters (Figure 2.8A). The nanoclusters and the primary particles exhibited similar magnetization, indicating that the constituent particles are separated inside the nanoclusters. The small *ca*. 1.85 emu/g increase in the magnetization of nanoclusters can be attributed to a cooperativity effect between closely spaced iron oxide cores.[41] Because the magnetic moment of a superparamagnetic nanoparticle in an external magnetic field is proportional to nanoparticle's volume, the nanoclusters exhibit greatly improved response to an external magnet (Figures 2.8B and 2.8C). A suspension of either primary particles or nanoclusters was placed next to a permanent magnet in a cuvette with a 1 cm pathlength, and the depletion of the nanoparticles from each dispersion was measured using UV-Vis spectrophotometry. The absorbance at time point zero (no magnet) at 590 nm for nanoclusters and 538 nm for primary particles gave 100% of the total amount of nanoparticles. After 5 min magnetic incubation, the nanocluster solution was depleted 53% versus a 7% for the primary particles (Figures 2.8B and 2.8C). After 15 min incubation, 73% of nanoclusters and 16% of primary particles were captured by the magnet. Therefore, the use of nanoclusters results in a significantly increased magnetic force while preserving superparamagnetic properties of the nanoparticles.

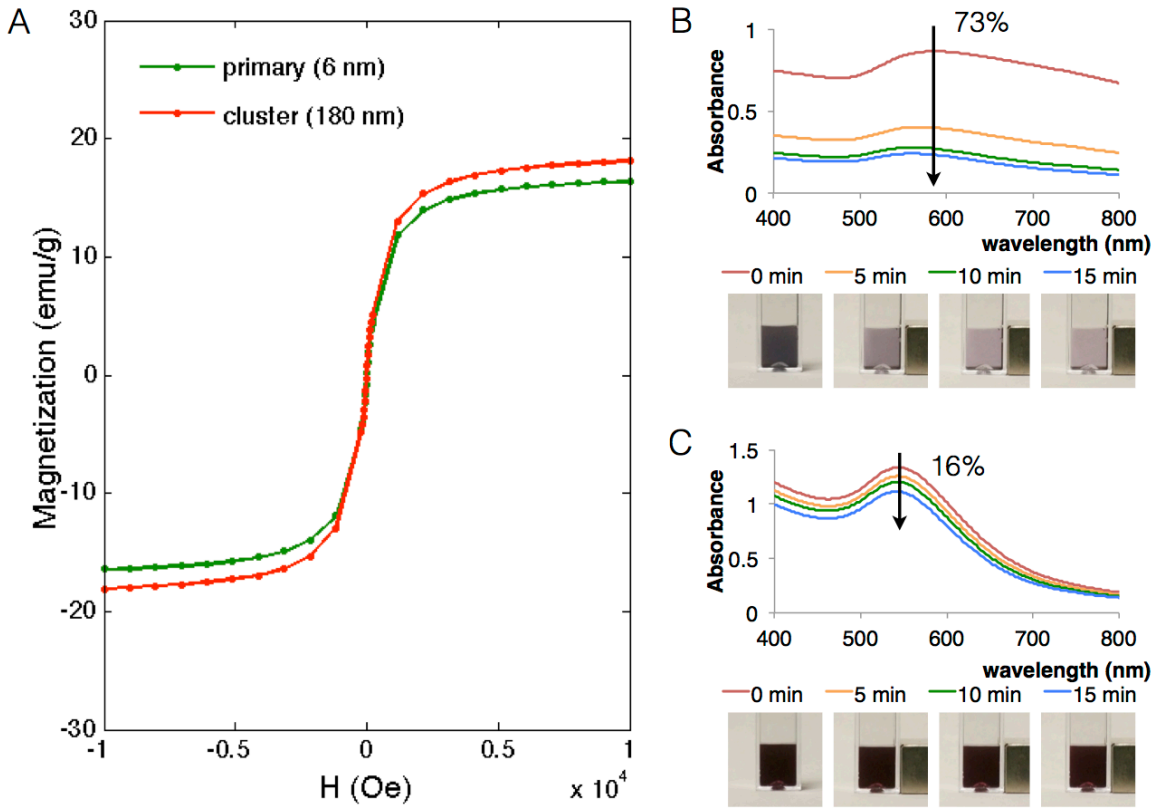

Figure 2.8 Characterization of magnetic properties of nanoclusters. (A) Magnetization hysteresis at 300 K of primary particles and nanoclusters. (B, C) Efficiency of magnetic separation of nanoclusters (B) and primary particles (C) from a colloidal suspension in a 1 cm cuvette in the presence of a permanent magnet. The yield (%) represents the portion of nanoparticles attracted to the magnet after 15 min magnet incubation as determined by the following formula: (1 – ([peak absorbance of magnet-treated sample]/[peak absorbance control sample without a magnet])) × 100%. The photographs show changes in turbidity of colloidal suspensions over time.

Biocompatibility of hybrid nanoclusters

It has been shown that biocompatibility of plasmonic nanoparticles is highly dependent on their surface coating.[42] Several strategies can be employed to ensure nanoparticle biocompatibility, including the use of biocompatible surfactants during particle synthesis or the conjugation of biocompatible molecules on nanostructures after

their synthesis. Here, we characterized the cellular toxicity of nanoclusters synthetized using CTAB and SDS capping ligands, as well as nanoclusters prepared by replacing SDS ligands with mPEG-SH molecules. Zeta potentials of the CTAB and SDS-capped nanoclusters were +48.5 ± 0.3 mV and –47.6 ± 6.0 mV, respectively (Figure 2.9). SDS replacement with mPEG-SH molecules results in a nearly neutral surface charge of +3.3 ± 2.6 mV, indicating successful ligand exchange.

surfactant	zeta potential (mV)
SDS	–47.6 ± 6.0
CTAB	+48.5 ± 0.3
PEGylation on SDS	+3.3 ± 2.6
Ab* conjugation then PEGylation	-7.0 ± 1.4

* monoclonal IgG1 anti-EGFR antibodies.

Figure 2.9 Zeta potential of nanoclusters with various surface coatings.

Cell viability studies were performed using the A-431 cancer cell line (Figure 2.10). Cell viability decreased by 80% and 65% after exposure to CTAB and SDS capped nanoclusters, respectively, while replacement of SDS with mPEG-SH molecules resulted in biocompatible nanoclusters which did not show any cytotoxic effects. These results are consistent with previous reports where CTAB coated nanoparticles exhibited high

cytotoxity.[43] Similarly, SDS molecules are widely used to linearize proteins in SDS-PAGE (sodium dodecyl sulfate polyacrylamide gel electrophoresis) and, therefore, can adversely affect the function of many proteins.[44] These results indicate that SDS is a preferable agent for nanocluster synthesis as it has a better biocompatibility when compared with CTAB. However, a ligand exchange of SDS with mPEG-SH is required in order to render biocompatible nanoclusters.

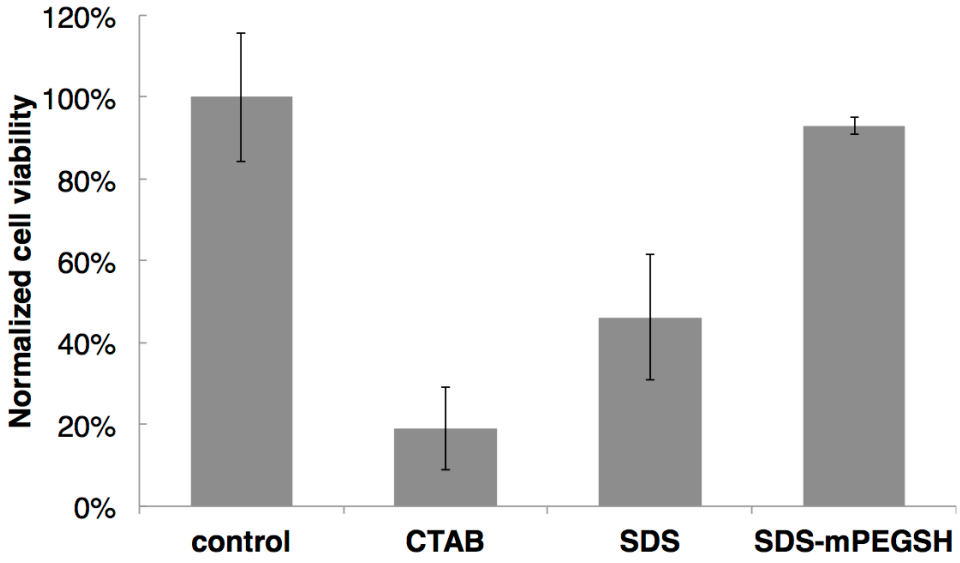

Figure 2.10 Cytotxicity of nanoclusters coated with CTAB, SDS, or methyl-PEG-thiol molecules.

Molecular targeted hybrid nanoclusters

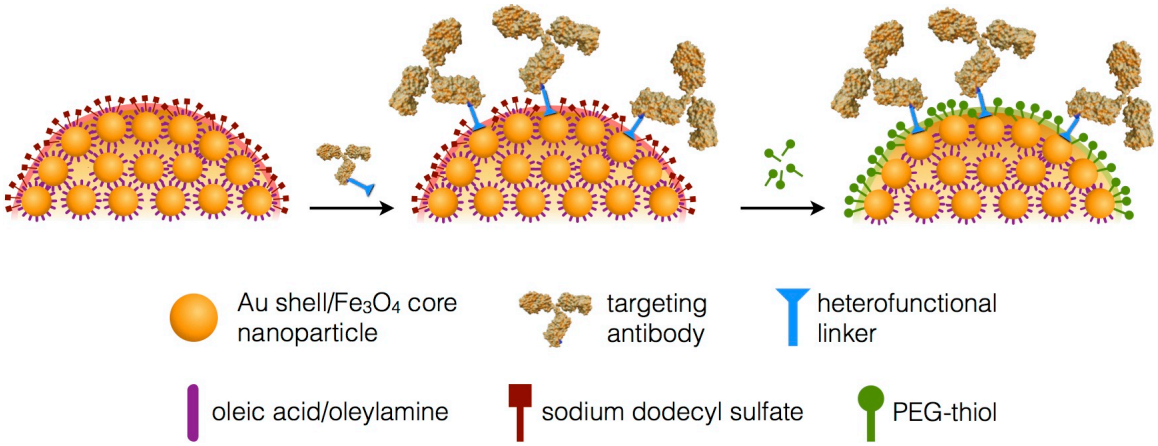

Figure 2.11 Schematic of the antibody conjugation to the nanoclusters through the antibody's Fc moiety using a hetero-functional linker.

Nanoclusters were conjugated with monoclonal antibodies for molecular specific targeting of cancer cells. We used a directional covalent attachment of antibodies to the gold surface of the nanoclusters, leaving antigen binding sites on the Fab antibody region directed outward from the surface and therefore available for targeting.[34] Briefly, a carbohydrate moiety on Fc antibody portion was first oxidized to an aldehyde group using sodium periodate. Then a heterobifunctional polyethylene glycol linker, terminated at one end by a hydrazide moiety and di-thiol group at the other end, was attached to the oxidized carbohydrates on the antibody *via* its hydrazide portion, which resulted in a stable hydrazone bond with aldehydes. The modified antibodies were attached to the nanoclusters through the di-thiol portion of the linker. Subsequently, mPEG-SH molecules were added to passivate the rest of the exposed surface to ensure biocompatibility of the molecular targeted nanoclusters (Figure 2.11). A red shift of *ca.* 32 nm of the absorbance peak of the nanoclusters were observed after the antibody

conjugation, which indicates an increase in the local dielectric constant and, therefore, successful protein conjugation on the surface of nanoclusters (Figure 2.12).[34] Furthermore, the attachment of clone 225 monoclonal EGFR antibodies resulted in a negative zeta potential of −7.0 ± 1.4 mV (Figure 2.9); a similar trend was previously reported for gold nanoparticles conjugated with antibodies.[43] The hydrodynamic radius of nanoclusters increases ~10 to 15 nm after antibody conjugation. This increase in diameter correlates well with *ca*. 12 nm size of an IgG antibody that is attached through the Fc moiety to the surface of nanoparticles. Therefore, the change in the hydrodynamic diameter is consistent with the directional conjugation chemistry for antibody attachment through the Fc portion.

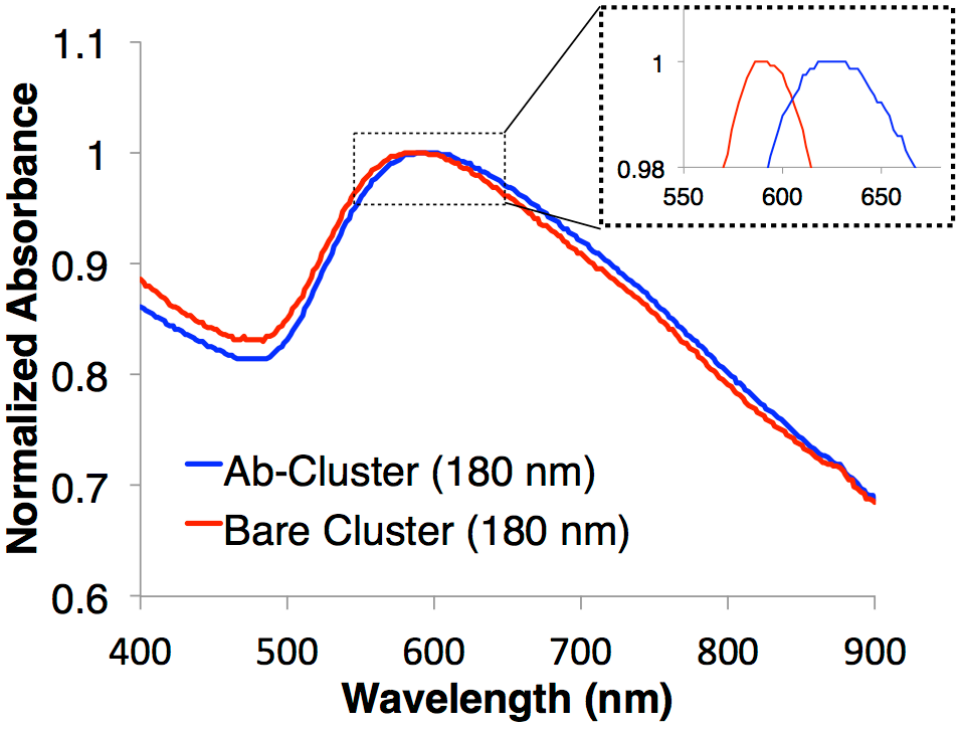

Figure 2.12 UV-Vis spectra of 180 nm diameter nanoclusters (red) and the nanoclusters conjugated with anti-EGFR antibodies (blue). Note a red shift in the absorbance of the functionalized nanoclusters.

Molecular specificity of immunotargeted nanoclusters

Molecular specificity of targeted nanoclusters was tested in two cell lines: (1) A-431 keratinocytes which express a high level of EGFR and are negative for epidermal growth factor receptor-2 (HER2), and (2) SK-BR-3 breast cancer cells which are negative for EGFR expression and positive for HER2. Nanoclusters targeted to either EGFR or HER2 and non-targeted PEGylated clusters were incubated with both cell types (Figure 2.13). Dark-field microscopy images illustrated a bright orange color that is associated with light scattering from the nanoclusters for both the A-431 and SK-BR-3 cells incubated with EGFR and HER2 targeted nanoclusters, respectively. In contrast, cells exhibited characteristic bluish-grey color due to intrinsic cellular scattering after incubation with either targeted nanoparticles that did not match their expression profile or with PEGylated nanoclusters. Therefore, these results demonstrate molecular specificity of immunotargeted nanoclusters.

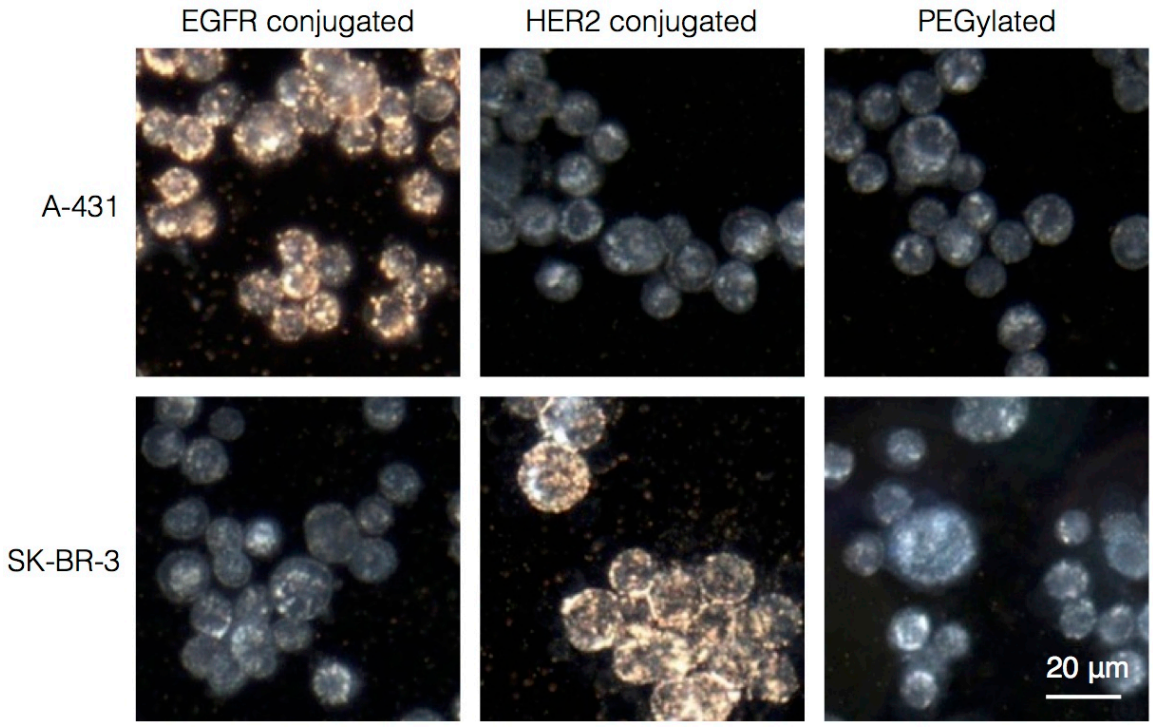

Figure 2.13 Dark-field reflectance images of cancer cells labeled with nanoclusters. Rows correspond to cancer cell with the following expression profiles: A-431(EGFR+/HER2–) and SK-BR-3 (EGFR–/HER2+). Columns show labeling results obtained with nanoclusters conjugated with anti-EGFR antibodies, anti-HER2 antibodies or PEG molecules. The yellow-orange color in the darkfield images is associated with nanocluster binding; unlabeled cells have a characteristic grey-bluish appearance.

Optical properties of particle-labeled cells

We compared the optical properties of cells labeled with either primary particles or nanoclusters, which were both targeted to EGFR molecules (Figure 2.14). The same mass of gold was used for each nanoparticle type in cell labeling experiments. Labeling with EGFR-targeted nanoclusters resulted in a greatly increased absorbance of the A-431 cells when compared with anti-EGFR primary particles (Figure 2.14A). This data demonstrates the advantage of using bigger nanoparticles with higher absorbances for molecular specific cellular imaging; this is not necessarily a trivial result as the use of a

bigger particle could result in a steric hindrance in labeling of closely spaced overexpressed molecules. Normalized absorbance spectra indicated significant broadening and an increase in the red-NIR spectral region of nanoparticles that are interacting with cells, compared with isolated particles in a suspension (Figure 2.14B). These spectral changes can be attributed to the surface plasmon resonance coupling between nanoparticles which are brought in close proximity through their interactions with cellular EGFR receptors; this effect has been previously observed and characterized by our group.[39, 45, 46] Optical imaging of single labeled cells confirms the results obtained using spectrophotometry of cell suspensions (Figure 2.14C-E). Both the bright-field and the dark-field imaging modalities show stronger contrast in the case of nanocluster labeled A-431 cells. Also, hyperspectral bright-field imaging revealed a much stronger absorbance in the red-NIR region of nanocluster labeled cells, compared with cells labeling with primary particles.

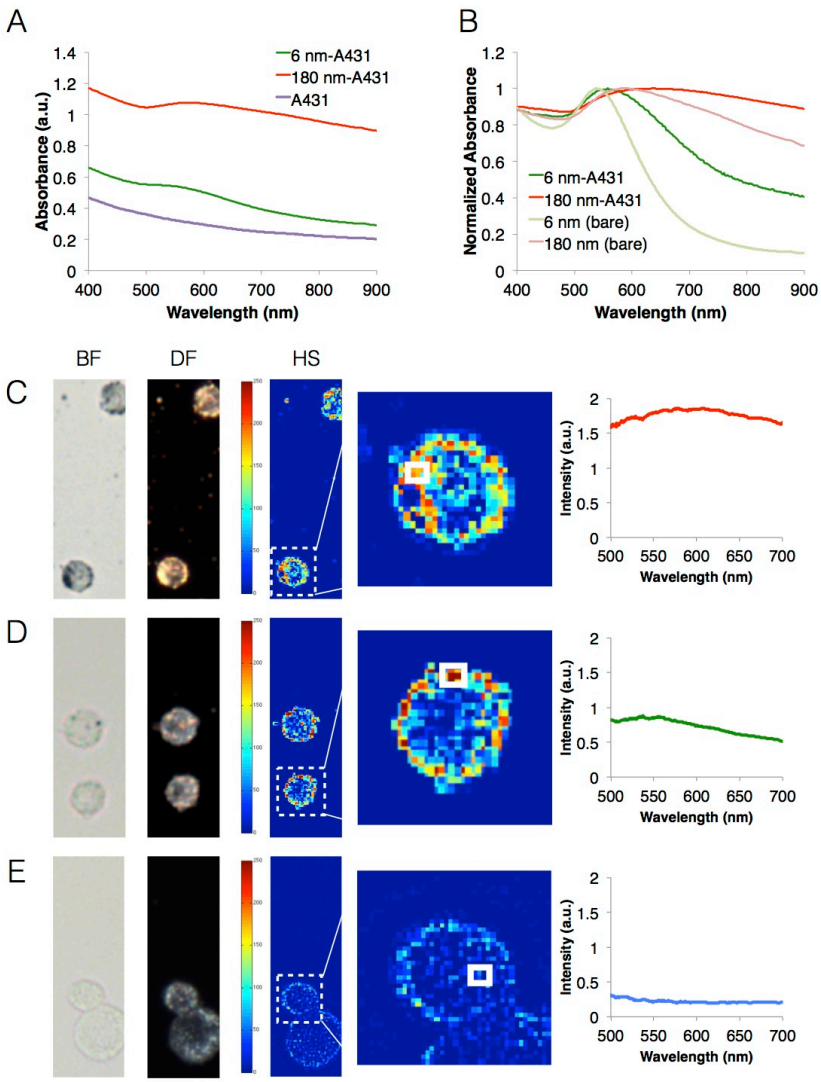

Figure 2.14 Optical properties of cells labeled with molecular targeted nanoparticles. (A, B) UV-Vis spectra of A-431 cells labeled with either EGFR-targeted primary particles or nanoclusters using the same mass of Au: (A) raw spectra, and (B) absorbance spectra of the labeled cells normalized to one after subtraction of the cell only spectrum in comparison with spectra from nanoparticle suspensions. (C – E) Optical properties of individual A-431 cells labeled with EGFR-targeted nanoclusters (C) or primary particles (D). The unlabeled cells are shown as a control (E). Columns from left to right: bright field (BF); dark field (DF); and hyperspectral absorbance (HS) images. The color bars show relative intensity distribution in the HS images for an integrated absorbance from 500 to 700 nm. Representative spectra at the right-hand side are obtained by integrating absorbance in the regions of interest highlighted by white boxes.

2.4 CONCLUSIONS

Here, we created an immunotargeted magneto-plasmonic nanoparticle platform with the size range of 6 nm to 180 nm. The unique feature of our method is synthesis of magneto-plasmonic nanoparticles of various sizes from primary blocks which also have magneto-plasmonic characteristics. This approach yields nanoparticles with a high density of magnetic and plasmonic functionalities which are uniformly distributed throughout the nanoparticle volume. Our method is essentially a simple one-pot reaction after primary particles are synthesized. The overall plasmon resonance strength and magnetic moment are determined by the number of primary particles and, therefore, can be easily optimized depending on an application. We also demonstrated that the choice of the right surfactant in synthesis of the magneto-plasmonic nanoclusters and subsequent surface modification with PEG molecules are both important steps in producing biocompatible nanoclusters, which do not exhibit cytotoxic properties. The nanoclusters show a greatly improved response to an external magnetic field when compared with the constituent primary particles. In addition, the nanoclusters also have a strong NIR absorbance that is absent in the primary particles. The hybrid nanoparticles can be easily functionalized by attaching monoclonal antibodies through the Fc moiety leaving the Fab portion that is responsible for antigen binding available for targeting both surface receptor molecules and intracellular biomarkers. Therefore, this biocompatible magneto-plasmonic nanoparticle platform exhibits the combination of properties which allow transition from highly promising feasibility studies to actual translation of magneto-plasmonic nanoparticles to a variety of biomedical applications, including multi-modal molecular imaging, cell tracking, highly efficient assays for simultaneous capture and enumeration of circulating cancer cells, and cell magnetic guidance under imaging monitoring.

2.5 REFERENCES

1. Bigall, N. C.; Parak, W. J.; Dorfs, D., Fluorescent, magnetic and plasmonic—Hybrid multifunctional colloidal nano objects. *Nano Today* **2012**, 7, 282-296.

2. Gautier, J.; Allard-Vannier, E.; Herve-Aubert, K.; Souce, M.; Chourpa, I., Design strategies of hybrid metallic nanoparticles for theragnostic applications. *Nanotechnology* **2013**, 24, 432002.

3. Wei, Q.; Wei, A., Optical imaging with dynamic contrast agents. *Chemistry* **2011**, 17, 1080-1091.

4. Aaron, J. S.; Oh, J.; Larson, T. A.; Kumar, S.; Milner, T. E.; Sokolov, K. V., Increased optical contrast in imaging of epidermal growth factor receptor using magnetically actuated hybrid gold/iron oxide nanoparticles. *Optics express* **2006**, 14, 12930-12943.

5. Song, H.-M.; Wei, Q.; Ong, Q. K.; Wei, A., Plasmon-resonant nanoparticles and nanostars with magnetic cores: synthesis and magnetomotive imaging. *ACS nano* **2010**, 4, 5163-5173.

6. Qu, M.; Mallidi, S.; Mehrmohammadi, M.; Truby, R.; Homan, K.; Joshi, P.; Chen, Y.-S.; Sokolov, K.; Emelianov, S., Magneto-photo-acoustic imaging. *Biomedical optics express* **2011**, 2, 385-396.

7. Jin, Y.; Jia, C.; Huang, S.-W.; O'Donnell, M.; Gao, X., Multifunctional nanoparticles as coupled contrast agents. *Nature communications* **2010**, 1, 41.

8. Wu, C.-H.; Huang, Y.-Y.; Chen, P.; Hoshino, K.; Liu, H.; Frenkel, E. P.; Zhang, J. X. J.; Sokolov, K. V., Versatile Immunomagnetic Nanocarrier Platform for Capturing Cancer Cells. *ACS nano* **2013**, 7, 8816-8823.

9. Galanzha, E. I.; Shashkov, E. V.; Kelly, T.; Kim, J.-W.; Yang, L.; Zharov, V. P., In vivo magnetic enrichment and multiplex photoacoustic detection of circulating tumour cells. *Nature nanotechnology* **2009**, 4, 855-860.

10. Larson, T. A.; Bankson, J.; Aaron, J.; Sokolov, K., Hybrid plasmonic magnetic nanoparticles as molecular specific agents for MRI/optical imaging and photothermal therapy of cancer cells. *Nanotechnology* **2007**, 18, 325101.

11. Yu, H.; Chen, M.; Rice, P. M.; Wang, S. X.; White, R. L.; Sun, S., Dumbbell-like bifunctional Au-Fe3O4 nanoparticles. *Nano Lett* **2005**, 5, 379-382.

12. Wang, L.; Luo, J.; Fan, Q.; Suzuki, M.; Suzuki, I. S.; Engelhard, M. H.; Lin, Y.; Kim, N.; Wang, J. Q.; Zhong, C. J., Monodispersed core-shell Fe3O4@Au nanoparticles. *J Phys Chem B* **2005**, 109, 21593-21601.

13. Wang, H.; Brandl, D. W.; Le, F.; Nordlander, P.; Halas, N. J., Nanorice: a hybrid plasmonic nanostructure. *Nano Lett* **2006**, 6, 827-832.

14. Hu, X.; Wei, C. W.; Xia, J.; Pelivanov, I.; O'Donnell, M.; Gao, X., Trapping and Photoacoustic Detection of CTCs at the Single Cell per Milliliter Level with Magneto–Optical Coupled Nanoparticles. *Small* **2013**, 9, 2046-2052.

15. Truby, R. L.; Emelianov, S. Y.; Homan, K. A., Ligand-mediated self-assembly of hybrid plasmonic and superparamagnetic nanostructures. *Langmuir* **2013**, 29, 2465-2470.

16. Bai, F.; Wang, D.; Huo, Z.; Chen, W.; Liu, L.; Liang, X.; Chen, C.; Wang, X.; Peng, Q.; Li, Y., A Versatile Bottom-up Assembly Approach to Colloidal Spheres from Nanocrystals. *Angewandte Chemie International Edition* **2007**, 46, 6650-6653.

17. Wang, L.; Luo, J.; Fan, Q.; Suzuki, M.; Suzuki, I. S.; Engelhard, M. H.; Lin, Y.; Kim, N.; Wang, J. Q.; Zhong, C.-J., Monodispersed Core−Shell Fe3O4@Au Nanoparticles. *The Journal of Physical Chemistry B* **2005**, 109, 21593-21601.

18. Wang, Y.; Wong, J. F.; Teng, X.; Lin, X. Z.; Yang, H., "Pulling" Nanoparticles into Water: Phase Transfer of Oleic Acid Stabilized Monodisperse Nanoparticles into Aqueous Solutions of α-Cyclodextrin. *Nano Letters* **2003**, 3, 1555-1559.

19. Devriese, L. A.; Voest, E. E.; Beijnen, J. H.; Schellens, J. H., Circulating tumor cells as pharmacodynamic biomarker in early clinical oncological trials. *Cancer Treatment Reviews* **2011**, 37, 579-589.

20. Kumar, S.; Aaron, J.; Sokolov, K. V., Directional conjugation of antibodies to nanoparticles for synthesis of multiplexed optical contrast agents with both delivery and targeting moieties. *Nature Protocols* **2008**, 3, 314-320.

21. Kumar, S.; Harrison, N.; Richards-Kortum, R.; Sokolov, K., Plasmonic Nanosensors for Imaging Intracellular Biomarkers in Live Cells. *Nano Letters* **2007**, 7, 1338-1343.

22. Hermanson, G. T., BioConjugate Techniques: 2nd Edition. **1996**, 761-764.

23. Bobbitt, J. M., Periodate Oxidation of Carbohydrates. *Adv Carbohydr Chem* **1956**, 11, 1-41.

24. Sieuwerts, A. M.; Kraan, J.; Bolt, J.; van der Spoel, P.; Elstrodt, F.; Schutte, M.; Martens, J. W.; Gratama, J. W.; Sleijfer, S.; Foekens, J. A., Anti-epithelial cell adhesion molecule antibodies and the detection of circulating normal-like breast tumor cells. *Journal of the National Cancer Institute (1988)* **2009**, 101, 61-66.

25. Rae, J. M.; Scheys, J. O.; Clark, K. M.; Chadwick, R. B.; Kiefer, M. C.; Lippman, M. E., EGFR and EGFRvIII expression in primary breast cancer and cell lines. *Breast Cancer Research and Treatment* **2004**, 87, 87-95.

26. Aaron, J.; Nitin, N.; Travis, K.; Kumar, S.; Collier, T.; Park, S. Y.; Jose-Yacaman, M.; Coghlan, L.; Follen, M.; Richards-Kortum, R.; Sokolov, K., Plasmon resonance coupling of metal nanoparticles for molecular imaging of carcinogenesis in vivo. *Journal of Biomedical Optics* **2007**, 12, 034007.

27. Aaron, J.; Travis, K.; Harrison, N.; Sokolov, K., Dynamic Imaging of Molecular Assemblies in Live Cells Based on Nanoparticle Plasmon Resonance Coupling. *Nano Letters* **2009**, 9, 3612-3618.

28. Wang, J.; Boriskina, S. V.; Wang, H.; Reinhard, B. M., Illuminating Epidermal Growth Factor Receptor Densities on Filopodia through Plasmon Coupling. *ACS Nano* **2011**, 5, 6619-6628.

29. Wang, J.; Yu, X.; Boriskina, S. V.; Reinhard, B. M., Quantification of Differential ErbB1 and ErbB2 Cell Surface Expression and Spatial Nanoclustering through Plasmon Coupling. *Nano Letters* **2012**, 12, 3231-3237.

30. Crow, M. J.; Seekell, K.; Ostrander, J. H.; Wax, A., Monitoring of Receptor Dimerization Using Plasmonic Coupling of Gold Nanoparticles. *ACS Nano* **2011**, 5, 8532-8540.

31. Mostert, B.; Kraan, J.; Bolt-de Vries, J.; van der Spoel, P.; Sieuwerts, A. M.; Schutte, M.; Timmermans, A. M.; Foekens, R.; Martens, J. W.; Gratama, J. W.; Foekens, J. A.; Sleijfer, S., Detection of circulating tumor cells in breast cancer may improve through enrichment with anti-CD146. *Breast Cancer Research and Treatment* **2011**, 127, 33-41.

32. Qiu, P.; Jensen, C.; Charity, N.; Towner, R.; Mao, C., Oil phase evaporation-induced self-assembly of hydrophobic nanoparticles into spherical clusters with controlled surface chemistry in an oil-in-water dispersion and comparison of behaviors of individual and clustered iron oxide nanoparticles. *Journal of the American Chemical Society* **2010**, 132, 17724-17732.

33. Xu, Z.; Hou, Y.; Sun, S., Magnetic core/shell Fe3O4/Au and Fe3O4/Au/Ag nanoparticles with tunable plasmonic properties. *Journal of the American Chemical Society* **2007**, 129, 8698-8699.

34. Kumar, S.; Aaron, J.; Sokolov, K., Directional conjugation of antibodies to nanoparticles for synthesis of multiplexed optical contrast agents with both delivery and targeting moieties. *Nature Protocols* **2008**, 3, 314-320.

35. Wang, L.; Wang, L.; Luo, J.; Fan, Q.; Suzuki, M.; Suzuki, I. S.; Engelhard, M. H.; Lin, Y.; Kim, N.; Wang, J. Q., Monodispersed core-shell Fe3O4@ Au nanoparticles. *The Journal of Physical Chemistry B* **2005**, 109, 21593-21601.

36. Khlebtsov, B.; Zharov, V.; Melnikov, A.; Tuchin, V.; Khlebtsov, N., Optical amplification of photothermal therapy with gold nanoparticles and nanoclusters. *Nanotechnology* **2006**, 17, 5167.

37. DeVries, G. A.; Brunnbauer, M.; Hu, Y.; Jackson, A. M.; Long, B.; Neltner, B. T.; Uzun, O.; Wunsch, B. H.; Stellacci, F., Divalent metal nanoparticles. *Science* **2007**, 315, 358-361.

38. Murthy, A. K.; Stover, R. J.; Borwankar, A. U.; Nie, G. D.; Gourisankar, S.; Truskett, T. M.; Sokolov, K. V.; Johnston, K. P., Equilibrium gold nanoclusters quenched with biodegradable polymers. *ACS Nano* **2013**, 7, 239-251.

39. Aaron, J.; Travis, K.; Harrison, N.; Sokolov, K., Dynamic imaging of molecular assemblies in live cells based on nanoparticle plasmon resonance coupling. *Nano Lett* **2009**, 9, 3612-3618.

40. Kreibig, U.; Vollmer, M., *Optical properties of metal clusters*. Springer: Berlin ; New York, 1995.

41. Su, C. H.; Sheu, H. S.; Lin, C. Y.; Huang, C. C.; Lo, Y. W.; Pu, Y. C.; Weng, J. C.; Shieh, D. B.; Chen, J. H.; Yeh, C. S., Nanoshell magnetic resonance imaging contrast agents. *J Am Chem Soc* **2007**, 129, 2139-2146.

42. Alkilany, A. M.; Nagaria, P. K.; Hexel, C. R.; Shaw, T. J.; Murphy, C. J.; Wyatt, M. D., Cellular uptake and cytotoxicity of gold nanorods: molecular origin of cytotoxicity and surface effects. *Small* **2009**, 5, 701-708.

43. Joshi, P. P.; Yoon, S. J.; Hardin, W. G.; Emelianov, S.; Sokolov, K. V., Conjugation of antibodies to gold nanorods through Fc portion: synthesis and molecular specific imaging. *Bioconjugate chemistry* **2013**, 24, 878-888.

44. Rath, A.; Glibowicka, M.; Nadeau, V. G.; Chen, G.; Deber, C. M., Detergent binding explains anomalous SDS-PAGE migration of membrane proteins. *Proceedings of the National Academy of Sciences* **2009**, 106, 1760-1765.

45. Sokolov, K.; Follen, M.; Aaron, J.; Pavlova, I.; Malpica, A.; Lotan, R.; Richards-Kortum, R., Real-time vital optical imaging of precancer using anti-epidermal growth factor receptor antibodies conjugated to gold nanoparticles. *Cancer Res* **2003**, 63, 1999-2004.

46. Aaron, J.; Nitin, N.; Travis, K.; Kumar, S.; Collier, T.; Park, S. Y.; Jose-Yacaman, M.; Coghlan, L.; Follen, M.; Richards-Kortum, R.; Sokolov, K., Plasmon resonance coupling of metal nanoparticles for molecular imaging of carcinogenesis in vivo. *J Biomed Opt* **2007**, 12, 034007.

Chapter 3: Development of Circulating Tumor Cell Detection Assays

3.1 INTRODUCTION

Detection of disseminated tumor cells or tumor biomarkers in human fluids such as blood, urine, and saliva can provide an opportunity to develop an accessible tool for cancer detection and monitoring.[1-3] In particular, accurate quantitation of cancer cells in the bloodstream helps determine prognosis and monitor the effectiveness of cancer therapy.[4-6] However, the challenge of detecting circulating tumor cells is their rare occurrence, estimated as one to few CTCs among millions of leukocytes and billions of erythrocytes.

Immunomagnetic-capture technology is one of the most popular and effective approaches to detect CTCs. Most blood cells are with very weak magnetic properties[7]; hence, selective enhancement on CTCs by targeting them with magnetic substances can help effectively isolate CTCs from the blood. Magnetic materials can be modified with specific antibody to tag CTCs. After mixing functionalized magnetic materials with blood for a defined time, the sample is incubated with a non-uniform magnetic field. The labeled cells migrate toward the region with stronger magnetic field where they are captured. Immunomagnetic methods usually yield viable cells with unaltered biological information which aid further gene expression analysis.

Several immunomagnetic-based capture assays have been introduced to detect and to count CTCs[8, 9] and they all rely on one common biomarker – epithelial cell surface marker (EpCAM) - expression on disseminated tumor cells. The single approved system, CellSearch™ (Veridex), utilizes ferrofluids conjugated with anti-EpCAM antibodies to immunomagnetically enrich CTCs that express EpCAM.[8] However, due to tumor heterogeneity and epithelial to mesenchymal transition (EMT), subpopulations of metastatic tumor cells do not often express this specific epithelial surface antigen or

express it at very low levels,[10, 11] thereby limiting the value of EpCAM based assays for CTC detection. Thus, EpCAM-dependent assays have limited capability to detect CTCs from "normal-like" subtype of breast cancers which lack such expression.[11, 12] Furthermore, in a recent prospective multicenter clinical study, CTCs were detected in only 61% of metastatic breast cancer patients.[4] Consequently, new approaches are required for an effective, highly sensitive, and specific detection of CTCs in whole blood. Our hypothesis is that a versatile platform that can target multiple clinical relevant cancer biomarkers may significantly improve CTC capture and, thus, provide a more accurate determination of the CTCs prevalence in cancer patients.

A key component of our approach to a versatile CTC assay is built around recent progress in development of core-shell nanostructures which have been used in a wide range of applications such as drug delivery, imaging and cellular trafficking.[13-16] Notably, bimetallic nanoparticles containing a magnetic core and a plasmonic gold shell enable novel imaging approaches and photothermal therapy.[17-19] Furthermore, the gold shell facilitates conjugation of biological molecules to the nanoparticle surface for molecular targeting. Previously, we introduced directional antibody conjugation method through the Fc portion that leaves the antigen binding sites on the Fab moiety available for targeting; this approach improves molecular specificity of the conjugates.[20, 21] In addition, nanoparticles with relatively small diameters (less than 10 nm) provide a number of unique advantages in molecular targeting such as reducing non-specific interactions, minimizing possible steric hindrance and increasing permeability in a biological environment such as cells and tissues.[22, 23]

We described a CTC assay in Chapter 3.2 that is based on advances in the synthesis of immunotargeted magneto-plasmonic nanocarriers in combination with a microfluidic device (Figure 3.1). The nanocarriers are based on 6 nm gold shell/iron

oxide core nanoparticles conjugated with monoclonal antibodies that are specific to common biomarkers of CTCs. The very thin gold shell of *ca*. 1 nm provides a convenient surface for antibody conjugation and the magnetic core is used for efficient magnetic force separation of the labeled cancer cells from normal cells in whole blood. The versatility of the nanoparticle platform for detection and enumeration of rare cells was demonstrated in capturing experiments of phenotypically different cancer cells including breast, colon and skin cancers. Furthermore, from the previous chapter we have observed the target-mediated aggregation of nanoparticles when hybrid magneto-plasmonic nanoclusters interacted with cancer cells, resulting in a red spectral shift and broadening of the absorbance spectra in red to near-infrared region. This effect is based on the phenomenon of plasmon resonance coupling between closely spaced noble metal nanoparticles. Thus, we took advantage of this property to explore the feasibility of photoacoustic (PA) detection of labeled cancer cells. The assay based on a simultaneous magnetic capture and PA detection of CTCs was described in Chapter 3.3. The contents of this chapter have been published in the journal ACS Nano[24], accepted in Advanced Functional Materials, and proposed to submit to Nanomedicine.

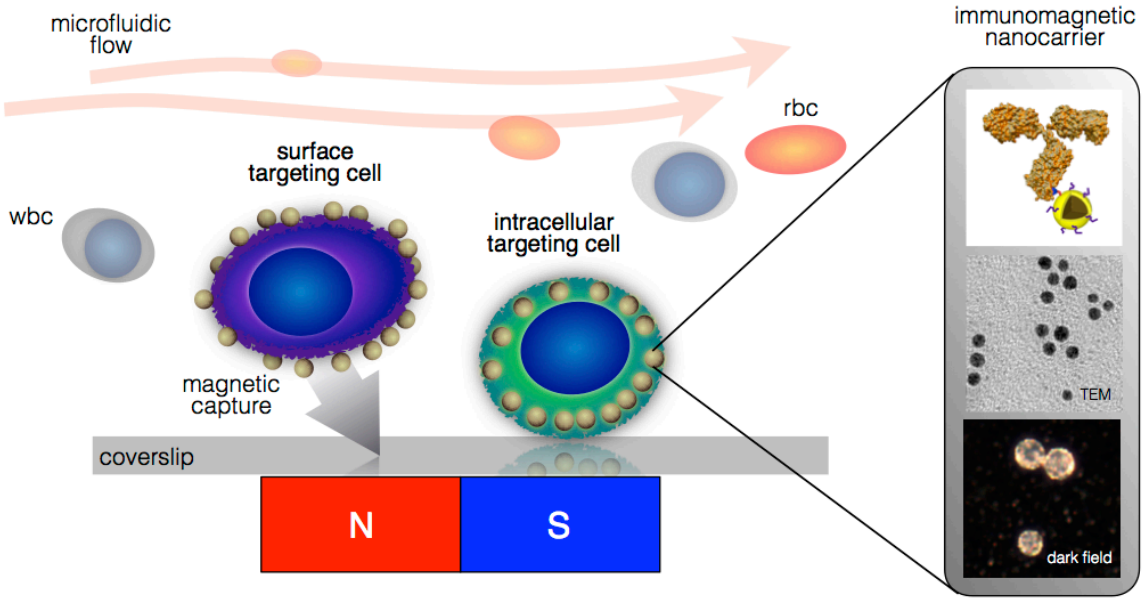

Figure 3.1 Conceptual cartoon of the versatile immunomagnetic nanocarrier platform in microfluidics for capturing circulating tumor cells in whole blood.

3.2 Microfluidic Device-Based Immunomagnetic Detection of Circulating Tumor Cells

3.2.1 Materials and Methods

Microchannel design

To screen blood samples, we used polydimethylsiloxane (PDMS)-based microchannel combined with magnetic field gradient generated by arrayed magnets with alternate polarities.[25] The microchannel with the height of 500 μm was fabricated through soft lithography using PDMS (Sylgard 184, Dow Corning, Midland, MI, 10:1 prepolymer to curing agent), with subsequent steps of bonding the PDMS channel with a glass coverslip (24 × 40 × 0.15 mm, Fisher Scientific).[9] Dimensions of the microchannel are shown in Figure 5a. The inlet of the microchannel was connected to a reservoir for sample loading and the outlet was connected to a syringe pump (Harvard Apparatus) to control flow rates.

Whole blood samples spiked with cancer cells

Blood samples from a healthy donor were spiked with a known number of cancer cells to determine sensitivity of the immunomagnetic nanocarrier platform. Whole blood samples were collected with CellSave tubes (Veridex). Three cell lines - COLO 205, SK-BR-3, and A-431 - with known phenotypes were harvested, centrifuged, and resuspended in phosphate buffered saline. Ten μL cell suspension at a concentration of approximately 20,000 cells per mL was added to a conical CellSave tube containing 2.5 mL of whole blood. The same amount of cell suspension was distributed on three glass slides to calculate the mean of cells spiked into the blood sample.

Immunotargeted nanoparticle preparation

A suspension of functionalized nanocarriers (100 μL, 50 nM) conjugated with either anti-EpCAM, anti-HER2, or anti-EGFR antibodies was added to the blood samples spiked with COLO 205, SK-BR-3, and A-431 cells, respectively. In addition, a combination of anti-EGFR and anti-EpCAM nanoparticles was used in capture experiments with A-431 cells and a combination of anti-HER2 and anti-EpCAM nanoparticles was applied for detection of SK-BR-3 cells. Each nanocarrier in the combinations was administered with equal volume (100 μL) and concentration (50 nM). BT-20 (ATCC) breast cancer cell line was used as a model of cells with a low EpCAM expression; this cell line was labeled with both anti-EpCAM nanocarriers and a combination of anti-EpCAM and anti-MUC1 nanocarriers.

The labeling with anti-CK nanoparticles targeting the intracellular cytokeratin biomarkers required a cell fixation/permeabilization step before addition of the nanoparticles. The whole blood samples containing cancer cells were incubated with 4% formaldehyde for 10 min at room temperature. Then, 1% Triton X-100 was added to the solution for 15 min followed by two washing steps in PBS.

Screening procedures and analysis of whole blood samples

The whole blood samples with spiked cancer cells and immunotargeted nanocarriers were incubated for 2 h under gentle shaking. Then, cancer cells were separated from the whole blood in the microfluidic chip described above that was operating at a continuous flow rate of 2.5 mL per hour. After the separation step, the microchannel was flushed with 3 to 4 mL of phosphate buffered saline to wash blood cells. Subsequently, 1 mL of ice-cold acetone was administered to the microchannel to fix captured cancer cells. The slides were stained using nuclear dye 4',6-diamidino-2-phenylindole (DAPI, Vector Laboratories), anti-cytokeratin pan-FITC (Sigma Aldrich), and the anti-CD45 antibodies labeled with Alexa Fluor 568 (Invitrogen). Captured cancer cells were defined as DAPI+/CK+/CD45−, and white blood cells were classified as DAPI+/CK−/CD45+. The capture yield was calculated by dividing the number of cells found in the sample by the mean number of spiked cells.

To determine dependence of capture efficiency on the number of cancer cells in whole blood, we conducted a series of experiments with a number of spiked COLO 205 cells ranging from 5 to 500 in 2.5 mL of whole blood. Anti-EpCAM nanocarriers were used for cell capture and the experiments were carried out as described above.

3.2.2 Results and Discussion

Detection of spiked cancer cells in whole blood

The efficiency of the immunomagnetic nanocarriers for the capture of cancer cells was examined with a microfluidic magnetic chip that we previously developed (Figure 3.2A).[9] In this device, a magnetic field gradient is generated by a permanent magnet that is placed on top of a 20 × 30 × 0.5 mm microfluidic chamber.[9] In an example, shown in Figure 3.2, 2.5 milliliters of whole blood from a normal volunteer was spiked with ~100-

200 COLO 205 cells and anti-EpCAM magnetic nanoparticles were added to label the cells. Then, the sample was passed through the microfluidic chamber at a continuous rate of 2.5 mL/h using a syringe pump. No additional purification or isolation steps were carried out prior to introduction of the blood sample to the chamber.

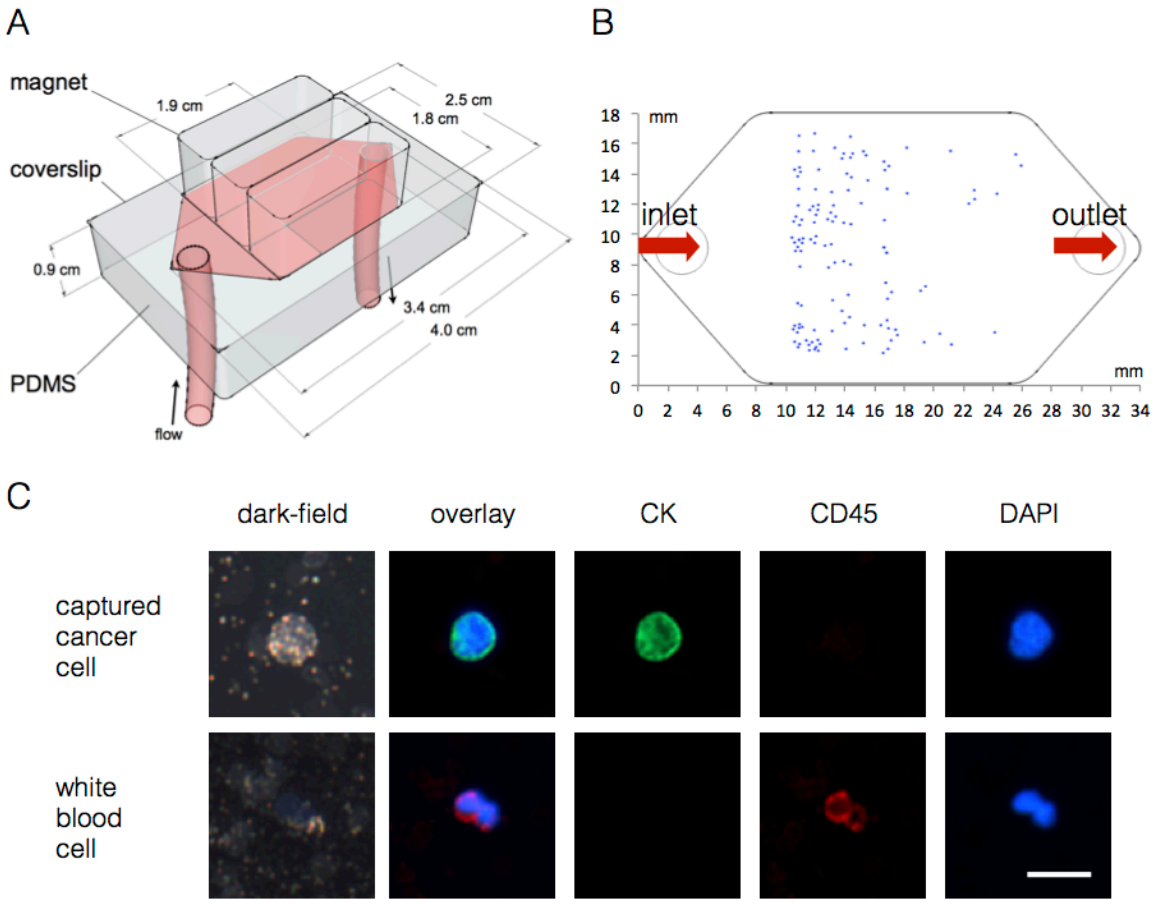

Figure 3.2 Design of a microfluidic channel for immunomagnetic capture, detection and characterization of CTCs (A). An example of distribution of captured COLO 205 cancer cells targeted with anti-EpCAM nanocarriers (B). Fluorescence and darkfield images of a captured COLO 205 cell (DAPI+/CK+/CD45–) and a white blood cell (DAPI+/CK–/CD45+); the cells were labeled using cytokeratin (CK), CD45 and DAPI stains (C).

The captured cancer cells were identified using fluorescent staining which allows distinguishing cancer cells with the epithelial tissue phenotype from the much larger population of nucleated white blood cells. The staining scheme that has been widely used in CTCs capture and enumeration experiments includes anti-CK, anti-CD45 and DAPI stains which are specific for epithelial cells, white blood cells and all nucleated cells, respectively.[4] Figure 3.2C shows an example of staining results for a captured cancer cell and a white blood cell where cancer cells can be easily identified by the positive CK and negative CD-45 staining, while white blood cells are CK negative and CD45 positive.

Most of the captured cancer cells were found where the first maximal magnetic field gradient exists (Figure 3.2B).[25] For this design, these capture sites were located around 10 mm away from the inlet of the microfluidic chamber. Cancer cells with less nanoparticle loading travelled a longer path in the microchamber and were captured at regions farther away from the inlet. In this assay, coordinates of captured cancer cells can be recorded to facilitate subsequent specific molecular characterization analyses such as fluorescence *in situ* hybridization (FISH) or hyperspectral microscopic imaging (HMI) which can identify and select a broad spectrum of molecular moieties for better delineation of the true status of the captured cells. No false positive cells were observed in experiments with normal blood without spiked cancer cells.

Capture efficiency

The combination of the microfluidic magnetic chip and the immunomagnetic nanocarriers provides flexibility in capturing rare cancer cells using different extracellular and intracellular biomarkers with high capturing efficiency (Figure 3.3). To demonstrate this concept, we carried out a series of spiked experiments in the whole blood where A-431 skin cancer cells, SK-BR-3 breast cancer cells and COLO 205 colon cancer cells were captured using cytoplasmic membrane protein targeted nanocarriers – anti-EGFR,

anti-HER2 and anti-EpCAM, respectively, according to an expression profile of each cell type (Figure 3.3A). In addition, the COLO 205 cells were also captured using nanocarriers targeted to the intracellular biomarker – cytokeratin. Notably, the capture efficiency exhibited by the cytokeratin targeting nanocarrier is the same as the efficiencies of the nanocarriers targeting cell surface proteins. The capture yield was 70–80% in cases where a single nanocarrier was used that is comparable to the FDA-approved CellSearch™ system and the recently described microchip system with antibody-coated microposts.[8, 26]

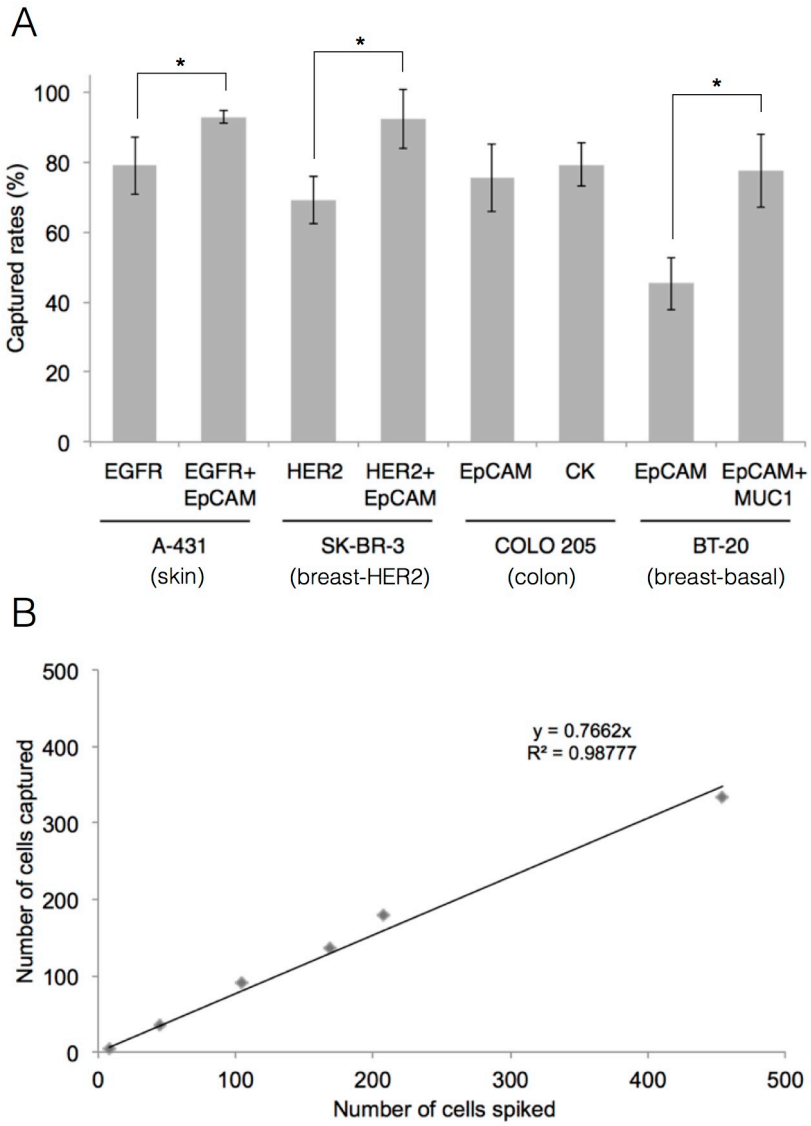

Figure 3.3 Cancer cell capture and enumeration. (A) Capture efficiency in spike experiments in 2.5 mL whole blood samples from a normal volunteer where COLO 205 (colon), SK-BR-3 (breast), A-431 (skin) or BT-20 (breast) cells were captured using immunomagnetic nanocarriers targeted to cancer biomarkers which are listed in the parentheses; each experiment was repeated at least 3 times. Note a significant increase ($*p < 0.05$) in the capture efficiency when a combination of nanocarriers is used for detection of A431, SK-BR-3 and BT-20 cells; this increase is especially pronounced in the case of a low EpCAM expressing BT-20 cells. (B) Number of captured cells as a function of spiked COLO 205 cells in 2.5 mL whole blood samples; the number of spiked cells was varied from 5 to 500 cells.

However, our approach to CTC assay allows straightforward multiplexing of immunotargeted nanocarriers to various cancer cell antigens, thereby increasing CTC detection.[27] For example, using anti-EGFR and anti-EpCAM nanocarriers simultaneously for detection of A-431 cells increases the capture yield from 79% in the case of anti-EGFR nanoparticles alone to 93% for the combination, similarly combining anti-HER2 and anti-EpCAM nanoparticles improves the capture yield of SK-BR-3 cells from 69% obtained in the case of HER2 targeting alone to 93% for the combination (Figure 3.3A).

We also explored the concept of using multiple nanocarriers to improve capture in cancers which express EpCAM antigen poorly or not at all. First, we manually reproduced CellSearch™ capture assay in spiked experiments in whole blood using the basal-like subtype of breast cancer cell line, BT-20, which expresses relative low EpCAM; the assay showed the capture efficiency of only *ca*. 44%. The same recovery rate was obtained using our anti-EpCAM immunomagnetic nanocarriers (Figure 3.3A). However, combining anti-EpCAM and anti-MUC1 nanocarriers together improved the capture efficiency from 45% to 78%. The nanocarriers in the combination were applied in 1:1 ratio and the concentration of each nanoparticle was the same as in experiments with a single nanocarrier.

Thus, utilizing multiple nanocarriers opens the route to significantly improve capture of CTCs with various expression profiles including capture of cancer cells that express EpCAM weakly on their surface.[4] We also demonstrated that cell capture efficiency exhibits a linear behavior (the R2 value for the linear regression fit is 0.988) in spiking experiments with a number of COLO 205 colon cancer cells ranging from 5 to 500 in whole blood (Figure 3.3B). For the group with only 5 cells, the capture yield was 86%, whereas an average ca. 77% capture yield was obtained from the linear graph shown on Figure 3.3B.

In addition to the multiplexing capabilities demonstrated above, the advantages of our platform include the use of whole blood in CTC detection that eliminates multiple pre-processing steps including plasma replacement, centrifugation and sample transfer between tubes which are commonly used in other assays such as CellSearch™. We also demonstrated the possibility of fluorescent staining inside the microfluidic chamber following cell capture. This in-channel procedure provides an efficient washing and fluorescent labeling due to short diffusion distances thus saving the amount of fluorescent reagents used, improving uniformity of staining and eliminating potential loss of captured cells. The CTC observation can be easily automated and individual cells can be analyzed using HMI to explore a large number of molecular markers for better delineation of the status of the captured cells.

3.3 Size-Selective Approach with Photoacoustic Detection of Circulating Tumor Cells

3.3.1 Materials and Methods

Photoacoustic imaging of nanocluster-labeled cells in tissue mimicking phantoms

Photoacoustic imaging experiments were carried out using tissue-mimicking ultrasonic phantoms.[28] First, a 5 cm thick base-layer was prepared using 8% gelatin, 0.25% 40-μm silica particles, and 0.1% formaldehyde.[29] Then, cell inclusions were made by mixing 7.5 μL of gelatin (16% gelatin, 0.5% 40-μm silica particles, and 0.2% formaldehyde) with 7.5 μL of formalin fixed pre-labeled A-431 cells. The inclusions contained *ca*. 10^5 cells and were pipetted onto the surface of the base-layer. After curing for 1 h at 4°C, the same procedure used to make the base layer was utilized to make a 1 cm thick layer on top of cell inclusions.

Cell phantoms were imaged using a Vevo 2100 (VisualSonics) for the photoacoustic signal acquisition and a Quanta-Ray PRO-290 pumping a premiScan/MB tunable OPO (Spectra-Physics Lasers) for the photoacoustic excitation. For photoacoustic images acquired using wavelengths shorter than 710 nm, the laser beam from the signal port of the OPO was coupled into an Optran WF multimode optical fiber (CeramOptec Industries, Inc.). The diameter of the laser spot on the surface of the phantom was 1 cm and the fluence was maintained at 3 mJ/cm^2 for all wavelengths using an array of neutral density (ND) filters. The 21 MHz transducer of the Vevo 2100 was positioned orthogonal to the surface of the phantom and was used to acquire the photoacoustic signals resulting from the nanosecond laser pulses. Photoacoustic images were acquired at 600 nm, 650 nm, and 700 nm with the optical fiber and ultrasound transducer being stationary and the phantom moving so that a single inclusion with either labeled or unlabeled A-431 cells was in the imaging plane. After the photoacoustic images were acquired, the laser source was switched from the signal port to the idler port of the OPO. The phantom was repositioned and photoacoustic images were acquired at 750 nm, 800 nm, 850 nm, 900 nm, 950 nm, and 1064 nm wavelengths. An average of 50 photoacoustic images were obtained at each wavelength. The photoacoustic signal intensity from a small region of interest (3 × 3 mm) in the phantom was averaged and plotted as a function of wavelength.

Magnetic capture efficiency test

A-431 cells in culture medium (5×10^5 cells) were labeled with either anti-EGFR conjugated primary particles or nanoclusters (both at concentration of 0.05 nM) for 1 h at room temperature. After labeling, A-431 cells were washed with 1x PBS. The labeled cells were then resuspended in 1 mL of 1x PBS and placed into a 1 cm cuvette. A cubic magnet (1 × 1 × 1 cm, NdFeB, K&J Magnetics) was positioned next to the cuvette's wall,

and a 10 μL sample was taken from the center of the cuvette at time points 5 min, 10 min, and 15 min.

CTC assay setup and photoacoustic detection

The whole blood samples (1 mL) with spiked A-431 cancer cells (1×10^3) and anti-EGFR conjugated nanoclusters (100 μl, 50 nM) were incubated for 1 h at room temperature under mild gentle shaking. Then, the labeled cell solution was transferred to a cell culture insert which contains polyethylene terephthalate membrane filter with 8 μm pore (Falcon, BD). The insert was placed in a 6-well plate and the well was then filled with 1 mL PBS (Figure 3.4A). A 0.5 T neodymium magnet (K&J Magnetics) was placed under the well and the entire setup was gently shaken for 30 min. The insert was gently washed three times with 1 mL PBS in the presence of the magnet and subsequently immersed in ice-cold acetone for 10 min to fix the cells on the membrane. The porous membrane was then carefully cut from the insert and placed on a glass microscope slide. A 50 μm diameter stainless steel wire was placed on the membrane as an optical and PA image co-registration marker. The membrane and wire marker was mounted with fluoromount (Sigma Aldrich) and covered with a glass coverslip for imaging (Figure 3.4C). Fingernail polish was used to seal the edges of the coverslip to provide a ridged watertight barrier.

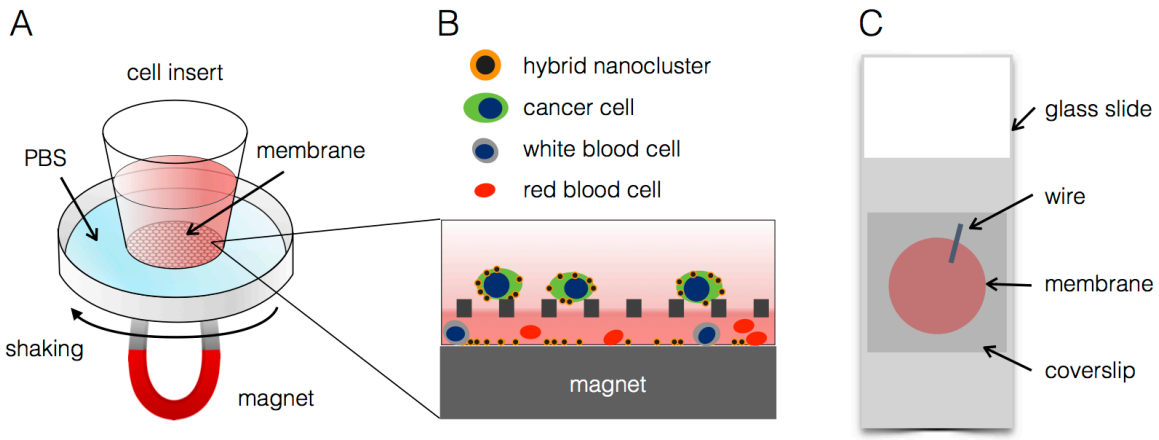

Figure 3.4 Schematic of the capture and enumeration of CTCs using a porous membrane and immunotageted hybrid nanoclusters. (A) Side-view of the magnetic enrichment setup. (B) Mechanism of magnetic capture where nanocluster-labeled cancer cells were attracted and captured by the magnet on a porous membrane whereas unbound free nanoclusters and blood cells were filtered through the pores. (C) Sample preparation for photoacoustic imaging with a wire marker on the cell-loaded porous membrane for co-registration.

The samples were first optically imaged using a DMI 3000 B inverted microscope (Leica Microsystems). Bright-field images of the porous membrane and wire co-registration marker were acquired using a 40x objective. The sample was then transferred to a modified PA microscope previously described.[30] Briefly, a Polaris II (New Wave Research) with 5 ns pulse width and 20 Hz pulse repetition rate was used to mediate the PA signal generation. The 532 nm wavelength beam was used. The resulting PA wave from the 532 nm pulsed laser light was measured using a 1 mm needle hydrophone (Precision Acoustics LTD), amplified using a 5073PR ultrasound receive amplifier (Olympus), and digitized using an CompuScope 12400 oscilloscope (Gage Applied Technologies). The PA intensity at each point was determined by the time of flight from the sample to the hydrophone, *ca*. 3.5 μs. To speed up the detection, the samples were scanned using two different spot sizes. The low resolution scan (100 μm spot size, 90 mJ/cm^2 fluence, 50 μm translation step size) was used to coarsely scan the sample.

After regions were identified, a high resolution scan (8 μm spot size, 90 mJ/cm^2 fluence, and 4 μm translation step size) was used to determine the distribution of the nanoclusters with subcellular resolution.

3.3.2 Results and Discussion

Photoacoustic imaging of nanocluster-labeled cells in tissue mimicking phantoms

Since magneto-plasmonic nanoparticles can be advantageous in a number of emerging biomedical applications including magnetic capture and simultaneous PA detection of CTCs, we evaluated nanocluster performance with PA imaging in the red-NIR region where blood and biological tissues are more transparent. A series of PA images at multiple wavelengths were acquired from A-431 cancer cells labeled with anti-EGFR nanoclusters and primary 6 nm particles (Figure 3.5). The use of nanoclusters increased the strength of PA signal from labeled cells in the NIR region by more than 4 times as compared with primary particles (Figure 3.5D). This quality makes the nanoclusters an attractive agent for *in vivo* imaging where absorption from endogenous chromophores, such as hemoglobin, is significantly reduced in the NIR region.[31]

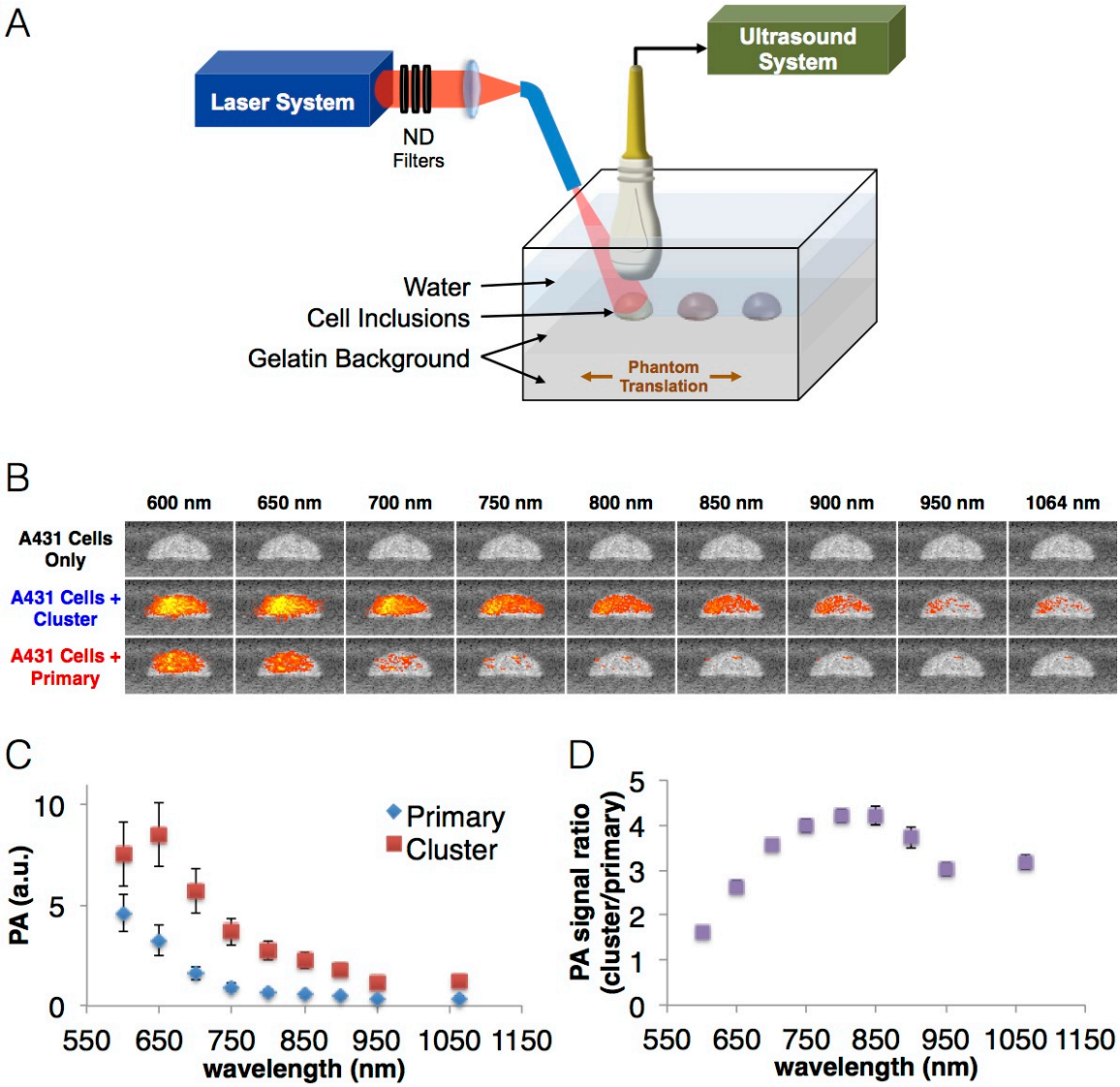

Figure 3.5 Photoacoustic imaging of labeled A-431 cells in tissue-mimicking cell phantoms. The cells were labeled with either EGFR-targeted nanoclusters or primary particles using the same mass of Au during labeling. (A) Schematic of the experimental setup for combined ultrasound and photoacoustic imaging. (B) Combined ultrasound and photoacoustic images of cell phantoms: unlabeled cells (top row), nanocluster labeled cells (middle row), and primary particles labeled cells (bottom row). (C) A plot of un-normalized PA signal intensity integrated over cell inclusions in the phantom as a function of wavelength. (D) The ratio of PA signal intensities from nanocluster labeled cells to primary particles labeled cells as a function of wavelength.

Magnetic capture efficiency

Previously, we showed that primary 6 nm magneto-plasmonic nanoparticles can be used for magnetic capture of cancer cells spiked in whole blood.[24] Here, we compared the performance of primary particles with magneto-plasmonic nanoclusters. The same mass of either anti-EGFR antibody conjugated primary particles or targeted nanoclusters were used to label the same amount of A-431 cells. Then, labeled cells were placed in a 1 cm cuvette with a permanent magnet positioned on one side (similar to the set-up shown in Figures 2.7B and 2.7C). The efficiency of cell separation was determined by comparing the amount of magnetically-trapped cells and cells in a control cuvette without a magnet:

$$\left(1 - \frac{cell\ count\ from\ magnet\ treated\ sample}{cell\ count\ from\ control\ (no\ magnet)}\right) \times 100\%$$

The results demonstrate enhanced magnetic cell separation by nanoclusters in shorter time periods (Figure 3.6), which is a key improvement because there is a critical need for development of faster CTC assays, especially in point-of-care applications. The capture yield of nanoclusters achieved *ca*. 93% after a 10 min magnetic incubation while the primary particles showed just *ca*. 70% capture efficiency at this time point. Hence, immunotargeted nanoclusters provide a more efficient agent for molecular specific magnetic separation of cells of interests.

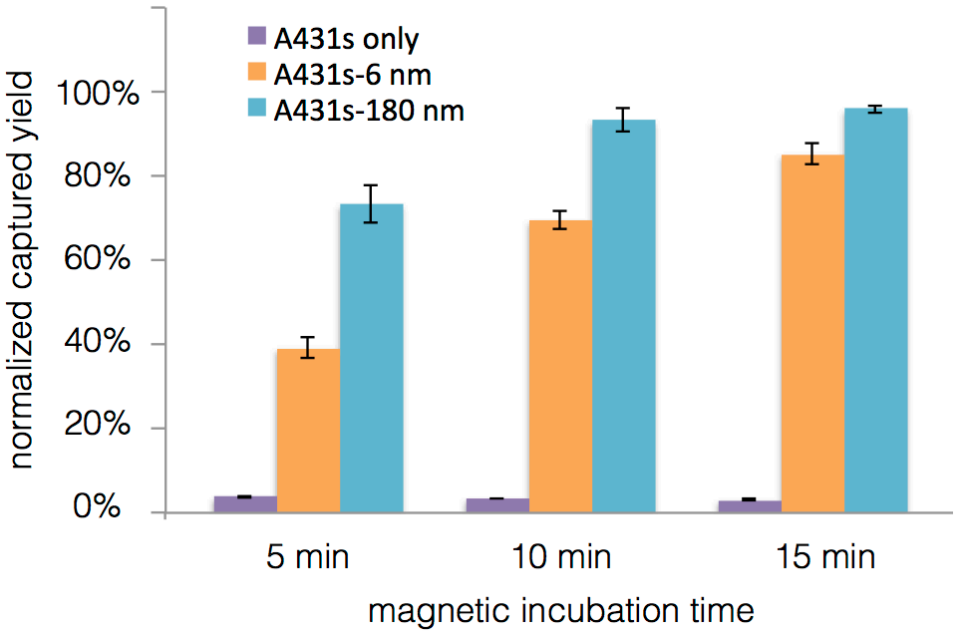

Figure 3.6 Magnetic capture efficiency as a function of time for A-431 cells labeled with either EGFR-targeted primary particles or nanoclusters. The experiment was carried out using the same approach as shown in Figures 2.8B and 2.8C. The bar graph shows a capture yield that was calculated as following: (1 – ([number of cells in suspension at a given time]/[number of cells before incubation with a magnet])) × 100%.

Detection of spiked cancer cells in whole blood

To illustrate the feasibility of CTC enrichment from whole blood using hybrid nanoclusters, two samples were prepared, blood only and blood spiked with A-431 cancer cells. The high contrast of the low resolution PA images indicated the presence of nanocluster-labeled cells (Figure 3.7A). The high resolution PA image provides the distribution of nanoclusters with subcellular resolution (Figure 3.7B). The spatial distribution of the nanoclusters correlates well with the positions of the cells in the bright-field image (Figure 3.7C). In contrast, the low resolution PA image of blood only group indicated that neither labeled cancer cells nor blood cells were present and 8 μm pores did not generate PA signal (Figure 3.7D and 3.7E).

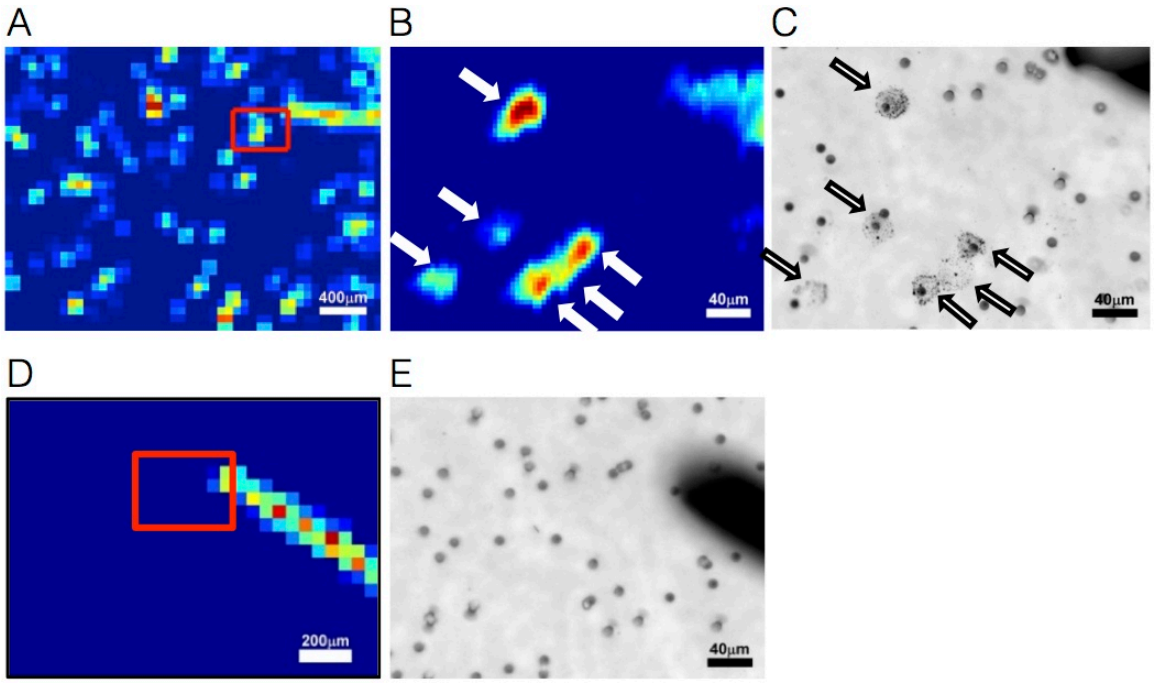

Figure 3.7 Photoacoustic and bright-field images of an enriched sample containing spiked cancer cells in whole blood (A – C) and an enriched sample containing whole blood only (D – E). (A) Low resolution PA images. (B) High resolution PA image and (C) bright-field image from the open red box in (A). (D) Low resolution PA images. (E) Bright-field image from the open red box in (D). Bright-field optical image co-registers with the photoacoustic image using a marker at the top right corner. The black dots in the optical image are membrane pores. The arrows in (B) and (C) show the labeled cancer cells in the photoacoustic and the optical images.

Although PA imaging alone can easily enumerate CTCs from blood cells, cases of high number of cancer cells or circulating tumor microemboli (multicellular aggregates or clusters of tumor cells) make accurate quantification difficult. This deficiency can be overcome by the combination of the PA imaging with optical imaging, thus the co-registration of images facilitates characterization and enumeration of CTCs. Furthermore, the sensitivity of PA imaging primarily depends on the nanoparticle labeling specificity of the targeted moiety. This detection method may compromise its efficiency due to the

tumor heterogeneity. Therefore, the introduction of a cocktail of nanoclusters against multiple biomarkers may prove to be essential for accurate CTC screening.

3.4 CONCLUSIONS

Sensitive and quantitative assessment of changes in circulating tumor cells CTCs help in cancer prognosis and in the evaluation of therapeutics efficacy. However, extremely low occurrence of CTCs in the peripheral blood (approximately one to few CTCs per billion blood cells) and potential changes in molecular biomarkers during the process of epithelial to mesenchymal transition create technical hurdles to the enrichment and enumeration CTCs. Recently, efforts have been directed toward development of antibody-capture assays based on the expression of the common biomarker - the epithelial cell adhesion molecule (EpCAM) of epithelium-derived cancer cells. Despite some promising results, the assays relying on EpCAM capture have shown inconsistent sensitivity in clinical settings and often fail to detect CTCs in patients with metastatic cancer. We have addressed this problem by the development of an assay based on hybrid magnetic/plasmonic nanocarriers and a microfluidic channel. In this assay cancer cells are specifically targeted by antibody-conjugated magnetic nanocarriers and are separated from normal blood cells by a magnetic force in a microfluidic chamber. Subsequently, immunofluorescence staining is used to differentiate CTCs from normal blood cells. We demonstrated in cell models of colon, breast and skin cancers that this platform can be easily adapted to a variety of biomarkers, targeting both surface receptor molecules and intracellular biomarkers of epithelial-derived cancer cells. Experiments in whole blood showed capture efficiency greater than 90% when two cancer biomarkers are used for cell capture. Thus, the combination of immunotargeted magnetic nanocarriers with microfluidics provides an important platform that can improve the effectiveness of

current CTC assays by overcoming the problem of heterogeneity of tumor cells in the circulation. In addition, we explored the feasibility of PA imaging to detect CTCs in whole blood. We demonstrated excellent detection sensitivity delineating the distribution of hybrid nanoclusters targeting the cancer cells on a porous membrane. The work paves the way for a novel CTC detection approach which utilizes immunotargeted magneto-plasmonic nanoclusters for a simultaneous magnetic capture and PA detection of CTCs. Thus, the post-processing steps can be minimized to prevent cell loss and a quick CTC readout can be established for better determination of the patient prognosis and assess tumor sensitivity to anticancer therapy.

3.5 REFERENCES

1. Meng, S.; Tripathy, D.; Shete, S.; Ashfaq, R.; Saboorian, H.; Haley, B.; Frenkel, E.; Euhus, D.; Leitch, M.; Osborne, C.; Clifford, E.; Perkins, S.; Beitsch, P.; Khan, A.; Morrison, L.; Herlyn, D.; Terstappen, L. W.; Lane, N.; Wang, J.; Uhr, J., uPAR and HER-2 gene status in individual breast cancer cells from blood and tissues. *Proceedings of the National Academy of Sciences of the United States of America* **2006**, 103, 17361-17365.

2. Zhang, L.; Farrell, J. J.; Zhou, H.; Elashoff, D.; Akin, D.; Park, N. H.; Chia, D.; Wong, D. T., Salivary Transcriptomic Biomarkers for Detection of Resectable Pancreatic Cancer. *Gastroenterology* **2010**, 138, 949-957.

3. Laxman, B.; Morris, D. S.; Yu, J.; Siddiqui, J.; Cao, J.; Mehra, R.; Lonigro, R. J.; Tsodikov, A.; Wei, J. T.; Tomlins, S. A.; Chinnaiyan, A. M., A first-generation multiplex biomarker analysis of urine for the early detection of prostate cancer. *Cancer Research* **2008**, 68, 645-649.

4. Cristofanilli, M.; Budd, G. T.; Ellis, M. J.; Stopeck, A.; Matera, J.; Miller, M. C.; Reuben, J. M.; Doyle, G. V.; Allard, W. J.; Terstappen, L. W.; Hayes, D. F., Circulating tumor cells, disease progression, and survival in metastatic breast cancer. *New England Journal of Medicine* **2004**, 351, 781-791.

5. Cristofanilli, M.; Hayes, D. F.; Budd, G. T.; Ellis, M. J.; Stopeck, A.; Reuben, J. M.; Doyle, G. V.; Matera, J.; Allard, W. J.; Miller, M. C.; Fritsche, H. A.; Hortobagyi, G. N.; Terstappen, L. W., Circulating tumor cells: a novel prognostic factor for newly diagnosed metastatic breast cancer. *Journal of Clinical Oncology* **2005**, 23, 1420-1430.

6. Coumans, F. A.; Doggen, C. J.; Attard, G.; de Bono, J. S.; Terstappen, L. W., All circulating EpCAM+CK+CD45- objects predict overall survival in castration-resistant prostate cancer. *Annals of Oncology* **2010**, 21, 1851-1857.

7. Gasparovic, C.; Matwiyoff, N. A., The magnetic properties and water dynamics of the red blood cell: a study by proton-NMR lineshape analysis. *Magn Reson Med* **1992**, 26, 274-299.

8. Riethdorf, S.; Fritsche, H.; Muller, V.; Rau, T.; Schindlbeck, C.; Rack, B.; Janni, W.; Coith, C.; Beck, K.; Janicke, F.; Jackson, S.; Gornet, T.; Cristofanilli, M.; Pantel, K., Detection of circulating tumor cells in peripheral blood of patients with metastatic breast cancer: a validation study of the CellSearch system. *Clinical Cancer Research* **2007**, 13, 920-928.

9. Hoshino, K.; Huang, Y. Y.; Lane, N.; Huebschman, M.; Uhr, J. W.; Frenkel, E. P.; Zhang, X., Microchip-based immunomagnetic detection of circulating tumor cells. *Lab on a Chip* **2011**, 11, 3449-3457.

10. Aktas, B.; Tewes, M.; Fehm, T.; Hauch, S.; Kimmig, R.; Kasimir-Bauer, S., Stem cell and epithelial-mesenchymal transition markers are frequently overexpressed in circulating tumor cells of metastatic breast cancer patients. *Breast Cancer Research and Treatment* **2009**, 11, R46.

11. Sieuwerts, A. M.; Kraan, J.; Bolt, J.; van der Spoel, P.; Elstrodt, F.; Schutte, M.; Martens, J. W.; Gratama, J. W.; Sleijfer, S.; Foekens, J. A., Anti-epithelial cell adhesion molecule antibodies and the detection of circulating normal-like breast tumor cells. *Journal of the National Cancer Institute (1988)* **2009**, 101, 61-66.

12. Mostert, B.; Kraan, J.; Bolt-de Vries, J.; van der Spoel, P.; Sieuwerts, A. M.; Schutte, M.; Timmermans, A. M.; Foekens, R.; Martens, J. W.; Gratama, J. W.; Foekens, J. A.; Sleijfer, S., Detection of circulating tumor cells in breast cancer may improve through enrichment with anti-CD146. *Breast Cancer Research and Treatment* **2011**, 127, 33-41.

13. Lee, H.; Lee, E.; Kim do, K.; Jang, N. K.; Jeong, Y. Y.; Jon, S., Antibiofouling polymer-coated superparamagnetic iron oxide nanoparticles as potential magnetic resonance contrast agents for in vivo cancer imaging. *Journal of the American Chemical Society* **2006**, 128, 7383-7389.

14. Farokhzad, O. C.; Langer, R., Impact of nanotechnology on drug delivery. *ACS Nano* **2009**, 3, 16-20.

15. Barcikowski, S.; Compagnini, G., Advanced nanoparticle generation and excitation by lasers in liquids. *Physical chemistry chemical physics: PCCP* **2013**, 15, 3022-3026.

16. Bigall, N. C.; Parak, W. J.; Dorfs, D., Fluorescent, magnetic and plasmonic-Hybrid multifunctional colloidal nano objects. *Nano Today* **2012**, 7, 282-296.

17. Larson, T. A.; Bankson, J.; Aaron, J.; Sokolov, K., Hybrid plasmonic magnetic nanoparticles as molecular specific agents for MRI/optical imaging and photothermal therapy of cancer cells. *Nanotechnology* **2007**, 18, 325101.

18. Song, H.-M.; Wei, Q.; Ong, Q. K.; Wei, A., Plasmon-Resonant Nanoparticles and Nanostars with Magnetic Cores: Synthesis and Magnetomotive Imaging. *ACS Nano* **2010**, 4, 5163-5173.

19. Wei, Q.; Song, H.-M.; Leonov, A. P.; Hale, J. A.; Oh, D.; Ong, Q. K.; Ritchie, K.; Wei, A., Gyromagnetic Imaging: Dynamic Optical Contrast Using Gold Nanostars with Magnetic Cores. *JACS* **2009**, 131, 9728-9734.

20. Kumar, S.; Aaron, J.; Sokolov, K. V., Directional conjugation of antibodies to nanoparticles for synthesis of multiplexed optical contrast agents with both delivery and targeting moieties. *Nature Protocols* **2008**, 3, 314-320.

21. Kumar, S.; Harrison, N.; Richards-Kortum, R.; Sokolov, K., Plasmonic Nanosensors for Imaging Intracellular Biomarkers in Live Cells. *Nano Letters* **2007**, 7, 1338-1343.

22. Huang, K.; Ma, H.; Liu, J.; Huo, S.; Kumar, A.; Wei, T.; Zhang, X.; Jin, S.; Gan, Y.; Wang, P. C.; He, S.; Zhang, X.; Liang, X. J., Size-dependent localization and penetration of ultrasmall gold nanoparticles in cancer cells, multicellular spheroids, and tumors in vivo. *ACS Nano* **2012**, 6, 4483-4493.

23. Anker, J. N.; Hall, W. P.; Lyandres, O.; Shah, N. C.; Zhao, J.; Van Duyne, R. P., Biosensing with plasmonic nanosensors. *Nature Materials* **2008**, 7, 442-453.

24. Wu, C.-H.; Huang, Y.-Y.; Chen, P.; Hoshino, K.; Liu, H.; Frenkel, E. P.; Zhang, J. X. J.; Sokolov, K. V., Versatile Immunomagnetic Nanocarrier Platform for Capturing Cancer Cells. *ACS nano* **2013**, 7, 8816-8823.

25. Hoshino, K.; Chen, P.; Huang, Y.-Y.; Zhang, X., Computational Analysis of Microfluidic Immunomagnetic Rare Cell Separation from a Particulate Blood Flow. *Analytical Chemistry* **2012**, 84, 4292-4299.

26. Nagrath, S.; Sequist, L. V.; Maheswaran, S.; Bell, D. W.; Irimia, D.; Ulkus, L.; Smith, M. R.; Kwak, E. L.; Digumarthy, S.; Muzikansky, A.; Ryan, P.; Balis, U. J.; Tompkins, R. G.; Haber, D. A.; Toner, M., Isolation of rare circulating tumour cells in cancer patients by microchip technology. *Nature* **2007**, 450, 1235-1239.

27. Punnoose, E. A.; Atwal, S. K.; Spoerke, J. M.; Savage, H.; Pandita, A.; Yeh, R. F.; Pirzkall, A.; Fine, B. M.; Amler, L. C.; Chen, D. S.; Lackner, M. R., Molecular biomarker analyses using circulating tumor cells. *PLoS One* **2010**, 5, e12517.

28. Yoon, S. J.; Mallidi, S.; Tam, J. M.; Tam, J. O.; Murthy, A.; Johnston, K. P.; Sokolov, K. V.; Emelianov, S. Y., Utility of biodegradable plasmonic nanoclusters in photoacoustic imaging. *Opt Lett* **2010**, 35, 3751-3753.

29. Cook, J. R.; Bouchard, R. R.; Emelianov, S. Y., Tissue-mimicking phantoms for photoacoustic and ultrasonic imaging. *Biomed Opt Express* **2011**, 2, 3193-3206.

30. Cook, J. R.; Frey, W.; Emelianov, S., Quantitative photoacoustic imaging of nanoparticles in cells and tissues. *ACS Nano* **2013**, 7, 1272-1280.

31. Emelianov, S. Y.; Li, P. C.; O'Donnell, M., Photoacoustics for molecular imaging and therapy. *Phys Today* **2009**, 62, 34-39.

Chapter 4: Development of Magnetically Guided Cell Delivery Methods for Adoptive Cell Therapy of Cancer

4.1 INTRODUCTION

Adoptive cell therapy (ACT) has emerged as an effective treatment for cancer patients, especially for metastatic melanoma.[1] ACT is a form of transfusion therapy which contains the infusion of selected T cells, often along with vaccines or growth factors to augment the impact *in vivo* of the transferred cells.[2] Anti-tumor lymphocytes are selected with appropriate effector functions and subsequently expanded *ex vivo* before reinfusion. Since effective therapeutic effect highly depends on the presence of anti-tumor lymphocytes at the tumor region, a very large cell number ($>10^{10}$ cells) per dose is usually demanded to seek out and kill cancer cell *in vivo*.[3] However, recent clinical studies demonstrate that inefficient homing of T cells becomes a rate-limiting step in anti-tumor efficacy, thus causing approximately half of metastatic melanoma patients fail to respond to the treatment.[4-6] Indeed, analysis of the transferred cells showed a lack of persistence *in vivo*. Less than 0.1% of the cells remained in the circulation in one week after infusion.[1] In fact, the majority of infused T cells have been found in lung, liver, and spleen, whereas less than 1% of the total transferred cells homed to tumor.[5, 7]

Different strategies have been employed to improve the homing efficiency of ACT. For example, introduction of an immunodepleting preparative regimen given before ACT resulted in a better T cell-to-target cell ratio at the tumor site, because the lymphodepletion can eliminate T regulatory cells and lymphocytes which usually compete with infused cells for homeostatic cytokines.[8] In addition, normal T cells can be genetically encoded with specific T-cell receptors, such as chimeric antigen receptors (CAR), which enhance the avidity of T cells for tumor-specific antigens and thereby improve anti-tumor efficacy.[9] Furthermore, chemokine signatures within tumor

microenvironment can be adjusted by genetically modified tumor-specific T cells.[10] Cells with corresponding chemokine receptors can migrate along with a chemokine gradient and initiate T cell-mediated antitumor immune responses.[11] Despite the promising results emerging from these improvements, several problems still need to be addressed. Recent studies have reported on-target toxicity to normal tissue following ACT of CAR-modified T cells in patients, thus eliciting the safety concern for this type of therapy.[12] Another major hurdle of ACT is the lengthy isolation and expansion process (4-16 weeks) to produce a large number of antigen-specific T cells. It may not be feasible for patients with progressive disease.[13] These problems prompt us to develop a magnetic-guided cell delivery approach with the expectation to enhance T cell homing efficiency (Figure 4.1), thus diminishing the cell dose and shortening laboratory preparation time.

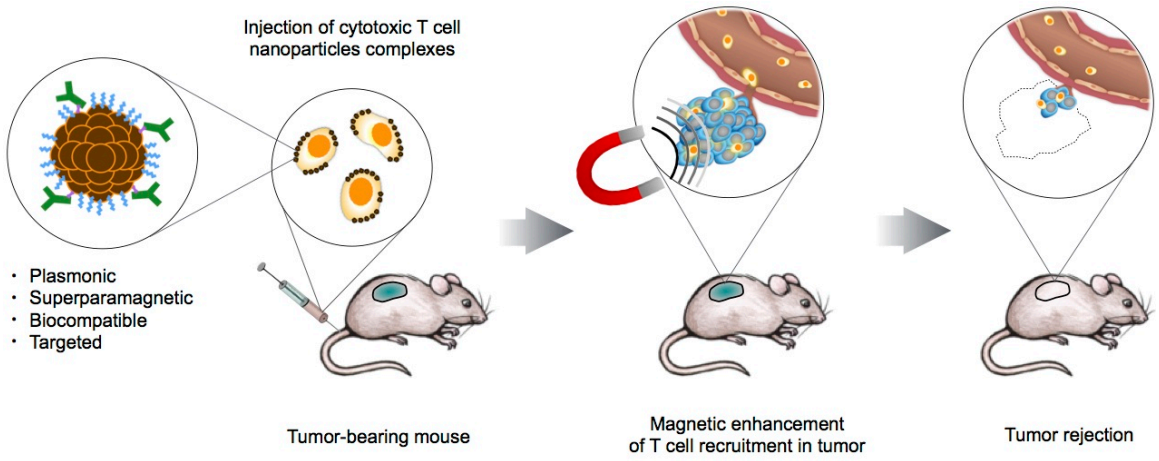

Figure 4.1 Conceptual cartoon of the magnet-guided delivery of cytotoxic T cells for adoptive cell therapy of cancer.

Magnetic nanoparticles have been received much attention due to their high biocompatibility and versatile applications for human health.[14] Cells labeled with magnetic nanoparticles are being explored for a range of applications, including magnetic resonance imaging [15], magnetic drug delivery[16, 17], and stem cell-based therapeutics.[18] In particular, magnetic particle-assisted positioning of human cells has been demonstrated to repair injured blood vessels,[19] heart,[20] and articular cartilage.[21] This strategy appears to be highly interesting for ACT because magnet-oriented positioning enables systemic delivery of the T cells aiming at tumor tissues. Further release of transferred cells from the tumor site is feasible by removing external magnetic stimuli. In addition, iron oxide-based magnetic nanoparticles offer unique properties for cell tracking and monitoring by MRI, thereby allowing us to delineate infused T cell survival, response and migration *in vivo* which has been a lack of deep understanding.[22]

Here, we tested the concept of nanoparticle-mediated cell labeling for controllable immune cell positioning. We engineered immune cells with magnetic properties by using nanoparticle platform derived from Chapter 2. Two cell labeling strategies were implemented: (1) cellular internalization of magnetic nanoclusters (described in Chapter 4.2) and (2) selective cell surface labeling by immunotargeted magneto-plasmonic nanoclusters (described in Chapter 4.3). The first strategy involved synthesis of iron oxide nanoclusters with particle surface modification to facilitate the cellular uptake and increase the biocompatibility. A macrophage cell line was loaded with biocompatible iron oxide nanoclusters and the response of engineered macrophages to magnetic stimuli was investigated. A series of feasibility studies for the magnet-assisted cell positioning was explored under simulated physiological conditions *in vitro*. The second strategy utilized immunotargeted magneto-plasmonic nanoclusters to label and enrich a subset of immune cells, cytotoxic T lymphocytes (CTL), which can kill cancer cells directly.[23] The viability

and *in vitro* magnetic response of CTL labeled with hybrid nanoclusters were evaluated. These results pave the way for an *in vivo* pilot study to investigate whether the magnet-guided cell delivery method can enhance T cell recruitment in tumor.

4.2 The Method Based on Cellular Internalization of Magnetic Nanoclusters

4.2.1 Materials and Methods

Synthesis and characterization of iron oxide nanoclusters

The 5 nm iron oxide nanoparticles were prepared according to a previously published protocol.[24] Briefly, 1 mM iron(III) acetylacetonate was mixed in 10 mL phenyl ether, followed by addition of 3 mM oleic acid, 2 mM oleylamine, and 3 mM 1,2-hexadecanediol (Fisher Scientific). The mixture was stirred vigorously, heated to 260 °C, and refluxed for 1 h yielding a suspension of highly uniform 5 nm Fe_3O_4 nanoparticles.

To synthesize nanoclusters, one volume of a suspension of the 5 nm Fe_3O_4 particles (5 mg/mL by total weight) in hexane was mixed with ten volumes of deionized water containing an anionic surfactant – sodium dodecyl sulfate (SDS, Sigma Aldrich) at 2.8 mg/mL.[25] The mixture was placed in a sonicator bath (Model 1510, Branson) for 2 h. After starting the sonication, the solution was shaken by hand gently to facilitate mixing between the phase containing primary hybrid nanoparticles and the bottom aqueous phase. The solution was heated in a water bath at 80 °C for 10 min to remove hexane. Nanoclusters with 130 nm in diameter were separated using the following sequence of centrifugation steps: (1) large nanoclusters, i.e. > 180 nm, were removed by centrifugation at 100 ×g for 30 min and the sediment was discarded; (2) the supernatant from step 1 was centrifuged at 400 ×g for 30 min and the sediment was collected and resuspended in 0.2 mM Na Citrate (Fisher Scientific) with 10 min sonication.

To coat magnetic nanoclusters with poly-l-lysine (PLL), the 130 nm magnetic nanocluster (1 mL at 0.15 mg Fe/mL) was spun down (830 ×g for 10 min), removed supernatant, and resuspended in 1 mg/mL PLL-FITC labeled (Sigma Aldrich). After 1 h sonication, the nanoclusters were incubated in oven at 70°C for 1 h. The solution was cooled down to room temperature, spun down again to remove excess PLL, and finally resuspended in PBS. The magnetic nanoclusters were characterized for morphology, size distribution, and charge using transmission electron microscopy (FEI TECNAI G2 F20 X-TWIN TEM at 80 keV.), dynamic light scattering (DLS, Beckman Coulter), and zeta potential measurements (Beckman Coulter), respectively.

Cellular uptake of magnetic nanoclusters

Murine macrophage cell line (J744.A1) were purchased from ATCC and grown in Dulbecco's Modified Eagle Medium (Life Technologies) supplemented with 5 % fetal bovine serum (FBS, Hyclone). When confluent, the sterile PLL-coated nanoclusters (100 μL at 10 μg/mL) were added to the cell culture medium. After incubation overnight, the cells were washed three times with PBS to remove excess magnetic nanoclusters. The dark-field and fluorescence images were taken using 20×, 0.5-NA, Leica DM6000 upright microscope.

Cell viability assay

J744.A1 cells (5×10^3 cells) were grown in 96-well and incubated with sterile PLL-coated magnet nanoclusters at two different concentration, 8.4 and 34.4 μg/mL for 24 h at 37°C. Afterwards, the cells incubated with magnetic nanoclusters and the untreated cell control were then washed twice with PBS and mixed with 100 μL MTS reagent, a mixture of MTS (3-(4,5-dimethylthiazol-2-yl)-5-(3-carboxymethoxyphenyl)-2-(4-sulfophenyl)-2H-tetrazolium) (0.32 mg/mL, Promega) and PMS (phenazine methosulfate) (7.3 μg/mL, Sigma Aldrich) in cell culture media. Absorbance at 490 nm

was taken 3 h after the addition of the MTS reagent using a BioTek Synergy HT micro-titer plate spectrophotometer; the absorbance is proportional to the number of metabolically active live cells in a sample.

In vitro magnetic attraction assay

First, we investigated whether internalized magnetic nanoclusters can respond to an external magnetic field. J744.A1 cells (5×10^5 cells) were grown on a coverslip and labeled with PLL-coated magnetic nanoclusters. After 24 h incubation at 37°C, the excess nanoclusters were washed out. A magnet (1 × 1 × 1 cm, NdFeB, K&J Magnetics) was positioned at one corner of the coverslip for 1 min, followed by imaging using 20×, 0.5-NA dark-field and bright-field objective under Leica DM6000 upright microscope.

Furthermore, we seeded magnetic nanocluster-loaded J744.A1 into a collagen I phantom as previously described.[26] The phantom was placed in a 6-well culture dish and undisturbed for 1 h for cell adhesion. A magnet (1 × 1 × 1 cm, NdFeB, K&J Magnetics) was then introduced and located next to the phantom. A series of bright-field pictures from the region of interest (*ca*. 5 mm from the magnet) was recorded as a function of time using an inverted bright-field microscopy (Olympus DP71).

To test the magnetic trapping in a flow condition, the magnetic nanocluster-loaded J744.A1 cell suspension was loaded into a reservoir that was connected to a tube (1/32” inner diameter). The other side of the tube was connected to a syringe pump to control flow rate at 10 mL/min. A magnet (1 × 1 × 1 cm, NdFeB, K&J Magnetics) was then placed underneath the tube, followed by recording a video with the presence of the magnet using an inverted bright-field microscopy (Olympus DP71).

4.2.2 Results and Discussion

Iron oxide nanoclusters

The synthetic scheme of PLL coated-Fe_3O_4 nanoclusters was shown in Figure 4.2A. A microemulsion approach was used to self-assemble 5 nm iron oxide seeds (Figure 4.2B) into nanoclusters (Figure 4.2C). The nanocluster formation utilizes a negatively charged amphiphilic surfactants SDS with a hydrophobic moiety to hold together the primary particles inside the cluster, through hydrophobic van der Waals interactions, and a polar group to provide aqueous solubility. The deposition of positively charged PLL layer onto the nanoclusters was then carried out by electrostatic interaction.[27] PLL is a polycationic polymer with great biocompatibility and solubility in water that has been used as carriers for gene delivery and coating materials for various purposes.[28] It contains plentiful active amino groups and a flexible molecular backbone which makes chemical modification easily.[29] Furthermore, the PLL coating has been shown to enhance cellular uptake of particles.[30] Thus, we coated our nanoclusters with PLL to facilitate cellular internalization of magnetic nanoclusters. The zeta potential of as-synthesized nanoclusters capped by SDS is −14.93 ± 0.63 mV. After coating nanoclusters with PLL, the zeta potential shifts to positive charge, +17.69 ± 0.44 mV. The hydrodynamic diameter of nanoclusters measured by dynamic light scattering indicates an increase of 33 nm (137.5 nm to 170.5 nm) after coating with PLL. Therefore, the change of surface charge and the increase of hydrodynamic diameter of the nanoclusters suggest the successful surface modification.

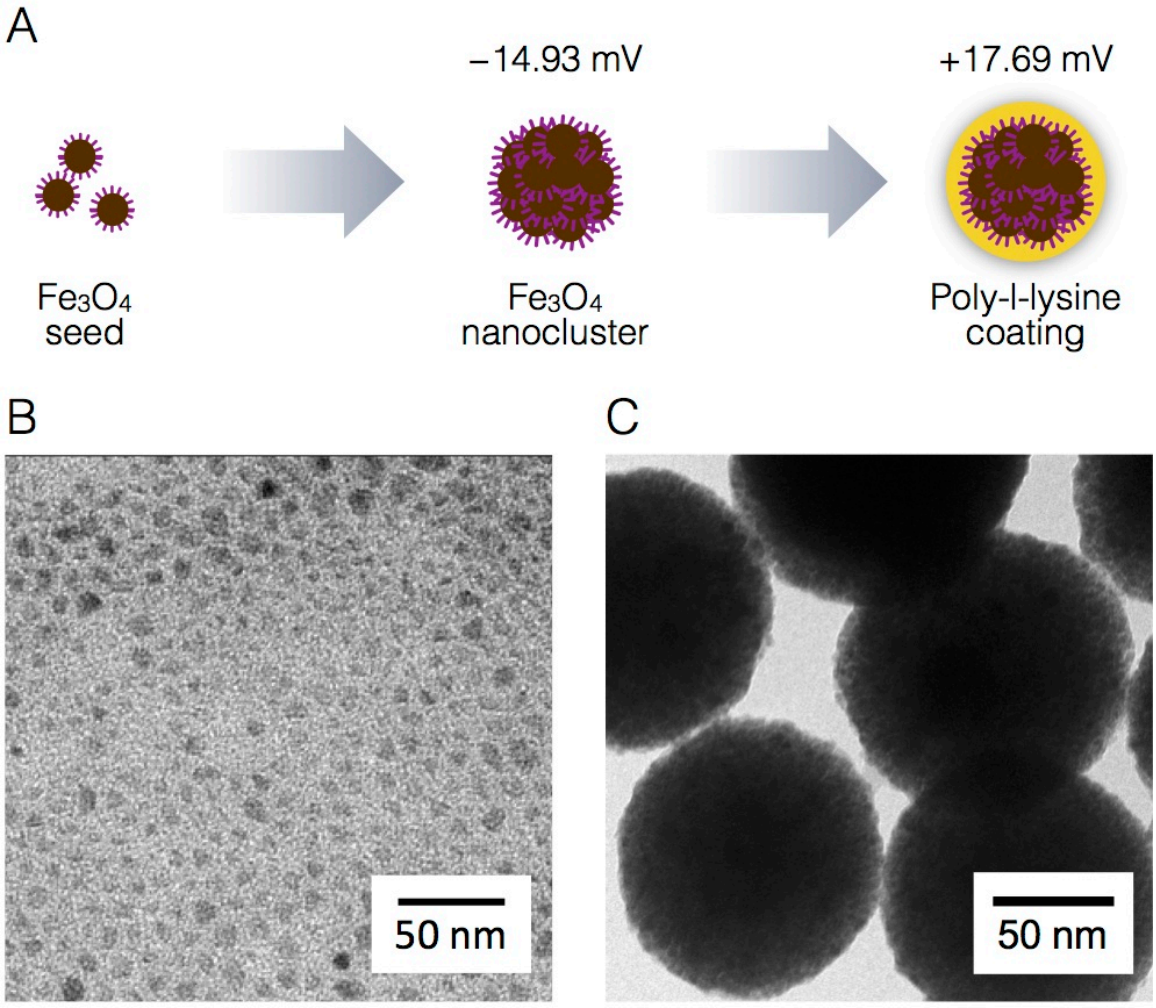

Figure 4.2 Iron oxide nanoclusters synthesis and characterization. (A) Synthetic scheme of poly-l-lysine coated magnetic nanoclusters. The charge indicates the zeta potential changes before and after coating with poly-l-lysine. TEM images of 5 nm iron oxide seeds (B) and nanoclusters with a diameter *ca*. 130 nm (C).

Cellular internalization of magnetic nanoclusters

To evaluate the cellular internalization of magnetic nanoclusters, we co-cultured PLL-FITC-modified iron oxide nanoclusters with a macrophage cell line, J744.A1. The nanoclusters were found to be internalized after 4 h incubation as determined by bright-field, dark-field, and fluorescence imaging (Figure 4.3). The brown color in the bright-

field image indicates the presence of nanoparticles, whereas untreated cell presents nearly transparent color (Figure 4.3). In dark-field images, a bright yellow color shows the uptake of the nanoclusters by macrophages, whereas a gray-bluish color corresponds to the endogenous scattering of the untreated cells. The effective cellular uptake can be further evidenced by the co-registration with the fluorescent images and the bright-field and dark-field optical images (Figure 4.3). Indeed, macrophages are capable of ingesting particular substances by phagocytosis, such as bacteria, damaged and dead cells, and foreign particles.[31] In our case, positive surface charge from the PLL modification further facilitated cellular uptake.

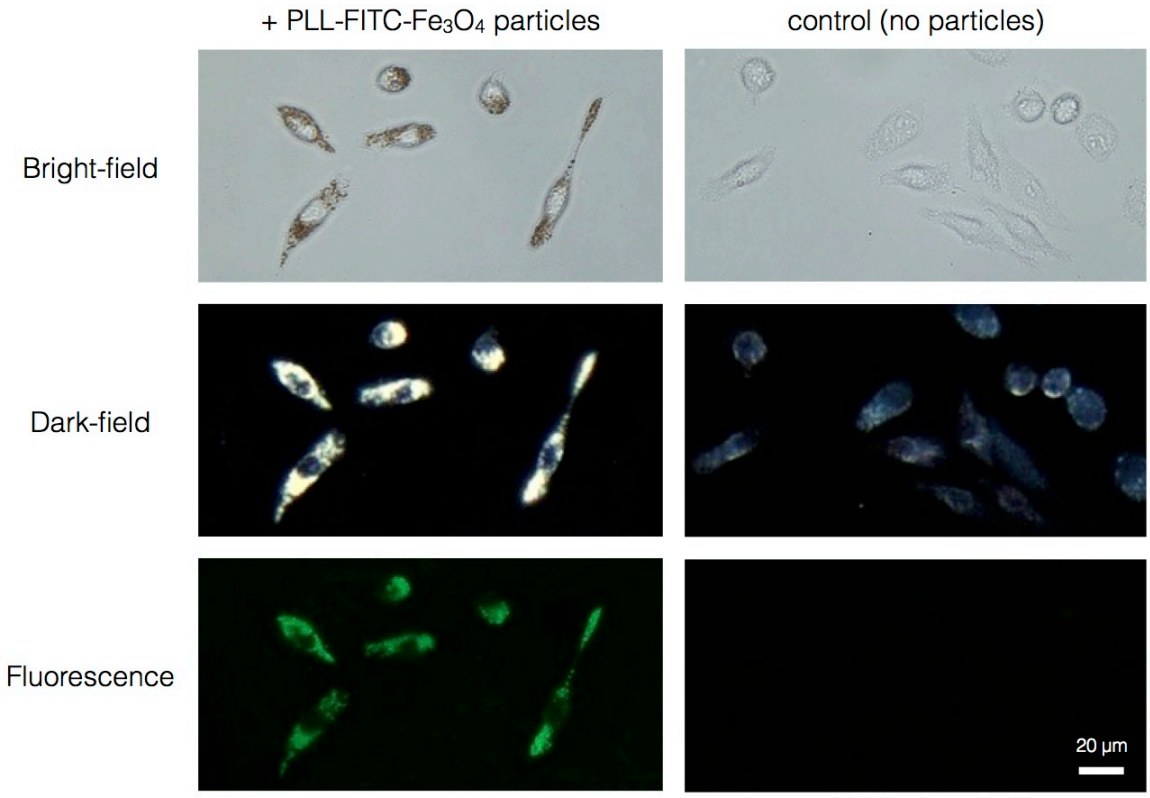

Figure 4.3 Images of macrophages labeled with poly-l-lysine-FITC coated iron oxide nanoclusters. Columns correspond to macrophages without and with particle loading. Rows show results obtained with (from top to bottom): bright-field, dark-field, and fluorescence microscope.

Biocompatibility of magnetic nanoclusters

Next, we investigated whether intracellular localization of the magnetic nanoclusters induced cytotoxicity. The viability assay was carried out by exposing macrophage cells with the nanoclusters for 24 h. At the concentration of 8.6 μg/mL, cell viability was similar to the untreated macrophages, suggesting high biocompatibility of the nanoclusters at this level (Figure 4.4). In the case loading with high concentration, 34.4 μg/mL, cell viability kept over 70%. Indeed, several studies have also shown that labeling cells with Fe_3O_4 nanoparticles did not affect the viability, proliferation, and differentiation capacity of cells.[15, 18, 32] Thus, we used the magnetic nanoclusters at a concentration of 10 μg/mL which is not cytotoxic and shows high cellular internalization efficiency (Figure 4.3).

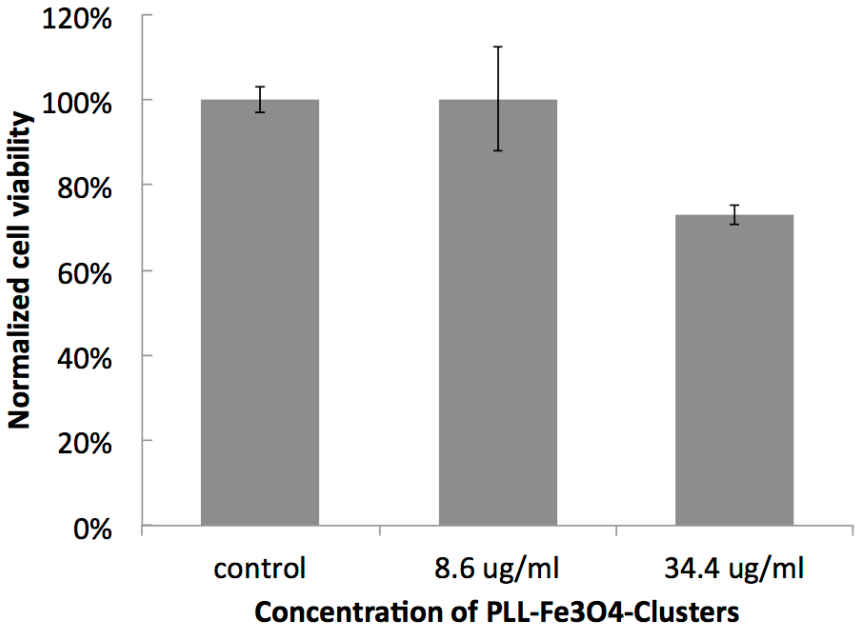

Figure 4.4 Viability assay of poly-l-lysine-coated iron oxide nanoclusters with macrophages. Cells were incubated with two different concentrations of the nanoclusters for 24 h followed by performing MTT cell viability assay.

Magnetic attraction of nanocluster-labeled macrophages under static conditions

Trafficking cells to a desirable region can be achieved in many ways, such as introducing a chemoattractants gradient or manipulating magnetic cells with a magnetic field.[16, 33] To elicit a significant therapeutic effect, functional cells should be trafficked to a region of interest in sufficient numbers. By yielding the cells with magnetic properties, cells can be presumably induced with preferential movement by applying and adjusting an external magnetic field. Thus, we conducted a series of experiments *in vitro* to evaluate the magnetic response of magnetic nanocluster-labeled cells. First, the macrophages were grown on a glass coverslip and labeled by the magnetic nanoclusters. A magnetic gradient field generated by a permanent magnet was then introduced underneath the coverslip (Figure 4.5A and 4.5B). The nanoclusters inside the cells close to the magnet (*ca*. 1.4 mm with 0.4 T) experienced the strong magnetic field and realigned its distribution accordingly (Figure 4.5C and 4.5D). In contrast, the nanoclusters away from the magnet (*ca*. 14 mm with 0.03 T) showed no response to the magnet (Figure 4.5E and 4.5F).

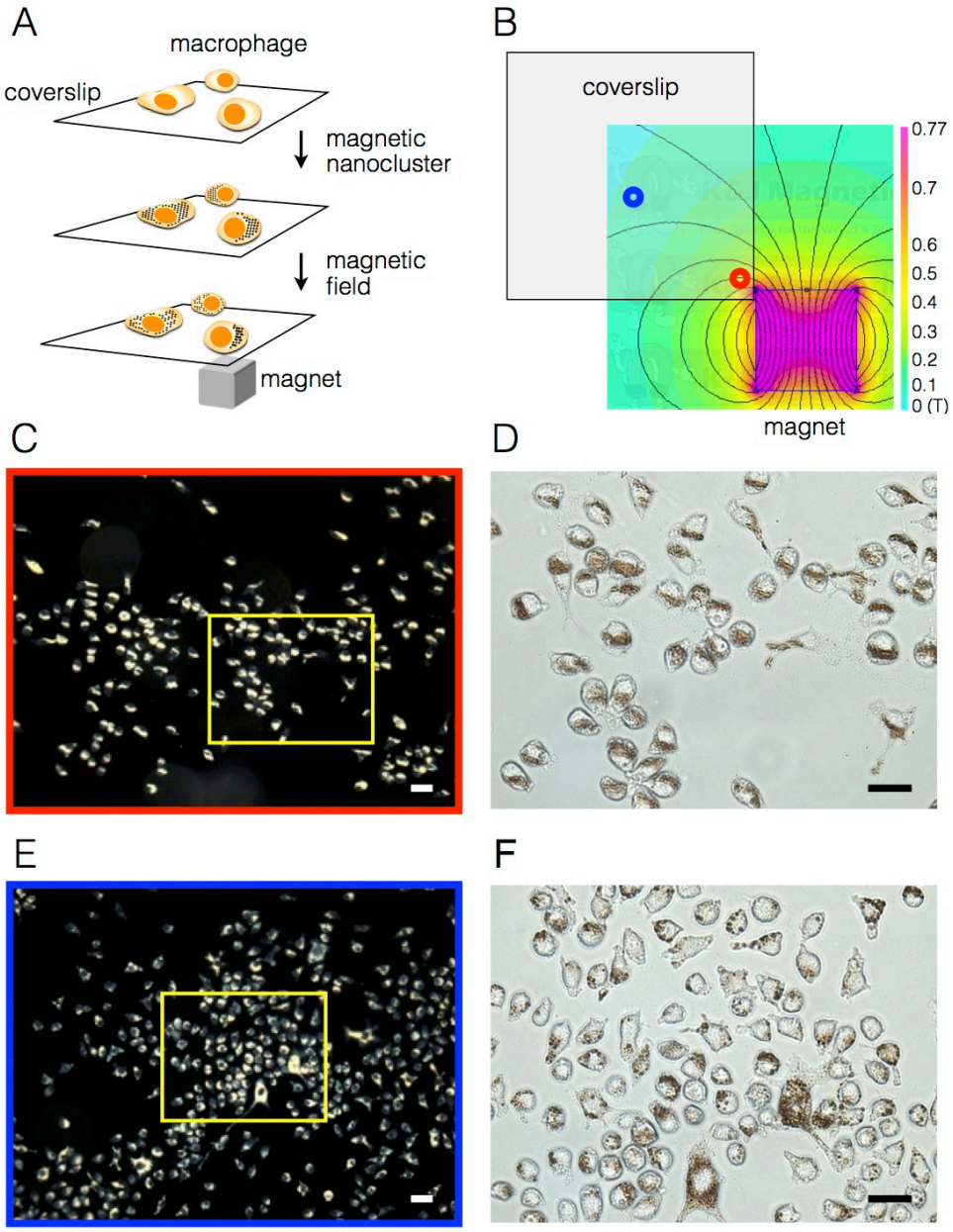

Figure 4.5 Magnet attract assay of magnet particle-loaded macrophages. (A) Experimental procedure. (B) Magnetic field distribution under the sample area. (C and E) Dark-field images were taken from the red circle (1.4 mm away from the magnet) and blue (14 mm away from the magnet), respectively. (D and F) Bright-field images were taken from the open yellow square from C and E, respectively.

We speculate that the realignment of magnetic nanoclusters can provide a source of force for attracting cells under a magnetic field. Therefore, we further embedded the magnetic nanocluster-labeled macrophages into a tissue-mimicking phantom. A magnet was applied externally next to the phantom (Figure 4.6A). A series of bright-field pictures from the region of interest (*ca*. 5 mm from the magnet) shows that the cells moved toward the magnet as time evolved (Figure 4.6B). The average speed is 0.46 ± 0.42 μm/min. A quicker movement can be expected when the cells are closer to the magnet. These findings demonstrate the potential to remotely control the engineered cells to specific sites. Even for the targeting site located in deep tissue, cells can possibly migrate under a local magnetic field generated by an implanted ferromagnet.

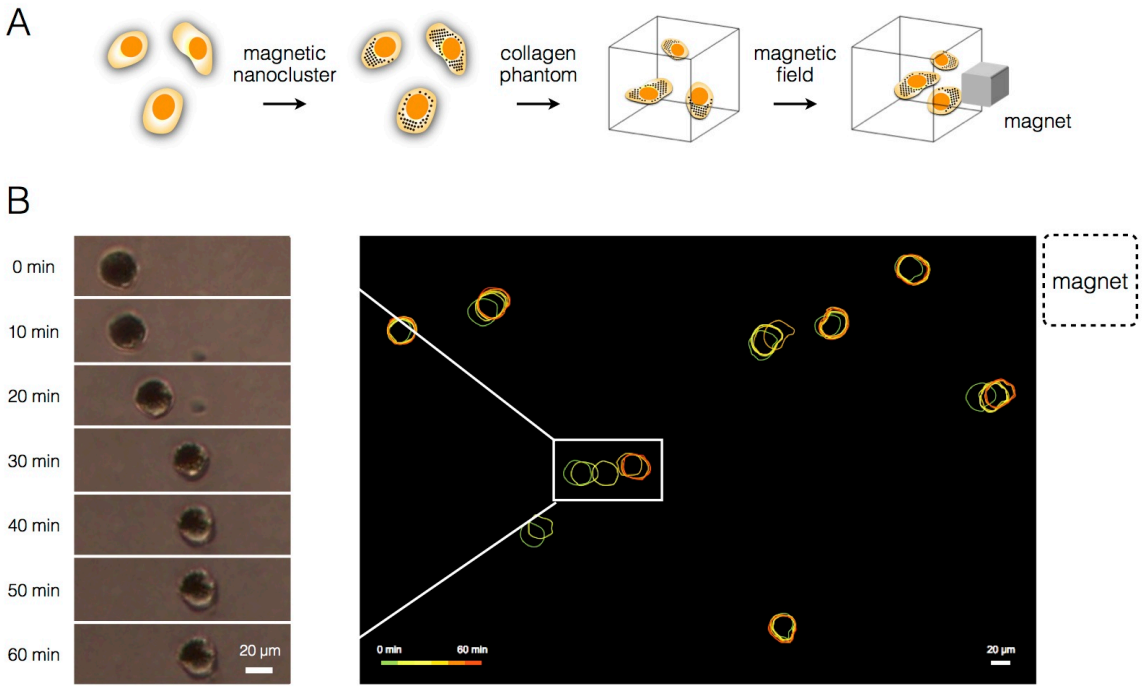

Figure 4.6 Motility assay of magnet particle-loaded macrophages as a function of time. (A) The macrophages were embedded in 3D tissue-mimicking phantom and an external magnet was placed at right-hand side. (B) The images were taken with ten min interval illustrated by the color locus. The average speed of the cell movement is 0.46 ± 0.42 μm/min.

Magnetic attraction of nanocluster-labeled macrophages under flow conditions

In addition to controllable migration, the adhesion of immune cells under flow condition and subsequent extravasation into surrounding tissues play the important step for site-specific targeting. In this assay, the magnetic nanocluster-labeled macrophages were loaded into a tube flowing at 10 mL/min which mimicked their passage through flowing blood vessels (Figure 4.7A).[34] The attraction of the cells was visualized under bright-field microscopy in the presence or absence of a magnetic field. In Figure 4.7B, introduction of the magnet resulted in a significant accumulation of labeled macrophages. In contrast, the labeled macrophages flowed by in the absence of the magnet. The nanocluster-loaded macrophages demonstrated high magnetic force so that they can be

magnetically trapped even at the fast flow condition. Overall, the internalization of magnetic nanoclusters creates efficient positioning of cells and enables their stable engraftment at specific sites. The engineered cells could potentially migrate to inaccessible areas of tumors aided by a magnetic force, which leads to destruction of tumor cells.

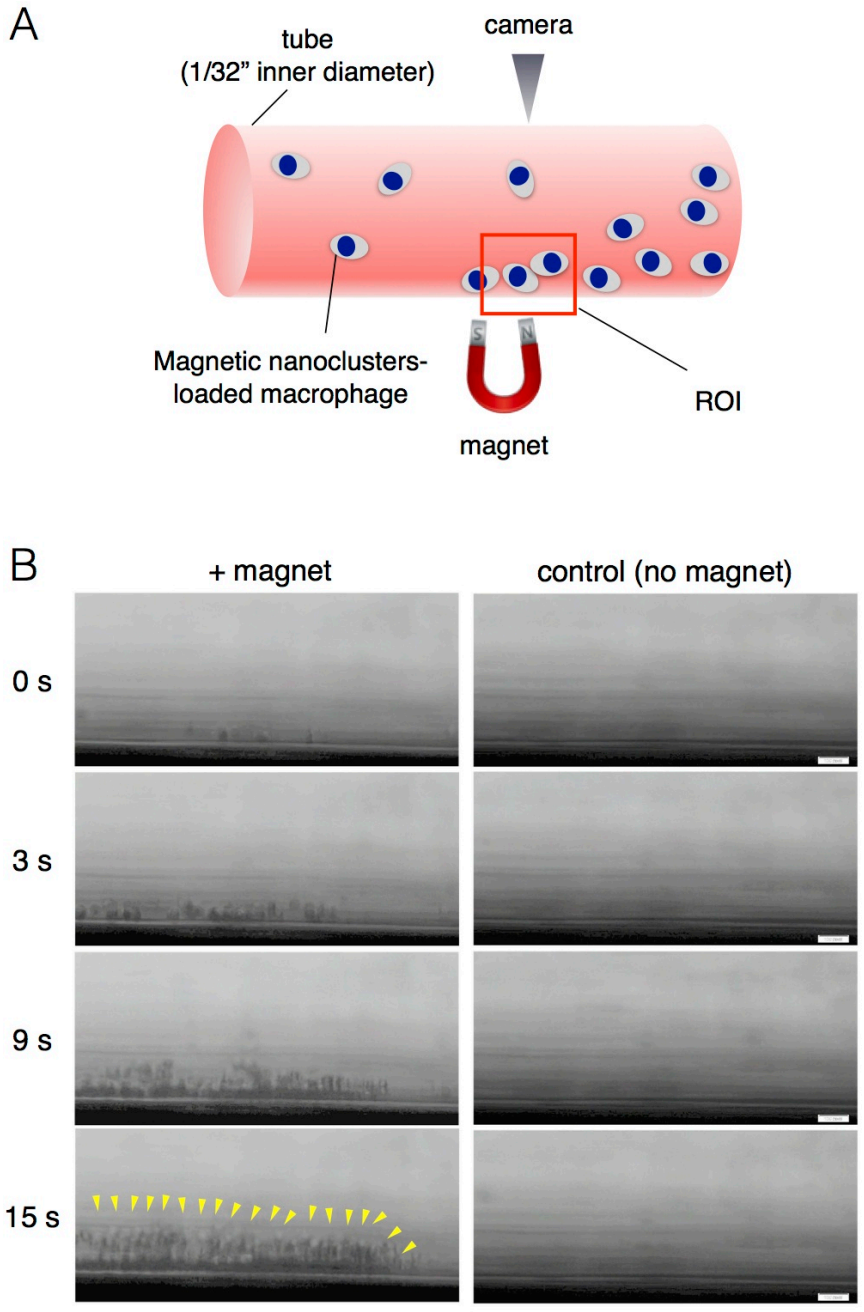

Figure 4.7 Magnetic attraction of nanocluster-labeled macrophages under flow conditions. (A) Schematic cartoon of the experimental setup. (B) Magnetic trapping study with and without the presence of a magnetic field under 10 mL/h flow rate. The yellow arrows indicate the accumulation of cells.

4.3 The Method Based on Selective Cell Surface Labeling by Immunotargeted Hybrid Nanoclusters

4.3.1 Materials and Methods

Synthesis of magneto-plasmonic nanoclusters and antibody conjugation

Hybrid magneto-plasmonic nanoparticles were synthesized in three steps as previously described (Chapter 2). First, 5 nm magnetic core nanoparticles were synthesized using thermal decomposition of $Fe(acac)_3$ (1 mmol, Sigma Aldrich) in the presence of oleic acid (2 mmol, Fisher), oleylamine (2 mmol, Fisher), 1,2-hexadecanediol (5 mmol, Sigma Aldrich), and phenyl ether (10 mL, Sigma Aldrich) at 250 to 260 °C with 1 h reflux. Second, a thin gold shell was then deposited onto the magnetic core nanoparticles. Five mL of as-synthesized magnetic nanoparticle suspension was mixed with gold acetate (1.1 mmol), oleic acid (0.75 mmol), oleylamine (3.0 mmol), 1,2-hexadecanediol (3 mmol), and 15 mL phenyl ether. The reaction was heated up to 180 °C and kept under reflux for 1 h. The resultant 6 nm seed particles were readily dispersed in hexane. Finally, the hybrid magneto-plasmonic nanoparticles were synthesized *via* oil-in-water microemulsion method. One volume of a suspension of the seed particles (5 mg/mL by total weight) in hexane was mixed with ten volumes of deionized water containing sodium dodecyl sulfate (2.8 mg/mL, Sigma Aldrich). After sonication (Model 1510, Branson) for 2 h, the solution was heated in a water bath at 80 °C for 10 min to remove residual hexane. The hybrid magneto-plasmonic nanoparticles with *ca*. 130 nm in diameter was collected by centrifugation at 400 ×g for 30 min and resuspended in 0.2 mM sodium citrate (Sigma Aldrich).

Antibody conjugation to magneto-plasmonic nanoclusters

Alexa Fluor 647 anti-mouse CD8 antibody (Biolegend) was thiolated at the carbohydrate moiety on Fc portion.[35] Briefly, 100 μL of antibody solution (1 mg/mL in

HEPES, pH 7.2) was incubated with 10 μL of 100 mM $NaIO_4$ (Sigma Aldrich) in dark for 30 min at room temperature. The reaction was quenched by 500 μL 1x PBS, followed by mixing with 2 μL of 46.5 mM linker solution (dithiolaromatic PEG6-CONHNH2, SensoPath) for 60 min at room temperature. Afterwards, the purified thiolated antibody solution was recovered by a 10k MWCO centrifuge filter (3,250 ×g for 20 min at 8 °C) and resuspended in 1x PBS. To conjugate antibodies to NP, 1 μL of thiolated antibodies (1 mg/mL) was mixed with 100 μL NP at O.D *ca*. 1.0 for 2 h at room temperature with mild shaking. To passivate the remaining NP surfaces, 10 μL of 10^{-3} M methoxyl polyethylene glycol thiol (5 kDa, SensoPath) was added to the solution with 20 min incubation at room temperature. Finally, the antibody-conjugated NPs were collected by centrifugation at 830 ×g for 3 min and resuspended in 100 μL 1x PBS.

Labeling and magnetic enrichment of CD8+ T cells

A single cell suspension from lymph nodes or spleens was derived from sacrificed mice. First, mouse lymph nodes or spleens were dissected out and washed in chilled PBS. Lymph node or spleen tissue was mechanically teased by clean forceps. A single cell suspension was prepared by passing through a 70 μm sterile filter and washed by 1x PBS through the mesh. The cells were then cultured in RPMI-1640 supplemented with 5% fetal bovine serum, 2 mM L-glutamine and 25 μg/mL Gentamicin (Life Technologies). Before NP labeling, 1 μg of Fc block antibody, CD16/CD32 (Biolegend), was added to 100 μL of suspended cells (*ca*. 1-3×10^6 cells) for 20 min at room temperature. Then, 100 μL of Alexa Fluor 647 anti-CD8 antibody conjugated NPs (0.05 nM) was mixed with cells for 1 h at room temperature. Cells were washed from any unbound NP by adding 5 mL PBS and centrifuging at 182 ×g for 3 minutes. The supernatant was discarded and the cells were resuspended in 1 mL PBS. Dark-field and fluorescence images of the cells

were performed using a Leica DM6000 upright microscope configured with 20×, 0.5-NA dark field objective, fluorescence filter cube (Chroma), and a Xe-lamp illumination.

For magnetic enrichment, labeled cells were first passed through a 30 μm filter (Miltenyi Biotec) to remove potential cell aggregates. The cell suspension was loaded into a PBS-rinsed MS column (Miltenyi Biotec) in presence of the MACS magnet. The column was then washed with 1 mL PBS for three times. The nanocluster-labeled CD8+ T cells retained in the MS column, whereas the non-labeled cells flowed through the MS column. Afterwards, the MS column was removed from the MACS magnet and washed out through with 1 mL PBS, resulting in release of NP-labeled CD8+ T cells from the MS column. The proportion of CD8+ T cells present in the total cell population was accessed by flow cytometry (BD LSRFortessa).

Measurement of cell viability after labeling with hybrid nanoclusters

A single cell suspension from spleens (1-5×10^6 cells in 100 μL) was labeled by Alexa Fluor 647 anti-CD8 antibody conjugated NPs (100 μL at 0.05 nM) for 1 h at room temperature. The cells were then washed with 5 mL PBS and resuspended in 3 mL cell culture medium. After 24 h incubation in CO_2 incubator at 37 °C, the cells were washed with 2 mL PBS and stained with 100 μL PBS containing 0.5 μg Zombie Violet dye (Biolegend) in dark for 20 min at room temperature. Afterwards, the cells were washed with 2 mL buffer (PBS containing 2% BSA) and resuspended in 100 μL PBS, followed by flow cytometry analysis (BD LSRFortessa).

In vitro Magnetic Trapping Test

The cells were derived from sacrificed transgenic mice expressing red fluorescent protein on CD2. The nanocluster labeling process was described above. Nanocluster-labeled cells or unlabeled cells (1.1×10^5 cells in 20 μL PBS) were distributed to a single well from inner side of a 96-well lid. A disc magnet (1 mm diameter × 0.5 mm thick,

NdFeB, N50, SuperMagnetMan) was placed toward the center of the well and a round glass coverslip was applied onto the top of the well. After incubation with the magnet for 1 min, the images were captured by TCS SP5 RS laser resonant scanning microscope using 4X objective (Leica Microsystems).

To investigate whether the nanocluster-labeled cells can be magnetically positioned, labeled cells (1.1×10^5) were distributed to a single well from inner side of a 96-well lid, followed by capping with a round glass coverslip. A disc magnet (1 mm diameter × 0.5 mm thick, NdFeB, SuperMagnetMan) was placed onto the glass coverslip with random movement. The images were captured as previously described.

4.3.2 Results and Discussion

Cell-based therapies based on anti-tumor lymphocytes are promising approaches for cancer immunotherapy.[9] The infusion of *ex vivo* cultured lymphocytes, called adoptive cell therapy, has demonstrated its effectiveness in tumor rejection in a few of early phase clinical trials.[36] The ability to genetically engineer lymphocytes *in vitro* yields further opportunity to increase the avidity of T cells for tumor antigens, thus improving the efficacy of ACT.[9, 10] In general, an effective cancer immunotherapy to seek out and reject cancer cells *in vivo* highly depends on the presence of large numbers of anti-tumor lymphocytes with appropriate homing and effector functions.[37] Although ACT involves the administration of lymphocytes that can be augmented *ex vivo* in very large numbers, inefficient migration of T cells to tumor tissue is still one major limited factor for ACT.[38, 39] Several lines of evidence have demonstrated that impaired tumor homing of T cells causes the disappointing clinical response rates.[40] Therefore, strategies to improve the migration of T cells to tumor microenvironment can possibly to enhance the efficacy of ACT.

Currently, most of the efforts have been focused on the improvement of T cell functions, including selection of antigen, antigen presentation systems, or expansion methods. For example, T cells from patients have been genetically engineered to express a T cell receptor or chimeric antigen receptor to specifically target a tumor-associate antigen.[41, 42] Several early clinical trials using CAR-modified T cells have shown some promising results.[43, 44] In addition, researchers have demonstrated a simplified and rapid method to expand tumor reactive lymphocytes for ACT, since the existed protocol has been criticized for its time-consuming and labor-intensive process.[45] However, to date, there have been very limited studies to improve ACT from the cell delivery perspective. Effective tumor rejection requires not only a sufficient number of activated T cells with high avidity that can recognize tumor antigens, but also the ability of these cells to migrate to the malignancy sites.[37] Thus, we proposed a magnet-guided approach which involves manipulating cells *ex vivo* with magnetic properties followed by precise positioning of lymphocytes using an external magnetic field. This novel approach could potentially lead to accumulate significant numbers of lymphocytes in tumor lesion and thereby achieve its desired therapeutic effect.

In the past two decades, the control of the interaction between live cells and magnetic nanomaterials has been intensively investigated. Magnetic nanomaterials, mainly iron oxide nanoparticles, with unique superparamagnetic properties and favorable biocompatibility are useful for biomedical applications.[46] For example, magnetic labeling of living cells has been successfully applied to diagnostic imaging and regenerative medicine for a variety of diseases, including neurological disease, myocardial infarction, and arthritis.[47-49] The use of "magnetic cells" provides not only the use in MR imaging for tracking and monitoring of transferred cells but also the remote manipulation of cells under a magnetic stimulus.[19, 50] However, we found that there are very few studies

utilizing the magnetic cell concept to combat one of the most prevalent diseases, cancer. Muthana *et al*. showed that administered magnetic NP-loaded monocytes can be pulled out from the circulation and pass across an endothelial cell barrier into the tumor mass.[51] However, their focus tends to utilize cells as cellular delivery vehicles for anti-cancer gene therapy. This is less straightforward than delivering either cytotoxic T lymphocytes or tumor-infiltrating lymphocytes to kill cancer cells directly. Thus, we present a novel approach to magnetically label and enrich cytotoxic T lymphocytes for *in vivo* reinfusion and subsequently positioning under an external magnetic field.

Magneto-plasmonic nanoclusters

We use our proprietary magneto-plasmonic nanoclusters to render cytotoxic T cells magnetic properties. The whole construct of the immunotargeted hybrid nanoclusters can be seen at Figure 4.8A. The hybrid nanoclusters were synthesized *via* self-assembly of the constituent Fe_3O_4 core–Au shell nanoparticles. The TEM image of nanoparticles (Figure 4.8B) shows a spherical shape with a size distribution of 130 ± 26 nm (Figure 4.9C). A distinctive plasmonic resonance peak was located *ca*. 556 nm (Figure 4.9D). The use of hybrid nanoclusters has been demonstrated enhancing magnetic force while preserving the superparamagnetic properties of the nanoparticles. Indeed, the hybrid nanoclusters can be quickly isolated from a colloidal suspension using a permanent magnet (inset in Figure 4.9D). Monoclonal targeted antibodies were attached to the nanoclusters using our proprietary directional conjugation through the Fc portion that leaves the antigen binding sites on the Fab moiety available for targeting.[35] This directional conjugation chemistry has been shown to diminish potential non-specific interactions through Fc receptors.[52-55] Subsequently, methyl-PEG-thiol is added to passivate the entire nanocluster surface and increase the biocompatibility of this nanoconstruct.

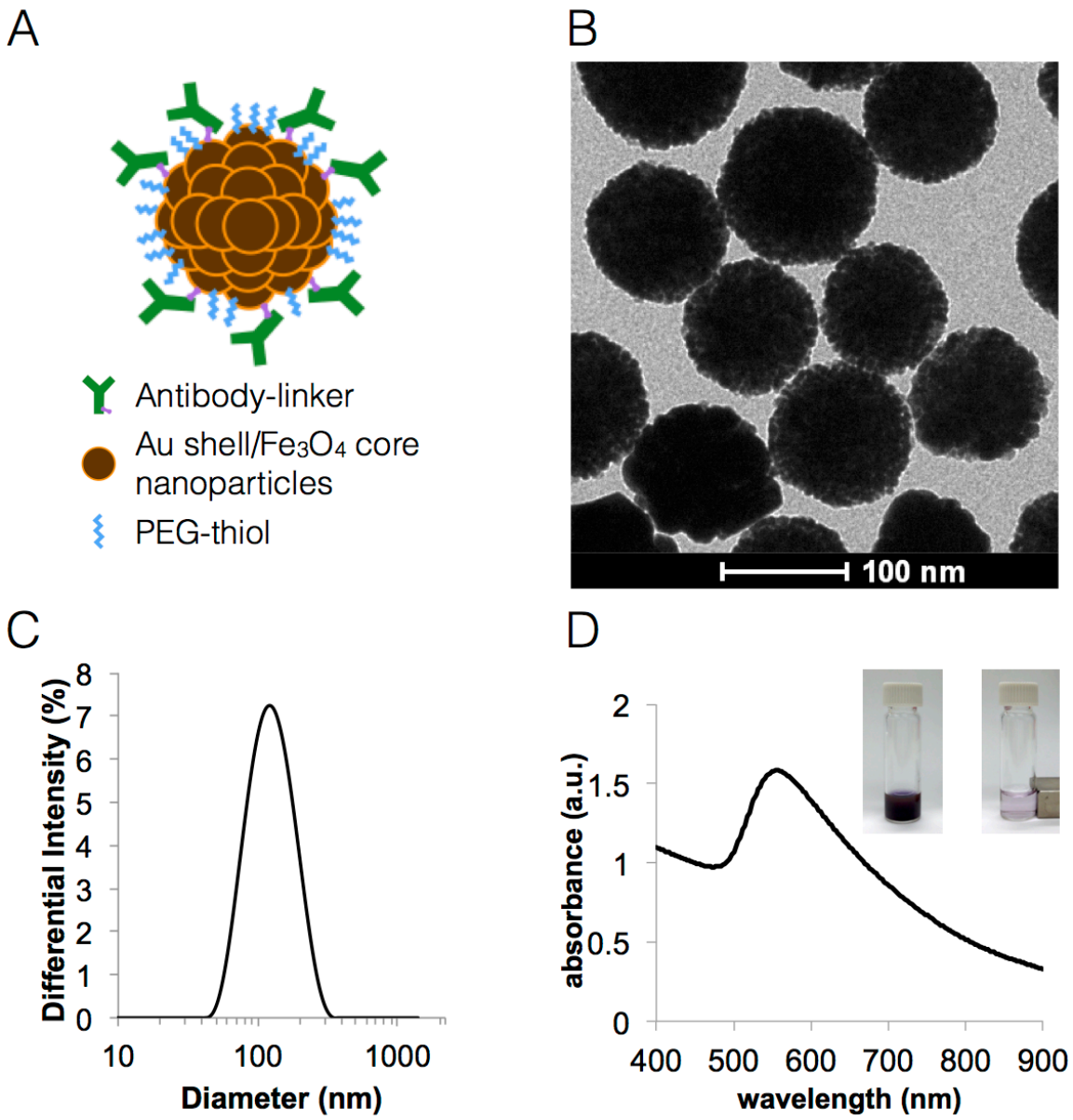

Figure 4.8 Characterization of magneto-plasmonic nanoparticles. (A) Schematic constituents of an immunotargeted magneto-plasmonic nanoparticles. (B) TEM image, (C) size distribution, and (D) UV-Vis spectrum of magneto-plasmonic nanoparticles. The insertion in (D) shows the separation of nanoparticles from a colloidal suspension using a permanent magnet.

Labeling CD8+ T cells

In this study, we chose anti-CD8 antibodies as our targeting biomarker which allows us to target cytotoxic T cells. The labeling specificity was first determined by comparing the cell binding using dark-field and fluorescence imaging. In Figure 4.9A, the cells from nanocluster-treated group show that bright orange color around their surface which is associated with strong light scattering from nanoclusters. The orange color matches well with the fluorescent signal from Alexa Fluor 647 anti-CD8 antibodies, therefore supporting the effective nanoparticle-antibody conjugation. In addition, we characterized the labeled cells using flow cytometry. Figure 4.9B shows similar expression of CD8 between nanoparticle- and antibody-treated samples, indicating the specific nanocluster labeling to CD8+ T cells. It is also noted that the CD8+ sub-population was slight lower for nanoparticle-labeled group (25.0%) in comparison with antibody alone group (31.5%). This phenomenon has been reported elsewhere that the particles affects binding kinetics between antibody and antigen, thus binding of antibody-conjugated beads to the cells is slower than that of the antibodies themselves[56]

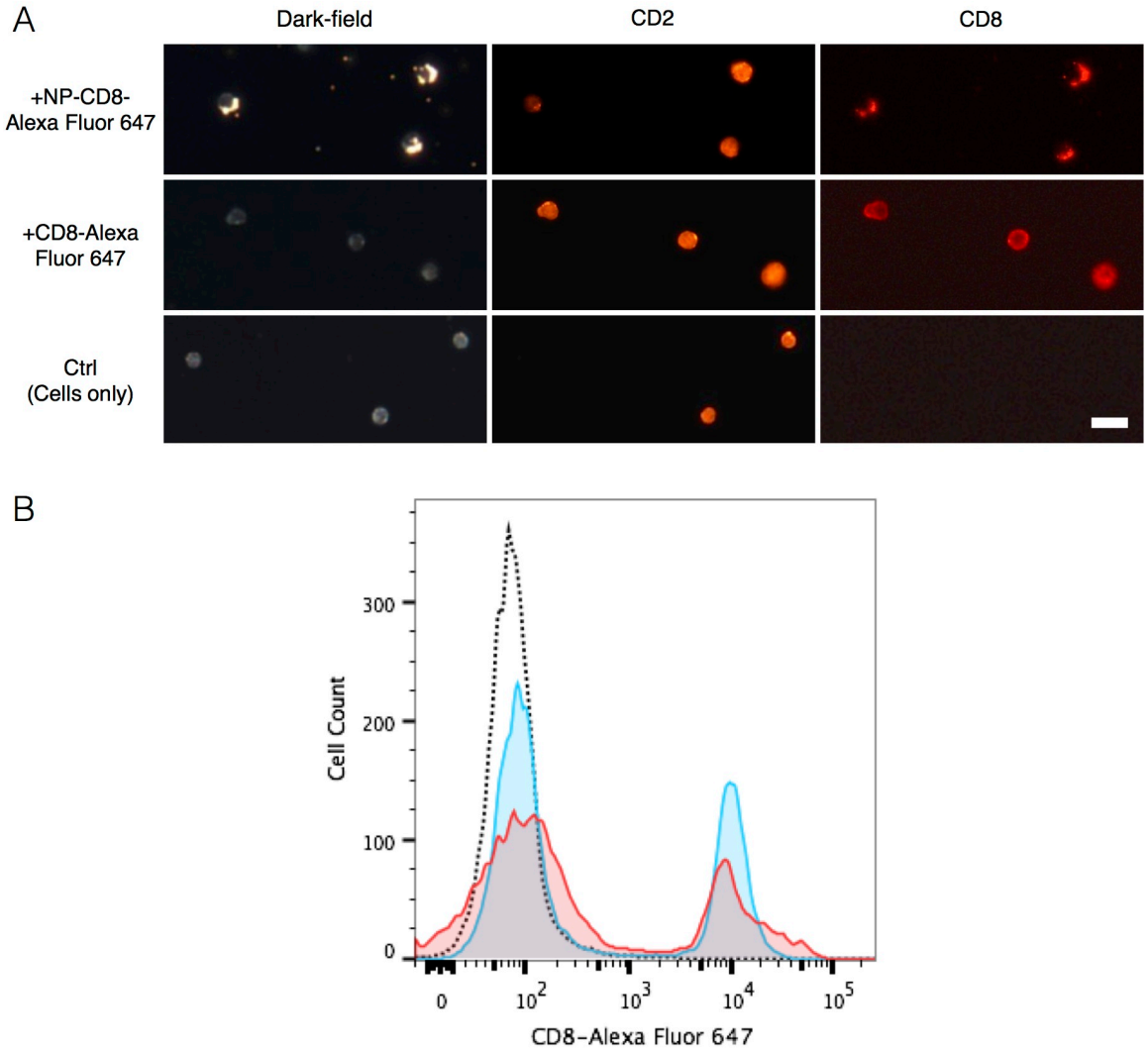

Figure 4.9 Characterization of T cells labeled by Alexa Flour 647-anti-CD8-conjugated nanoparticles using (A) imaging analysis and (B) flow cytometry. The yellow-orange color in the dark-field images is associated with binding of the nanoparticles to the cells; unlabeled cells show greyish color that represents the intrinsic scattering properties of cells. CD2 is a marker for T cells whose fluorescent signal was from red fluorescent protein on CD2. Flow cytometry analysis shows that CD8+ subset was 25% for nanoparticle-labeled group (red solid) in comparison with 31.5% for antibody-alone group (blue solid). An isotype-matched IgG2a Alexa Flour 647 (black dot) serves as negative control.

Magnetic enrichment of CD8+ T cells

We investigated whether the labeled CD8+ T cells can be isolated magnetically. We used the commercially available magnetic cell sorting apparatus, MACS™ column which is widely utilized in biological field.[57] In brief, nanoparticle-labeled cells were loaded into magnetic cell separation columns filled with ferromagnetic beads, followed by introduction of a magnetic field generated by a strong external magnet (Figure 4.10A). The cells labeled with hybrid nanoclusters were efficiently retarded in the column and unlabeled cells were eluted. The labeled cells were then recovered when the column was de-magnetized by removal from the magnetic field. Before separation, 3.9% of the cells expressed CD8+ (Figure 4.10B). After magnetic enrichment, the CD8+ T cell population increased to 80.5% (Figure 4.10C). In contrast, the un-retained fraction, eluted from the column during the washing step, contained only 0.5% of CD8+ T cell population (Figure 4.10D). The more than 20-fold enrichment rates explained that the hybrid nanocluster-labeled cells generated enough magnetic strength, thus contributing the high efficiency of magnetic enrichment of CD8+ T cells. To the best of our knowledge, it is the first hybrid magneto-plasmonic nanoparticles used for immunological cell labeling and separation.

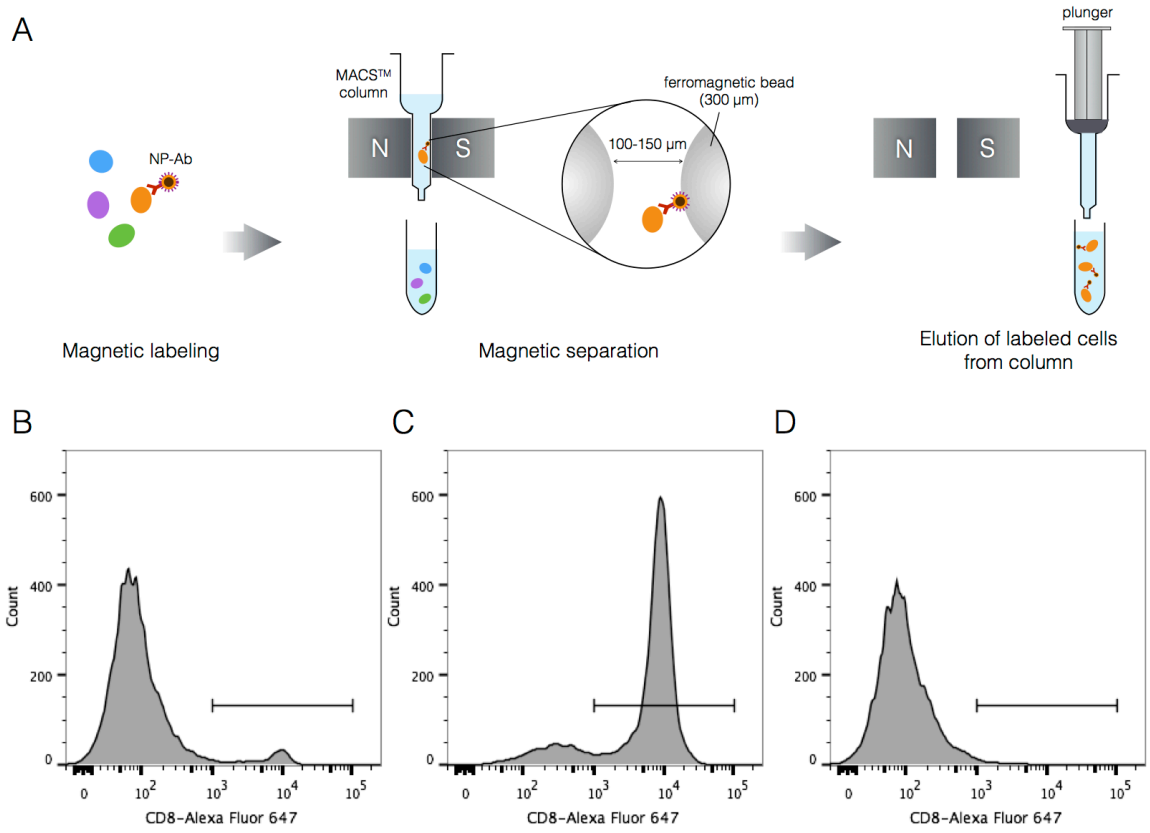

Figure 4.10 Magnetic enrichment of CD8+ T cells from mouse splenocytes. (A) Experimental produce for magnetic enrichment. The cells were labeled by Alexa Flour 647-anti-CD8-conjugated nanoparticles followed by running MACS™ column: before (B), after (C), and eluent of isolation (D) where the CD8+ cell subsets are 5.9%, 85%, and 2.2%, respectively.

Biocompatibility of hybrid nanoclusters

The utility of nanoparticle-labeled cells for ACT highly depends on the extent of cytotoxicity induced by nanoparticles. The cells should be kept viable during nanoparticle labeling process and subsequent reinfusion *in vivo*. Thus, we assessed whether the nanocluster labeling would interfere the viability of cells. Several reports have been shown the coating on nanoparticles highly determines their biocompatibility.[58, 59] Among the choice of surfactants, nanoparticles modified with polyethylene glycol achieved enhanced biocompatibility.[60-62] In our nanoparticle platform, co-attachment of PEG

molecules to the nanocluster surface is feasible. The process involves only mixing the nanoparticles with methyl-PEG-thiol so that the original surfactants can be exchanged with PEG. In the viability assay, a single cell suspension from mouse spleen was labeled by anti-CD8-conjugated nanoclusters or antibody alone for 1 h. After washing step, the cells were then incubated for 24 h in the CO_2 incubator at 37°C. The cells were then stained with amine-reactive viability dye. The positive control prepared by heat-killed approach showed more than 95% cell death which indicates the effectiveness of this viability dye (Figure 4.11B). In contrast, nanoparticle-labeled cells showed the similar viability as compared with untreated or antibody-treated cells after 24 h incubation (Figure 4.11). Therefore, the great biocompatibility suggests high utility of the hybrid nanoclusters for labeling and enriching cytotoxic T lymphocytes.

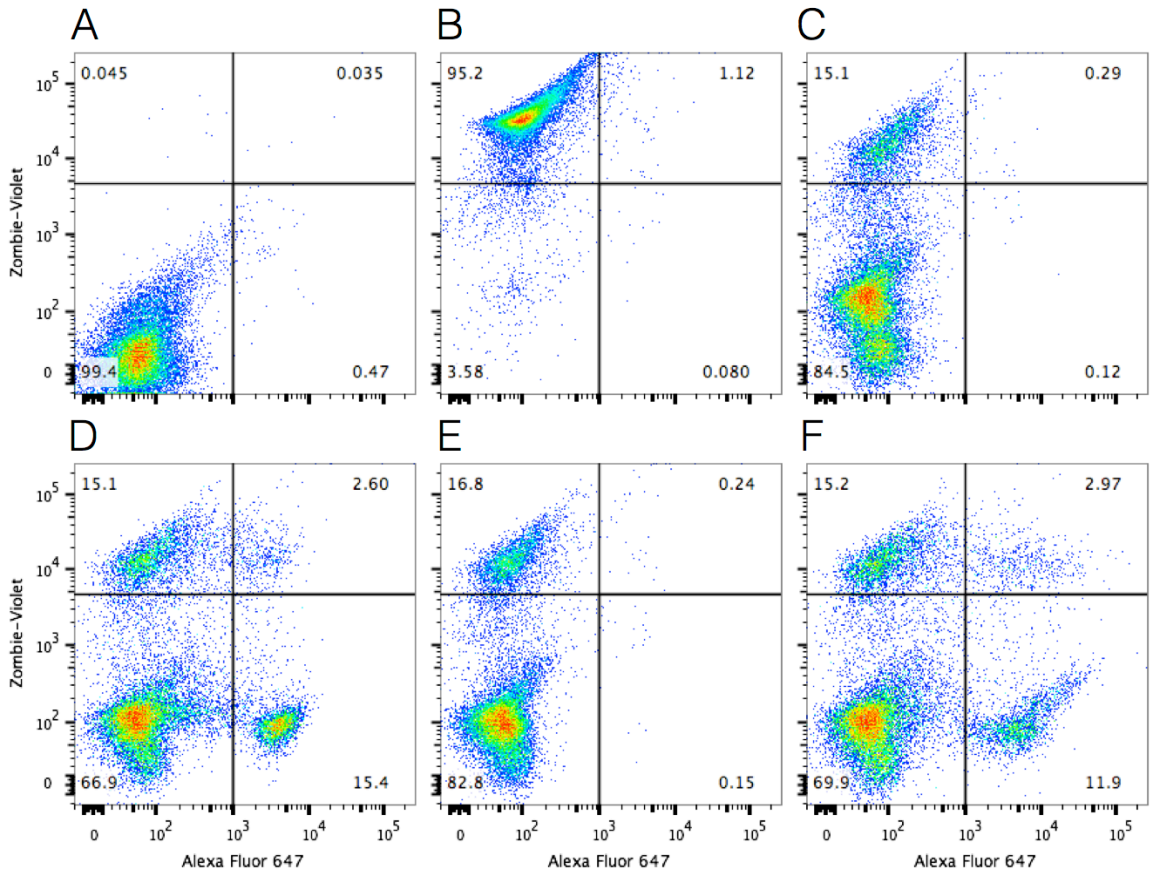

Figure 4.11 Flow cytometry evaluation of cell viability on splenocytes treated with nanoparticles and incubated for 24 h thereafter. Live and dead cells were distinguished by using Zombie Aqua™ Fixable Viability Kit. (A) unstained; (B) heat-killed (positive control); (C) untreated (negative control); (D) Alexa Flour 647 anti-CD8 Ab; (E) Alexa Flour 647 IgG2a isotype ctrl; (F) Alexa Flour 647-anti-CD8-conjugated nanoparticles. Upper quadrants represent the live cell population which is distinguished from the killed population at lower quadrants. The right quadrants contain events that are positive for the CD8-Alexa Flour 647.

In vitro magnetic trapping test

Cell-based cancer therapies typically rely on intravenous delivery of cells which are expected to home to sites of diseases. However, homing efficiency is typically inefficient.[11, 22, 63] We propose that delivery and retention of cells could be enhanced by magnetic labeling of cells and subsequent introduction of an external magnetic gradient at the site of interest. To investigate the feasibility of this approach, we first evaluated the magnetic attraction of labeled cells under *in vitro* static conditions. We dropped a tiny disc magnet (1 mm diameter × 0.5 mm thick) into a well loaded with nanocluster-labeled T cells (Figure 4.12A). The nanoparticle-labeled cells demonstrated strong response to the magnetic field gradients and retained at the sites with highest magnetic field gradient (Figure 4.12B). In contrast, the unlabeled cells remained in a cell suspension and distributed uniformly in the well without disturbance by the magnet. (Figure 4.12B).

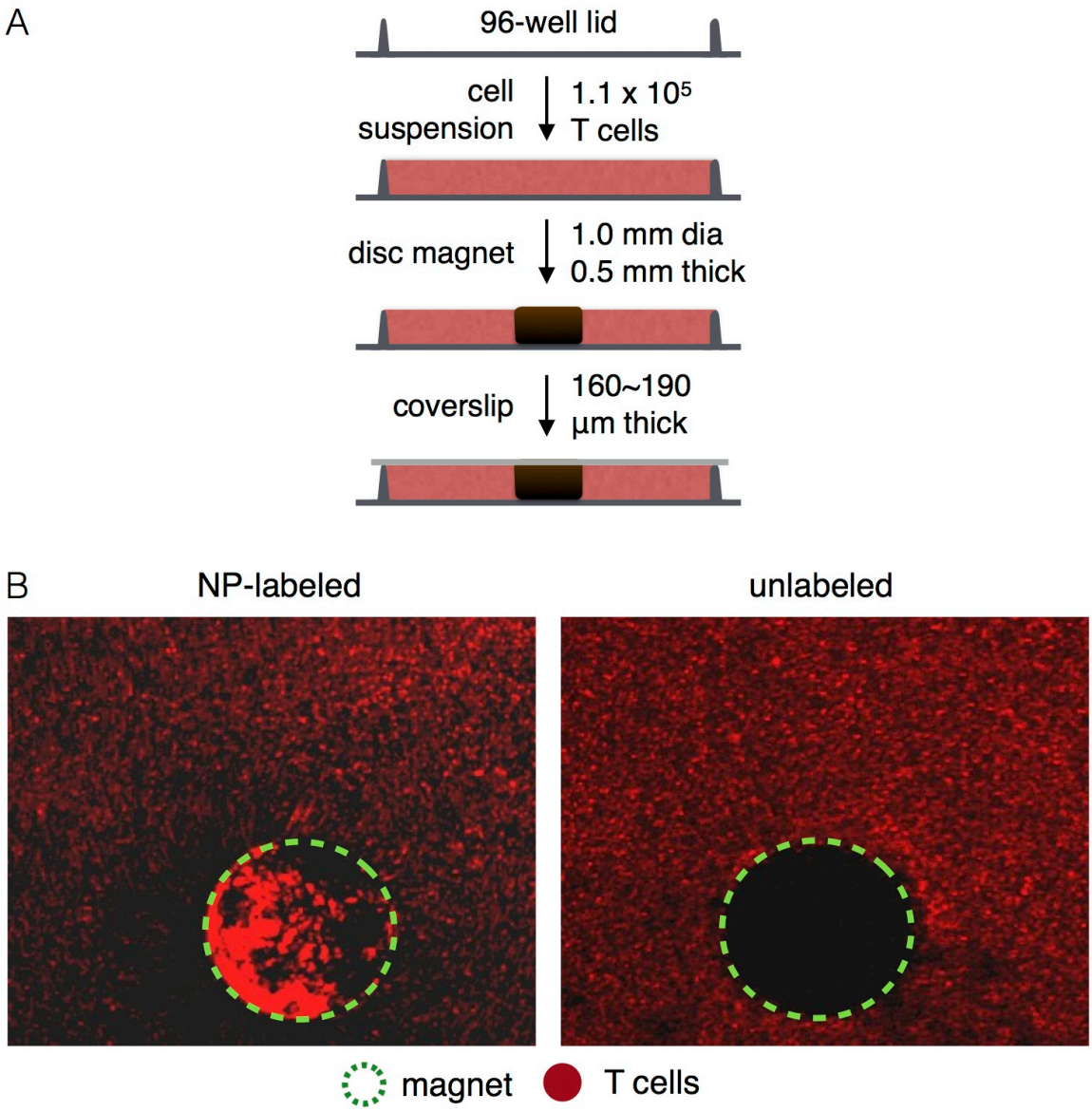

Figure 4.12 Magnetic attraction assay of nanoparticle-labeled CD8+ T cells under static conditions. (A) Experimental procedure. (B) Magnetic attraction of enriched CD8+ T cells or unlabeled T cells after incubation of a disc magnet for 1 min. Green dot line represents the magnet and the red cells are T cells from transgenic mice expressing red fluorescent protein on CD2.

We further investigated whether nanocluster-labeled T cells can be positioned under magnetic guidance. The nanocluster-labeled cells were loaded into a small chamber created by a well from the inner side of a 96-well lid and a glass coverslip. A disc magnet was placed on top of the coverslip. Then, the disc magnet was repositioned at later time points (Figure 4.13A). The nanocluster-labeled cells moved toward the magnet when the magnet was static at one position. After moving the disc magnet to another region, nanocluster-labeled cells shifted to the magnet accordingly (Figure 4.13B). As can be seen from the last timeframe in Figure 4.13B, T cells formed a high-density cell cluster after removing the magnet. This enhancement of T cell recruitment suggests a high potential for therapeutic use. Overall, these *in vitro* findings clearly indicate that nanocluster-labeled cells can be magnetically positioned and confined in a specific area.

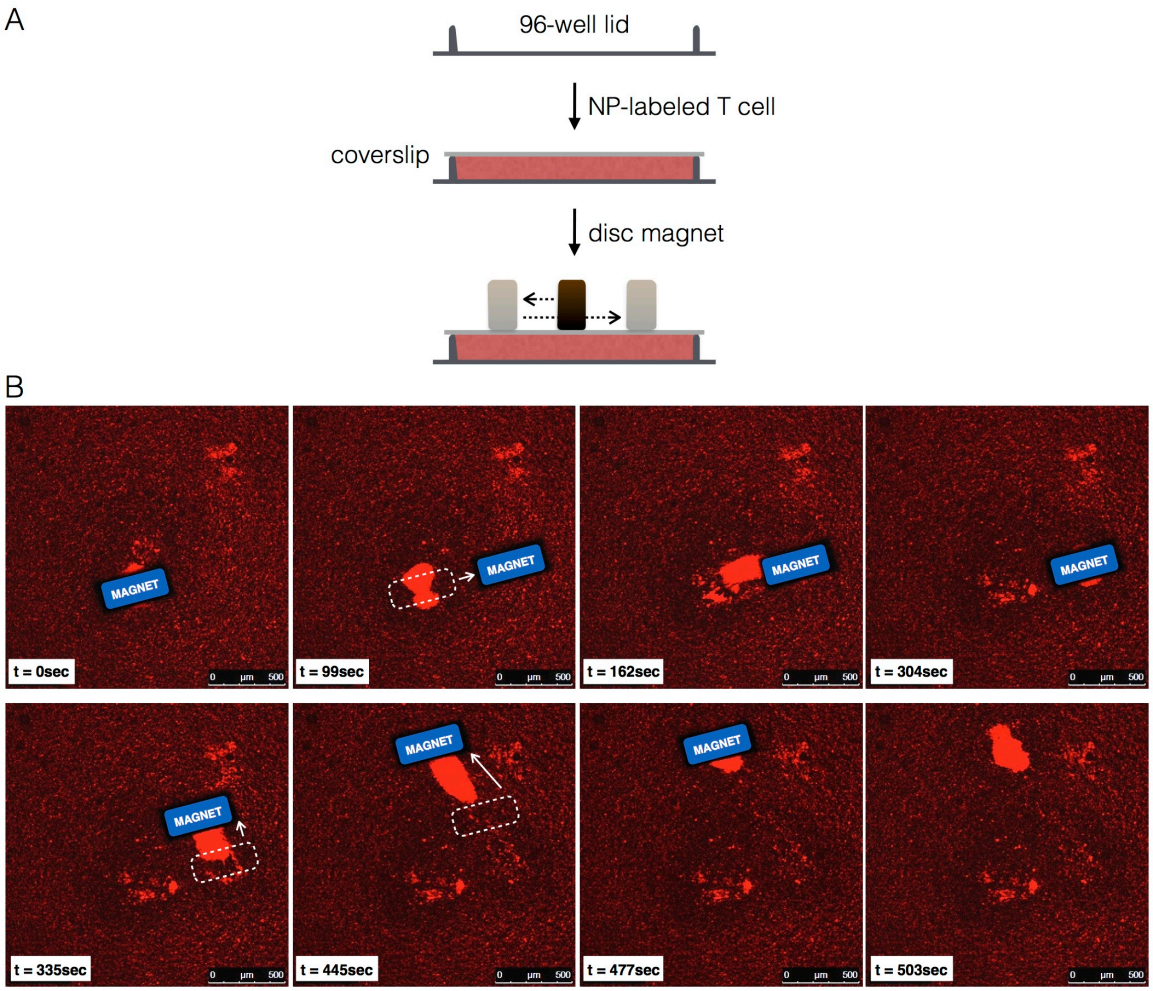

Figure 4.13 Magnetic motility assay of nanoparticle-labeled CD8+ T cells. (A) Experimatal procedure. (B) Magnetic manipulation of labeled T cells by an external magnet. White dot line indicates the location of the magnet (solid blue) from the previous time point. Red cells are T cells from transgenic mice expressing red fluorescent protein on CD2.

4.4 CONCLUSIONS

Here, we introduced a concept to mediate immune cells with magnetic properties and a magnetic field to improve cellular delivery of ACT. We showed that the immune cells were well labeled by the nanoparticles based either cellular internalization or selective surface labeling. It is also found that none of the nanoparticle labeling induced noticeable cytotoxic to immune cells. Importantly, the retention of the magnetically engineered cells can be elevated under physiological conditions by applying a magnetic field. These engineered cells can be potentially manipulated to inaccessible areas of tumors with an aid of a magnetic force. Thus, infiltration of immune cells into tumor tissues could be expected to reject tumor cells in a more efficient manner.

4.3 REFERENCES

1. Rosenberg, S. A.; Dudley, M. E., Adoptive cell therapy for the treatment of patients with metastatic melanoma. *Curr Opin Immunol* **2009**, 21, 233-240.

2. Rosenberg, S. A.; Aebersold, P.; Cornetta, K.; Kasid, A.; Morgan, R. A.; Moen, R.; Karson, E. M.; Lotze, M. T.; Yang, J. C.; Topalian, S. L.; et al., Gene transfer into humans--immunotherapy of patients with advanced melanoma, using tumor-infiltrating lymphocytes modified by retroviral gene transduction. *N Engl J Med* **1990**, 323, 570-578.

3. Rosenberg, S. A.; Restifo, N. P.; Yang, J. C.; Morgan, R. A.; Dudley, M. E., Adoptive cell transfer: a clinical path to effective cancer immunotherapy. *Nat Rev Cancer* **2008**, 8, 299-308.

4. Pockaj, B. A.; Sherry, R. M.; Wei, J. P.; Yannelli, J. R.; Carter, C. S.; Leitman, S. F.; Carasquillo, J. A.; Steinberg, S. M.; Rosenberg, S. A.; Yang, J. C., Localization of 111indium-labeled tumor infiltrating lymphocytes to tumor in patients receiving adoptive immunotherapy. Augmentation with cyclophosphamide and correlation with response. *Cancer* **1994**, 73, 1731-1737.

5. Fisher, B.; Packard, B. S.; Read, E. J.; Carrasquillo, J. A.; Carter, C. S.; Topalian, S. L.; Yang, J. C.; Yolles, P.; Larson, S. M.; Rosenberg, S. A., Tumor localization of

adoptively transferred indium-111 labeled tumor infiltrating lymphocytes in patients with metastatic melanoma. *J Clin Oncol* **1989**, 7, 250-261.

6. Rosenberg, S. A.; Dudley, M. E., Cancer regression in patients with metastatic melanoma after the transfer of autologous antitumor lymphocytes. *Proc Natl Acad Sci U S A* **2004**, 101 Suppl 2, 14639-14645.

7. Bobisse, S.; Rondina, M.; Merlo, A.; Tisato, V.; Mandruzzato, S.; Amendola, M.; Naldini, L.; Willemsen, R. A.; Debets, R.; Zanovello, P.; Rosato, A., Reprogramming T lymphocytes for melanoma adoptive immunotherapy by T-cell receptor gene transfer with lentiviral vectors. *Cancer Res* **2009**, 69, 9385-9394.

8. Dudley, M. E.; Wunderlich, J. R.; Yang, J. C.; Sherry, R. M.; Topalian, S. L.; Restifo, N. P.; Royal, R. E.; Kammula, U.; White, D. E.; Mavroukakis, S. A.; Rogers, L. J.; Gracia, G. J.; Jones, S. A.; Mangiameli, D. P.; Pelletier, M. M.; Gea-Banacloche, J.; Robinson, M. R.; Berman, D. M.; Filie, A. C.; Abati, A.; Rosenberg, S. A., Adoptive cell transfer therapy following non-myeloablative but lymphodepleting chemotherapy for the treatment of patients with refractory metastatic melanoma. *J Clin Oncol* **2005**, 23, 2346-2357.

9. June, C. H., Adoptive T cell therapy for cancer in the clinic. *J Clin Invest* **2007**, 117, 1466-1476.

10. Peng, W.; Ye, Y.; Rabinovich, B. A.; Liu, C.; Lou, Y.; Zhang, M.; Whittington, M.; Yang, Y.; Overwijk, W. W.; Lizee, G.; Hwu, P., Transduction of tumor-specific T cells with CXCR2 chemokine receptor improves migration to tumor and antitumor immune responses. *Clin Cancer Res* **2010**, 16, 5458-5468.

11. Pittet, M. J.; Mempel, T. R., Regulation of T-cell migration and effector functions: insights from in vivo imaging studies. *Immunol Rev* **2008**, 221, 107-129.

12. Kershaw, M. H.; Westwood, J. A.; Slaney, C. Y.; Darcy, P. K., Clinical application of genetically modified T cells in cancer therapy. *Clinical & Translational Immunology* **2014**, 3, e16.

13. Yee, C., Adoptive T cell therapy: Addressing challenges in cancer immunotherapy. *J Transl Med* **2005**, 3, 17.

14. Gallo, J.; Long, N. J.; Aboagye, E. O., Magnetic nanoparticles as contrast agents in the diagnosis and treatment of cancer. *Chem Soc Rev* **2013**, 42, 7816-7833.

15. Qiao, R.; Yang, C.; Gao, M., Superparamagnetic iron oxide nanoparticles: from preparations to in vivo MRI applications. *Journal of Materials Chemistry* **2009**, 19, 6274-6293.

16. Wilczewska, A. Z.; Niemirowicz, K.; Markiewicz, K. H.; Car, H., Nanoparticles as drug delivery systems. *Pharmacol Rep* **2012**, 64, 1020-1037.

17. Sun, C.; Lee, J. S.; Zhang, M., Magnetic nanoparticles in MR imaging and drug delivery. *Adv Drug Deliv Rev* **2008**, 60, 1252-1265.

18. Landazuri, N.; Tong, S.; Suo, J.; Joseph, G.; Weiss, D.; Sutcliffe, D. J.; Giddens, D. P.; Bao, G.; Taylor, W. R., Magnetic targeting of human mesenchymal stem cells with internalized superparamagnetic iron oxide nanoparticles. *Small* **2013**, 9, 4017-4026.

19. Hofmann, A.; Wenzel, D.; Becher, U. M.; Freitag, D. F.; Klein, A. M.; Eberbeck, D.; Schulte, M.; Zimmermann, K.; Bergemann, C.; Gleich, B.; Roell, W.; Weyh, T.; Trahms, L.; Nickenig, G.; Fleischmann, B. K.; Pfeifer, A., Combined targeting of lentiviral vectors and positioning of transduced cells by magnetic nanoparticles. *Proc Natl Acad Sci U S A* **2009**, 106, 44-49.

20. Cheng, K.; Malliaras, K.; Li, T. S.; Sun, B.; Houde, C.; Galang, G.; Smith, J.; Matsushita, N.; Marban, E., Magnetic enhancement of cell retention, engraftment, and functional benefit after intracoronary delivery of cardiac-derived stem cells in a rat model of ischemia/reperfusion. *Cell Transplant* **2012**, 21, 1121-1135.

21. Kamei, G.; Kobayashi, T.; Ohkawa, S.; Kongcharoensombat, W.; Adachi, N.; Takazawa, K.; Shibuya, H.; Deie, M.; Hattori, K.; Goldberg, J. L.; Ochi, M., Articular cartilage repair with magnetic mesenchymal stem cells. *Am J Sports Med* **2013**, 41, 1255-1264.

22. Zhang, L.; Dokouhaki, P., Recent Advances in T Cell Adoptive Immunotherapy of Cancer. *Current Cancer Therapy Reviews* **2008**, 4, 1-13.

23. Stone, J. D.; Kranz, D. M., Role of T cell receptor affinity in the efficacy and specificity of adoptive T cell therapies. *Front Immunol* **2013**, 4, 244.

24. Wang, L.; Luo, J.; Fan, Q.; Suzuki, M.; Suzuki, I. S.; Engelhard, M. H.; Lin, Y.; Kim, N.; Wang, J. Q.; Zhong, C.-J., Monodispersed Core–Shell Fe3O4@Au Nanoparticles. *The Journal of Physical Chemistry B* **2005**, 109, 21593-21601.

25. Bai, F.; Wang, D.; Huo, Z.; Chen, W.; Liu, L.; Liang, X.; Chen, C.; Wang, X.; Peng, Q.; Li, Y., A Versatile Bottom-up Assembly Approach to Colloidal Spheres from Nanocrystals. *Angewandte Chemie International Edition* **2007**, 46, 6650-6653.

26. Sokolov, K.; Galvan, J.; Myakov, A.; Lacy, A.; Lotan, R.; Richards-Kortum, R., Realistic three-dimensional epithelial tissue phantoms for biomedical optics. *J Biomed Opt* **2002**, 7, 148-156.

27. Satake, I.; Yang, J. T., Interaction of sodium decyl sulfate with poly(L-ornithine) and poly(L-lysine) in aqueous solution. *Biopolymers* **1976**, 15, 2263-2275.

28. Luhmann, T.; Rimann, M.; Bittermann, A. G.; Hall, H., Cellular uptake and intracellular pathways of PLL-g-PEG-DNA nanoparticles. *Bioconjug Chem* **2008**, 19, 1907-1916.

29. Hartono, S. B.; Gu, W.; Kleitz, F.; Liu, J.; He, L.; Middelberg, A. P.; Yu, C.; Lu, G. Q.; Qiao, S. Z., Poly-L-lysine functionalized large pore cubic mesostructured silica nanoparticles as biocompatible carriers for gene delivery. *ACS Nano* **2012**, 6, 2104-2117.

30. Riggio, C.; Calatayud, M. P.; Hoskins, C.; Pinkernelle, J.; Sanz, B.; Torres, T. E.; Ibarra, M. R.; Wang, L.; Keilhoff, G.; Goya, G. F.; Raffa, V.; Cuschieri, A., Poly-l-lysine-coated magnetic nanoparticles as intracellular actuators for neural guidance. *Int J Nanomedicine* **2012**, 7, 3155-3166.

31. Metz, S.; Bonaterra, G.; Rudelius, M.; Settles, M.; Rummeny, E. J.; Daldrup-Link, H. E., Capacity of human monocytes to phagocytose approved iron oxide MR contrast agents in vitro. *Eur Radiol* **2004**, 14, 1851-1858.

32. Tong, L.; Zhao, M.; Zhu, S.; Chen, J., Synthesis and application of superparamagnetic iron oxide nanoparticles in targeted therapy and imaging of cancer. *Front Med* **2011**, 5, 379-387.

33. Bear, A. S.; Cruz, C. R.; Foster, A. E., T cells as vehicles for cancer vaccination. *J Biomed Biotechnol* **2011**, 417403.

34. Lawrence, M. B.; Springer, T. A., Leukocytes roll on a selectin at physiologic flow rates: distinction from and prerequisite for adhesion through integrins. *Cell* **1991**, 65, 859-873.

35. Kumar, S.; Aaron, J.; Sokolov, K., Directional conjugation of antibodies to nanoparticles for synthesis of multiplexed optical contrast agents with both delivery and targeting moieties. *Nature Protocols* **2008**, 3, 314-320.

36. Dudley, M. E.; Yang, J. C.; Sherry, R.; Hughes, M. S.; Royal, R.; Kammula, U.; Robbins, P. F.; Huang, J.; Citrin, D. E.; Leitman, S. F.; Wunderlich, J.; Restifo, N. P.; Thomasian, A.; Downey, S. G.; Smith, F. O.; Klapper, J.; Morton, K.; Laurencot, C.; White, D. E.; Rosenberg, S. A., Adoptive cell therapy for patients with metastatic melanoma: evaluation of intensive myeloablative chemoradiation preparative regimens. *J Clin Oncol* **2008**, 26, 5233-5239.

37. Blattman, J. N.; Greenberg, P. D., Cancer immunotherapy: a treatment for the masses. *Science* **2004**, 305, 200-205.

38. Peterson, A. C.; Harlin, H.; Gajewski, T. F., Immunization with Melan-A peptide-pulsed peripheral blood mononuclear cells plus recombinant human interleukin-12 induces clinical activity and T-cell responses in advanced melanoma. *Journal of clinical oncology* **2003**, 21, 2342-2348.

39. Rosenberg, S. A.; Sherry, R. M.; Morton, K. E.; Scharfman, W. J.; Yang, J. C.; Topalian, S. L.; Royal, R. E.; Kammula, U.; Restifo, N. P.; Hughes, M. S., Tumor progression can occur despite the induction of very high levels of self/tumor antigen-specific CD8+ T cells in patients with melanoma. *The Journal of Immunology* **2005**, 175, 6169-6176.

40. Rosenberg, S. A.; Yang, J. C.; Restifo, N. P., Cancer immunotherapy: moving beyond current vaccines. *Nat Med* **2004**, 10, 909-915.

41. Kalos, M.; Levine, B. L.; Porter, D. L.; Katz, S.; Grupp, S. A.; Bagg, A.; June, C. H., T cells with chimeric antigen receptors have potent antitumor effects and can establish memory in patients with advanced leukemia. *Science translational medicine* **2011**, 3, 95ra73-95ra73.

42. Song, D.-G.; Ye, Q.; Carpenito, C.; Poussin, M.; Wang, L.-P.; Ji, C.; Figini, M.; June, C. H.; Coukos, G.; Powell, D. J., In vivo persistence, tumor localization, and

antitumor activity of CAR-engineered T cells is enhanced by costimulatory signaling through CD137 (4-1BB). *Cancer research* **2011**, 71, 4617-4627.

43. Kohn, D. B.; Dotti, G.; Brentjens, R.; Savoldo, B.; Jensen, M.; Cooper, L. J. N.; June, C. H.; Rosenberg, S.; Sadelain, M.; Heslop, H. E., CARs on Track in the Clinic: Workshop of the Blood and Marrow Transplant Clinical Trials Network Subcommittee on Cell and Gene Therapy Washington DC, 18 May 2010. *Molecular Therapy* **2011**, 19, 432.

44. Porter, D. L.; Levine, B. L.; Kalos, M.; Bagg, A.; June, C. H., Chimeric antigen receptor–modified T cells in chronic lymphoid leukemia. *New England Journal of Medicine* **2011**, 365, 725-733.

45. Somerville, R. P.; Devillier, L.; Parkhurst, M. R.; Rosenberg, S. A.; Dudley, M. E., Clinical scale rapid expansion of lymphocytes for adoptive cell transfer therapy in the WAVE(R) bioreactor. *J Transl Med* **2012**, 10, 69.

46. Chorny, M.; Alferiev, I. S.; Fishbein, I.; Tengood, J. E.; Folchman-Wagner, Z.; Forbes, S. P.; Levy, R. J., Formulation and in vitro characterization of composite biodegradable magnetic nanoparticles for magnetically guided cell delivery. *Pharm Res* **2012**, 29, 1232-1241.

47. Schlorf, T.; Meincke, M.; Kossel, E.; Gluer, C. C.; Jansen, O.; Mentlein, R., Biological properties of iron oxide nanoparticles for cellular and molecular magnetic resonance imaging. *Int J Mol Sci* **2010**, 12, 12-23.

48. Shimizu, K.; Ito, A.; Arinobe, M.; Murase, Y.; Iwata, Y.; Narita, Y.; Kagami, H.; Ueda, M.; Honda, H., Effective cell-seeding technique using magnetite nanoparticles and magnetic force onto decellularized blood vessels for vascular tissue engineering. *J Biosci Bioeng* **2007**, 103, 472-478.

49. Sykova, E.; Jendelova, P.; Herynek, V., MR tracking of stem cells in living recipients. *Methods Mol Biol* **2009**, 549, 197-215.

50. Arbab, A. S.; Jordan, E. K.; Wilson, L. B.; Yocum, G. T.; Lewis, B. K.; Frank, J. A., In vivo trafficking and targeted delivery of magnetically labeled stem cells. *Hum Gene Ther* **2004**, 15, 351-360.

51. Muthana, M.; Scott, S. D.; Farrow, N.; Morrow, F.; Murdoch, C.; Grubb, S.; Brown, N.; Dobson, J.; Lewis, C. E., A novel magnetic approach to enhance the efficacy of cell-based gene therapies. *Gene Ther* **2008**, 15, 902-910.

52. Sokolov, K.; Follen, M.; Aaron, J.; Pavlova, I.; Malpica, A.; Lotan, R.; Richards-Kortum, R., Real-time vital optical imaging of precancer using anti-epidermal growth factor receptor antibodies conjugated to gold nanoparticles. *Cancer Res* **2003**, 63, 1999-2004.

53. Aaron, J.; Nitin, N.; Travis, K.; Kumar, S.; Collier, T.; Park, S. Y.; Jose-Yacaman, M.; Coghlan, L.; Follen, M.; Richards-Kortum, R.; Sokolov, K., Plasmon resonance coupling of metal nanoparticles for molecular imaging of carcinogenesis in vivo. *Journal of Biomedical Optics* **2007**, 12, 034007.

54. Ricles, L. M.; Nam, S. Y.; Sokolov, K.; Emelianov, S. Y.; Suggs, L. J., Function of mesenchymal stem cells following loading of gold nanotracers. *Int J Nanomedicine* **2011**, 6, 407-416.

55. Chung, E.; Nam, S. Y.; Ricles, L. M.; Emelianov, S. Y.; Suggs, L. J., Evaluation of gold nanotracers to track adipose-derived stem cells in a PEGylated fibrin gel for dermal tissue engineering applications. *Int J Nanomedicine* **2013**, 8, 325-336.

56. Grutzkau, A.; Radbruch, A., Small but mighty: how the MACS-technology based on nanosized superparamagnetic particles has helped to analyze the immune system within the last 20 years. *Cytometry A* **2010**, 77, 643-647.

57. Sachlos, E.; Risueno, R. M.; Laronde, S.; Shapovalova, Z.; Lee, J. H.; Russell, J.; Malig, M.; McNicol, J. D.; Fiebig-Comyn, A.; Graham, M.; Levadoux-Martin, M.; Lee, J. B.; Giacomelli, A. O.; Hassell, J. A.; Fischer-Russell, D.; Trus, M. R.; Foley, R.; Leber, B.; Xenocostas, A.; Brown, E. D.; Collins, T. J.; Bhatia, M., Identification of drugs including a dopamine receptor antagonist that selectively target cancer stem cells. *Cell* **2012**, 149, 1284-1297.

58. Anton, N.; Benoit, J. P.; Saulnier, P., Design and production of nanoparticles formulated from nano-emulsion templates-a review. *J Control Release* **2008**, 128, 185-199.

59. Shukla, R.; Bansal, V.; Chaudhary, M.; Basu, A.; Bhonde, R. R.; Sastry, M., Biocompatibility of gold nanoparticles and their endocytotic fate inside the cellular compartment: a microscopic overview. *Langmuir* **2005**, 21, 10644-10654.

60. Sun, J.; Zhou, S.; Hou, P.; Yang, Y.; Weng, J.; Li, X.; Li, M., Synthesis and characterization of biocompatible Fe3O4 nanoparticles. *J Biomed Mater Res A* **2007**, 80, 333-341.

61. Joshi, P. P.; Yoon, S. J.; Hardin, W. G.; Emelianov, S.; Sokolov, K. V., Conjugation of antibodies to gold nanorods through Fc portion: synthesis and molecular specific imaging. *Bioconjugate chemistry* **2013**, 24, 878-888.

62. O'Neal, D. P.; Hirsch, L. R.; Halas, N. J.; Payne, J. D.; West, J. L., Photo-thermal tumor ablation in mice using near infrared-absorbing nanoparticles. *Cancer Lett* **2004**, 209, 171-176.

63. Zheng, S.; Shen, Y.; Song, Y.; Yuan, Y., How to detour Treg cells in T cell-based antitumor immune therapy. *Onco Targets Ther* **2013**, 6, 1243-1247.

Chapter 5: Conclusions and Future Work

5.1 Conclusions

In Chapter 2, an immunotargeted magneto-plasmonic nanoparticle platform was created. The unique feature of the platform is the synthesis of magneto-plasmonic nanoparticles of various sizes from primary blocks which also have magneto-plasmonic characteristics. This platform yields nanoparticles with a high density of magnetic and plasmonic functionalities which are uniformly distributed throughout the nanoparticle volume. The dense packing of primary particles does not change their superparamagnetic behavior; however, the close proximity of the constituent particles in the nanoclusters leads to a greatly improved response to an external magnetic field and strong near-infrared plasmon resonances. Thus, our approach provides the combination of the tunability of magnetic moment without sacrificing superparamagnetic properties and strong visible-NIR absorbance, thus addressing many of the major limitations of previous synthetic methods. Furthermore, the hybrid nanoparticles can be easily functionalized by attaching antibodies through the Fc moiety leaving the Fab portion that is responsible for antigen binding available for targeting. We also demonstrated that the choice of the suitable surfactant in synthesis of the magneto-plasmonic nanoparticles and subsequent surface modification with PEG molecules are both important steps in producing biocompatible nanoconstructs.

In Chapter 3, we utilized the immunotargeted magneto-plasmonic nanoparticle platform for labeling of rare cancer cells in the whole blood. The combination of nanocarriers and a magnetic microfluidic chip allows highly efficient capture, enumeration and molecular characterization of CTCs. Our platform provides flexibility in capturing phenotypically different CTCs by using nanocarriers that are targeted to different molecular tumor biomarkers; this can significantly improve the effectiveness of

CTC assays. Furthermore, the use of targeted nanoparticles allows a straightforward extension to multiplexed approaches where capture of cancer cells is carried out by a mixture of nanoparticles with different target specificities. Experiments in whole blood showed capture efficiency greater than 90% when two cancer biomarkers are used for cell capture. In addition, we explored the feasibility of PA imaging to detect CTCs in whole blood. We demonstrated excellent detection sensitivity delineating the distribution of hybrid nanoclusters targeting the cancer cells on a porous membrane. The work paved the way for a novel and efficient CTC assay which utilizes immunotargeted magneto-plasmonic nanoclusters for a simultaneous magnetic capture and PA detection of CTCs.

In Chapter 4, we demonstrated a concept to mediate immune cells with magnetic properties and a magnetic field to improve cellular delivery for immunotherapy of cancer. We showed that the immune cells were well labeled by our nanoparticle platform based either cellular internalization or selective surface targeting approach. None of the nanoparticle labeling approaches induced noticeable cytotoxic to immune cells. The magnetically engineered cells can be trafficked with an aid of a magnetic field. Thus, our results highlight the promise of using our nanoparticle platform as a multifunctional probe to manipulate and track the transferred immune cells *in vivo* and encourage further evaluation of therapeutic efficacy in the magnet-guided cellular immunotherapy.

5.2 FUTURE WORK

Targeted metal nanoparticles for imaging and delivery are designed to interact with specific subsets of cells. It is important to ensure that these nanoparticles are not causing long-term toxicity.[1,2] As gold nanoparticles are barely biodegradable, they may cause concerns about clinical translation. FDA mandates that contrast agents should be cleared in a reasonable time.[1] Therefore, one of the future works is to modify the

synthetic chemistry of our hybrid nanoparticle platform for efficient body clearance. Several studies indicate that the nanoparticles less than 6 nm in diameter can be efficiently cleared.[1, 3, 4] This is encouraging for us because the size of constituent nanoparticles for building the hybrid nanoparticle platform is in the same range. The nanocluster formation can be aided by the use of weakly adsorbing biodegradable polymers that allows the control of nanocluster size and the enhancement of magnetic and optical functionalities.[5] The biodegradable polymer stabilizer can degrade over time under physiological conditions which leads to disassembly of nanoclusters into sub-6 nm constituent nanoparticles[6], thus holding the promise for efficient body clearance.

The high sensitivity of PA imaging enables a new method to detect CTC; however, this method should be further tested its accuracy which can be carried out by comparison with the current standard detection based on immunofluorescence staining. Specifically, the samples can be divided into two groups: half of the samples will be examined under PA imaging, whereas the other half of the samples will be stained with DAPI, CD45, and CK and observed under fluorescent microscope. The accuracy can be determined by comparing the counts of CTCs from PA detection and fluorescent staining. Furthermore, lower CTC number, e.g. 1-5 cells per mL blood, is necessary to test detection efficiency.[7] Ultimately, creating a special magnetic microchip designed for simultaneous magnet capture and PA detection would be beneficial for a highly sensitive, low cost, facile CTC assay. The design of the microchip will include a fluidic chamber which accommodates a porous array at the bottom. The size of the holes should be larger than the nanoparticles but smaller the targeted cells. With a magnet field gradient applied to the chamber, targeted cells can be retained in the chip whereas the free nanoparticles will be filtered out through the pores and unlabeled cells will be washed away. Then, the captured CTCs can be detected using PA imaging through an acoustically transparent

window on the top of the flow chamber. Signal intensity from PA imaging and size/shape of identified objects will be used as discriminative parameters in recognizing and counting labeled cancer cells. After PA imaging, CTCs can be collected through the outlet after removal of the magnet for downstream molecular analyses.

A new magnetic approach to enhance cell delivery of immunotherapy of cancer has been proposed to overcome the poor homing efficiency of transferred cells. A series of *in vitro* experiments demonstrated highly magnet-controlled manipulation of labeled immune cells. However, a systemic *in vivo* evaluation will be needed to validate the feasibility of this magnetic approach under more sophisticated physiological conditions. Furthermore, the trafficking of the labeled immune cells *in vivo* can be monitored by a variety of imaging modalities, such as photoacoustic imaging, MRI, or X-ray imaging, since the hybrid nanoparticles provide very good contrast for them. Ultimately, the magnetic approach should be investigated whether the enhancement of cytotoxic T lymphocyte recruitment can be exploited as a fatal attraction for tumor therapy.

5.3 REFERENCES

1. Choi, H. S.; Liu, W.; Misra, P.; Tanaka, E.; Zimmer, J. P.; Ipe, B. I.; Bawendi, M. G.; Frangioni, J. V., Renal clearance of quantum dots. *Nature biotechnology* **2007**, 25, 1165-1170.

2. Lewinski, N.; Colvin, V.; Drezek, R., Cytotoxicity of nanoparticles. *Small* **2008**, 4, 26-49.

3. Chithrani, B. D.; Ghazani, A. A.; Chan, W. C., Determining the size and shape dependence of gold nanoparticle uptake into mammalian cells. *Nano Lett* **2006**, 6, 662-668.

4. Zhou, C.; Long, M.; Qin, Y.; Sun, X.; Zheng, J., Luminescent gold nanoparticles with efficient renal clearance. *Angewandte Chemie* **2011**, 123, 3226-3230.

5. Tam, J. M.; Tam, J. O.; Murthy, A.; Ingram, D. R.; Ma, L. L.; Travis, K.; Johnston, K. P.; Sokolov, K. V., Controlled assembly of biodegradable plasmonic nanoclusters for near-infrared imaging and therapeutic applications. *ACS nano* **2010**, 4, 2178-2184.

6. Murthy, A. K.; Stover, R. J.; Borwankar, A. U.; Nie, G. D.; Gourisankar, S.; Truskett, T. M.; Sokolov, K. V.; Johnston, K. P., Equilibrium gold nanoclusters quenched with biodegradable polymers. *ACS Nano* **2013**, 7, 239-251.

7. Cristofanilli, M.; Hayes, D. F.; Budd, G. T.; Ellis, M. J.; Stopeck, A.; Reuben, J. M.; Doyle, G. V.; Matera, J.; Allard, W. J.; Miller, M. C.; Fritsche, H. A.; Hortobagyi, G. N.; Terstappen, L. W., Circulating tumor cells: a novel prognostic factor for newly diagnosed metastatic breast cancer. *Journal of Clinical Oncology* **2005**, 23, 1420-1430.

References

Aaron, J.; Nitin, N.; Travis, K.; Kumar, S.; Collier, T.; Park, S. Y.; Jose-Yacaman, M.; Coghlan, L.; Follen, M.; Richards-Kortum, R.; Sokolov, K., Plasmon resonance coupling of metal nanoparticles for molecular imaging of carcinogenesis in vivo. *Journal of Biomedical Optics* 2007, 12, 034007.

Aaron, J.; Travis, K.; Harrison, N.; Sokolov, K., Dynamic Imaging of Molecular Assemblies in Live Cells Based on Nanoparticle Plasmon Resonance Coupling. Nano Letters 2009, 9, 3612-3618.

Aaron, J. S.; Oh, J.; Larson, T. A.; Kumar, S.; Milner, T. E.; Sokolov, K. V., Increased optical contrast in imaging of epidermal growth factor receptor using magnetically actuated hybrid gold/iron oxide nanoparticles. Optics express 2006, 14, 12930-12943.

Aktas, B.; Tewes, M.; Fehm, T.; Hauch, S.; Kimmig, R.; Kasimir-Bauer, S., Stem cell and epithelial-mesenchymal transition markers are frequently overexpressed in circulating tumor cells of metastatic breast cancer patients. Breast Cancer Research and Treatment 2009, 11, R46.

Alkilany, A. M.; Nagaria, P. K.; Hexel, C. R.; Shaw, T. J.; Murphy, C. J.; Wyatt, M. D., Cellular uptake and cytotoxicity of gold nanorods: molecular origin of cytotoxicity and surface effects. Small 2009, 5, 701-708.

Allard, W. J.; Matera, J.; Miller, M. C.; Repollet, M.; Connelly, M. C.; Rao, C.; Tibbe, A. G.; Uhr, J. W.; Terstappen, L. W., Tumor cells circulate in the peripheral blood of all major carcinomas but not in healthy subjects or patients with nonmalignant diseases. Clin Cancer Res 2004, 10, 6897-6904.

Anker, J. N.; Hall, W. P.; Lyandres, O.; Shah, N. C.; Zhao, J.; Van Duyne, R. P., Biosensing with plasmonic nanosensors. Nature Materials 2008, 7, 442-453.

Anton, N.; Benoit, J. P.; Saulnier, P., Design and production of nanoparticles formulated from nano-emulsion templates-a review. J Control Release 2008, 128, 185-199.

Arbab, A. S.; Jordan, E. K.; Wilson, L. B.; Yocum, G. T.; Lewis, B. K.; Frank, J. A., In vivo trafficking and targeted delivery of magnetically labeled stem cells. Hum Gene Ther 2004, 15, 351-360.

Bai, F.; Wang, D.; Huo, Z.; Chen, W.; Liu, L.; Liang, X.; Chen, C.; Wang, X.; Peng, Q.; Li, Y., A Versatile Bottom-up Assembly Approach to Colloidal Spheres from Nanocrystals. Angewandte Chemie International Edition 2007, 46, 6650-6653.

Barcikowski, S.; Compagnini, G., Advanced nanoparticle generation and excitation by lasers in liquids. Physical chemistry chemical physics: PCCP 2013, 15, 3022-3026.

Bear, A. S.; Cruz, C. R.; Foster, A. E., T cells as vehicles for cancer vaccination. J Biomed Biotechnol 2011, 417403.

Berry, D. A.; Cronin, K. A.; Plevritis, S. K.; Fryback, D. G.; Clarke, L.; Zelen, M.; Mandelblatt, J. S.; Yakovlev, A. Y.; Habbema, J. D.; Feuer, E. J., Effect of screening and adjuvant therapy on mortality from breast cancer. N Engl J Med 2005, 353, 1784-1792.

Bigall, N. C.; Parak, W. J.; Dorfs, D., Fluorescent, magnetic and plasmonic—Hybrid multifunctional colloidal nano objects. Nano Today 2012, 7, 282-296.

Blattman, J. N.; Greenberg, P. D., Cancer immunotherapy: a treatment for the masses. Science 2004, 305, 200-205.

Bobbitt, J. M., Periodate Oxidation of Carbohydrates. Adv Carbohydr Chem 1956, 11, 1-41.

Bobisse, S.; Rondina, M.; Merlo, A.; Tisato, V.; Mandruzzato, S.; Amendola, M.; Naldini, L.; Willemsen, R. A.; Debets, R.; Zanovello, P.; Rosato, A., Reprogramming T lymphocytes for melanoma adoptive immunotherapy by T-cell receptor gene transfer with lentiviral vectors. Cancer Res 2009, 69, 9385-9394.

Bogart, L. K.; Pourroy, G.; Murphy, C. J.; Puntes, V.; Pellegrino, T.; Rosenblum, D.; Peer, D.; Levy, R., Nanoparticles for imaging, sensing, and therapeutic intervention. ACS Nano 2014, 8, 3107-3122.

Carelle, N.; Piotto, E.; Bellanger, A.; Germanaud, J.; Thuillier, A.; Khayat, D., Changing patient perceptions of the side effects of cancer chemotherapy. Cancer 2002, 95, 155-163.

Casanovas, O.; Hicklin, D. J.; Bergers, G.; Hanahan, D., Drug resistance by evasion of antiangiogenic targeting of VEGF signaling in late-stage pancreatic islet tumors. Cancer Cell 2005, 8, 299-309.

Cheng, K.; Malliaras, K.; Li, T. S.; Sun, B.; Houde, C.; Galang, G.; Smith, J.; Matsushita, N.; Marban, E., Magnetic enhancement of cell retention, engraftment, and functional benefit after intracoronary delivery of cardiac-derived stem cells in a rat model of ischemia/reperfusion. Cell Transplant 2012, 21, 1121-1135.

Chithrani, B. D.; Ghazani, A. A.; Chan, W. C., Determining the size and shape dependence of gold nanoparticle uptake into mammalian cells. Nano Lett 2006, 6, 662-668.

Choi, H. S.; Liu, W.; Misra, P.; Tanaka, E.; Zimmer, J. P.; Ipe, B. I.; Bawendi, M. G.; Frangioni, J. V., Renal clearance of quantum dots. Nature biotechnology 2007, 25, 1165-1170.

Chorny, M.; Alferiev, I. S.; Fishbein, I.; Tengood, J. E.; Folchman-Wagner, Z.; Forbes, S. P.; Levy, R. J., Formulation and in vitro characterization of composite biodegradable magnetic nanoparticles for magnetically guided cell delivery. Pharm Res 2012, 29, 1232-1241.

Chung, E.; Nam, S. Y.; Ricles, L. M.; Emelianov, S. Y.; Suggs, L. J., Evaluation of gold nanotracers to track adipose-derived stem cells in a PEGylated fibrin gel for dermal tissue engineering applications. Int J Nanomedicine 2013, 8, 325-336.

Colombo, M.; Carregal-Romero, S.; Casula, M. F.; Gutierrez, L.; Morales, M. P.; Bohm, I. B.; Heverhagen, J. T.; Prosperi, D.; Parak, W. J., Biological applications of magnetic nanoparticles. Chem Soc Rev 2012, 41, 4306-4334.

Cook, J. R.; Bouchard, R. R.; Emelianov, S. Y., Tissue-mimicking phantoms for photoacoustic and ultrasonic imaging. Biomed Opt Express 2011, 2, 3193-3206.

Cook, J. R.; Frey, W.; Emelianov, S., Quantitative photoacoustic imaging of nanoparticles in cells and tissues. ACS Nano 2013, 7, 1272-1280.

Coumans, F. A.; Doggen, C. J.; Attard, G.; de Bono, J. S.; Terstappen, L. W., All circulating EpCAM+CK+CD45- objects predict overall survival in castration-resistant prostate cancer. Annals of Oncology 2010, 21, 1851-1857.

Crisan, D.; Ruark, D. S.; Decker, D. A.; Drevon, A. M.; Dicarlo, R. G., Detection of circulating epithelial cells after surgery for benign breast disease. Mol Diagn 2000, 5, 33-38.

Cristofanilli, M.; Budd, G. T.; Ellis, M. J.; Stopeck, A.; Matera, J.; Miller, M. C.; Reuben, J. M.; Doyle, G. V.; Allard, W. J.; Terstappen, L. W.; Hayes, D. F., Circulating tumor cells, disease progression, and survival in metastatic breast cancer. New England Journal of Medicine 2004, 351, 781-791.

Cristofanilli, M.; Hayes, D. F.; Budd, G. T.; Ellis, M. J.; Stopeck, A.; Reuben, J. M.; Doyle, G. V.; Matera, J.; Allard, W. J.; Miller, M. C.; Fritsche, H. A.; Hortobagyi, G. N.; Terstappen, L. W., Circulating tumor cells: a novel prognostic factor for newly diagnosed metastatic breast cancer. Journal of Clinical Oncology 2005, 23, 1420-1430.

Crow, M. J.; Seekell, K.; Ostrander, J. H.; Wax, A., Monitoring of Receptor Dimerization Using Plasmonic Coupling of Gold Nanoparticles. ACS Nano 2011, 5, 8532-8540.

Delaney, G.; Jacob, S.; Featherstone, C.; Barton, M., The role of radiotherapy in cancer treatment: estimating optimal utilization from a review of evidence-based clinical guidelines. Cancer 2005, 104, 1129-1137.

Desitter, I.; Guerrouahen, B. S.; Benali-Furet, N.; Wechsler, J.; Janne, P. A.; Kuang, Y.; Yanagita, M.; Wang, L.; Berkowitz, J. A.; Distel, R. J.; Cayre, Y. E., A new device for rapid isolation by size and characterization of rare circulating tumor cells. Anticancer Res 2011, 31, 427-441.

DeVries, G. A.; Brunnbauer, M.; Hu, Y.; Jackson, A. M.; Long, B.; Neltner, B. T.; Uzun, O.; Wunsch, B. H.; Stellacci, F., Divalent metal nanoparticles. Science 2007, 315, 358-361.

Devriese, L. A.; Voest, E. E.; Beijnen, J. H.; Schellens, J. H., Circulating tumor cells as pharmacodynamic biomarker in early clinical oncological trials. Cancer Treatment Reviews 2011, 37, 579-589.

Doane, T. L.; Burda, C., The unique role of nanoparticles in nanomedicine: imaging, drug delivery and therapy. Chem Soc Rev 2012, 41, 2885-2911.

Dreaden, E. C.; Alkilany, A. M.; Huang, X.; Murphy, C. J.; El-Sayed, M. A., The golden age: gold nanoparticles for biomedicine. Chem Soc Rev 2012, 41, 2740-2779.

Dudley, M. E.; Wunderlich, J. R.; Yang, J. C.; Sherry, R. M.; Topalian, S. L.; Restifo, N. P.; Royal, R. E.; Kammula, U.; White, D. E.; Mavroukakis, S. A.; Rogers, L. J.;

Gracia, G. J.; Jones, S. A.; Mangiameli, D. P.; Pelletier, M. M.; Gea-Banacloche, J.; Robinson, M. R.; Berman, D. M.; Filie, A. C.; Abati, A.; Rosenberg, S. A., Adoptive cell transfer therapy following non-myeloablative but lymphodepleting chemotherapy for the treatment of patients with refractory metastatic melanoma. J Clin Oncol 2005, 23, 2346-2357.

Dudley, M. E.; Yang, J. C.; Sherry, R.; Hughes, M. S.; Royal, R.; Kammula, U.; Robbins, P. F.; Huang, J.; Citrin, D. E.; Leitman, S. F.; Wunderlich, J.; Restifo, N. P.; Thomasian, A.; Downey, S. G.; Smith, F. O.; Klapper, J.; Morton, K.; Laurencot, C.; White, D. E.; Rosenberg, S. A., Adoptive cell therapy for patients with metastatic melanoma: evaluation of intensive myeloablative chemoradiation preparative regimens. J Clin Oncol 2008, 26, 5233-5239.

Emelianov, S. Y.; Li, P. C.; O'Donnell, M., Photoacoustics for molecular imaging and therapy. Phys Today 2009, 62, 34-39.

Esmaeilsabzali, H.; Beischlag, T. V.; Cox, M. E.; Parameswaran, A. M.; Park, E. J., Detection and isolation of circulating tumor cells: Principles and methods. Biotechnol Adv 2013, 31, 1063-1084.

Etzioni, R.; Tsodikov, A.; Mariotto, A.; Szabo, A.; Falcon, S.; Wegelin, J.; DiTommaso, D.; Karnofski, K.; Gulati, R.; Penson, D. F.; Feuer, E., Quantifying the role of PSA screening in the US prostate cancer mortality decline. Cancer Causes Control 2008, 19, 175-181.

Farokhzad, O. C.; Langer, R., Impact of nanotechnology on drug delivery. ACS Nano 2009, 3, 16-20.

Figueras, J.; Torras, J.; Valls, C.; Llado, L.; Ramos, E.; Marti-Rague, J.; Serrano, T.; Fabregat, J., Surgical resection of colorectal liver metastases in patients with expanded indications: a single-center experience with 501 patients. Dis Colon Rectum 2007, 50, 478-488.

Fisher, B.; Packard, B. S.; Read, E. J.; Carrasquillo, J. A.; Carter, C. S.; Topalian, S. L.; Yang, J. C.; Yolles, P.; Larson, S. M.; Rosenberg, S. A., Tumor localization of adoptively transferred indium-111 labeled tumor infiltrating lymphocytes in patients with metastatic melanoma. J Clin Oncol 1989, 7, 250-261.

Galanzha, E. I.; Shashkov, E. V.; Kelly, T.; Kim, J.-W.; Yang, L.; Zharov, V. P., In vivo

magnetic enrichment and multiplex photoacoustic detection of circulating tumour cells. Nature nanotechnology 2009, 4, 855-860.

Gallo, J.; Long, N. J.; Aboagye, E. O., Magnetic nanoparticles as contrast agents in the diagnosis and treatment of cancer. Chem Soc Rev 2013, 42, 7816-7833.

Gasparovic, C.; Matwiyoff, N. A., The magnetic properties and water dynamics of the red blood cell: a study by proton-NMR lineshape analysis. Magn Reson Med 1992, 26, 274-299.

Gautier, J.; Allard-Vannier, E.; Herve-Aubert, K.; Souce, M.; Chourpa, I., Design strategies of hybrid metallic nanoparticles for theragnostic applications. Nanotechnology 2013, 24, 432002.

Gerber, D. E.; Schiller, J. H., Maintenance chemotherapy for advanced non-small-cell lung cancer: new life for an old idea. J Clin Oncol 2013, 31, 1009-1020.

Gerges, N.; Rak, J.; Jabado, N., New technologies for the detection of circulating tumour cells. Br Med Bull 2010, 94, 49-64.

Giuliano, M.; Giordano, A.; Jackson, S.; Hess, K. R.; De Giorgi, U.; Mego, M.; Handy, B. C.; Ueno, N. T.; Alvarez, R. H.; De Laurentiis, M.; De Placido, S.; Valero, V.; Hortobagyi, G. N.; Reuben, J. M.; Cristofanilli, M., Circulating tumor cells as prognostic and predictive markers in metastatic breast cancer patients receiving first-line systemic treatment. Breast Cancer Res 2011, 13, R67.

Grutzkau, A.; Radbruch, A., Small but mighty: how the MACS-technology based on nanosized superparamagnetic particles has helped to analyze the immune system within the last 20 years. Cytometry A 2010, 77, 643-647.

Hanahan, D.; Weinberg, R. A., Hallmarks of cancer: the next generation. Cell 2011, 144, 646-674.

Hartono, S. B.; Gu, W.; Kleitz, F.; Liu, J.; He, L.; Middelberg, A. P.; Yu, C.; Lu, G. Q.; Qiao, S. Z., Poly-L-lysine functionalized large pore cubic mesostructured silica nanoparticles as biocompatible carriers for gene delivery. ACS Nano 2012, 6, 2104-2117.

Henry, M. D.; Wen, S.; Silva, M. D.; Chandra, S.; Milton, M.; Worland, P. J., A prostate-specific membrane antigen-targeted monoclonal antibody-chemotherapeutic

conjugate designed for the treatment of prostate cancer. Cancer Res 2004, 64, 7995-8001.

Hermanson, G. T., BioConjugate Techniques: 2nd Edition. 1996, 761-764.

Hirsch, L. R.; Stafford, R. J.; Bankson, J. A.; Sershen, S. R.; Rivera, B.; Price, R. E.; Hazle, J. D.; Halas, N. J.; West, J. L., Nanoshell-mediated near-infrared thermal therapy of tumors under magnetic resonance guidance. Proc Natl Acad Sci U S A 2003, 100, 13549-13554.

Hofmann, A.; Wenzel, D.; Becher, U. M.; Freitag, D. F.; Klein, A. M.; Eberbeck, D.; Schulte, M.; Zimmermann, K.; Bergemann, C.; Gleich, B.; Roell, W.; Weyh, T.; Trahms, L.; Nickenig, G.; Fleischmann, B. K.; Pfeifer, A., Combined targeting of lentiviral vectors and positioning of transduced cells by magnetic nanoparticles. Proc Natl Acad Sci U S A 2009, 106, 44-49.

Hoshino, K.; Chen, P.; Huang, Y.-Y.; Zhang, X., Computational Analysis of Microfluidic Immunomagnetic Rare Cell Separation from a Particulate Blood Flow. Analytical Chemistry 2012, 84, 4292-4299.

Hoshino, K.; Huang, Y. Y.; Lane, N.; Huebschman, M.; Uhr, J. W.; Frenkel, E. P.; Zhang, X., Microchip-based immunomagnetic detection of circulating tumor cells. Lab on a Chip 2011, 11, 3449-3457.

Hu, X.; Wei, C. W.; Xia, J.; Pelivanov, I.; O'Donnell, M.; Gao, X., Trapping and Photoacoustic Detection of CTCs at the Single Cell per Milliliter Level with Magneto–Optical Coupled Nanoparticles. Small 2013, 9, 2046-2052.

Huang, K.; Ma, H.; Liu, J.; Huo, S.; Kumar, A.; Wei, T.; Zhang, X.; Jin, S.; Gan, Y.; Wang, P. C.; He, S.; Zhang, X.; Liang, X. J., Size-dependent localization and penetration of ultrasmall gold nanoparticles in cancer cells, multicellular spheroids, and tumors in vivo. ACS Nano 2012, 6, 4483-4493.

Ito, A.; Kuga, Y.; Honda, H.; Kikkawa, H.; Horiuchi, A.; Watanabe, Y.; Kobayashi, T., Magnetite nanoparticle-loaded anti-HER2 immunoliposomes for combination of antibody therapy with hyperthermia. Cancer Lett 2004, 212, 167-175.

Jain, P. K.; Huang, X.; El-Sayed, I. H.; El-Sayed, M. A., Noble metals on the nanoscale: optical and photothermal properties and some applications in imaging, sensing,

biology, and medicine. Acc Chem Res 2008, 41, 1578-1586.

Jin, Y.; Jia, C.; Huang, S.-W.; O'Donnell, M.; Gao, X., Multifunctional nanoparticles as coupled contrast agents. Nat Commun 2010, 1, 41.

Jing, Y.; Moore, L. R.; Williams, P. S.; Chalmers, J. J.; Farag, S. S.; Bolwell, B.; Zborowski, M., Blood progenitor cell separation from clinical leukapheresis product by magnetic nanoparticle binding and magnetophoresis. Biotechnol Bioeng 2007, 96, 1139-1154.

Joshi, P. P.; Yoon, S. J.; Hardin, W. G.; Emelianov, S.; Sokolov, K. V., Conjugation of antibodies to gold nanorods through Fc portion: synthesis and molecular specific imaging. Bioconjugate chemistry 2013, 24, 878-888.

June, C. H., Principles of adoptive T cell cancer therapy. J Clin Invest 2007, 117, 1204-1212.

June, C. H., Adoptive T cell therapy for cancer in the clinic. J Clin Invest 2007, 117, 1466-1476.

Kalos, M.; Levine, B. L.; Porter, D. L.; Katz, S.; Grupp, S. A.; Bagg, A.; June, C. H., T cells with chimeric antigen receptors have potent antitumor effects and can establish memory in patients with advanced leukemia. Science translational medicine 2011, 3, 95ra73-95ra73.

Kamei, G.; Kobayashi, T.; Ohkawa, S.; Kongcharoensombat, W.; Adachi, N.; Takazawa, K.; Shibuya, H.; Deie, M.; Hattori, K.; Goldberg, J. L.; Ochi, M., Articular cartilage repair with magnetic mesenchymal stem cells. Am J Sports Med 2013, 41, 1255-1264.

Kershaw, M. H.; Westwood, J. A.; Slaney, C. Y.; Darcy, P. K., Clinical application of genetically modified T cells in cancer therapy. Clinical & Translational Immunology 2014, 3, e16.

Khlebtsov, B.; Zharov, V.; Melnikov, A.; Tuchin, V.; Khlebtsov, N., Optical amplification of photothermal therapy with gold nanoparticles and nanoclusters. Nanotechnology 2006, 17, 5167.

Kobayashi, S.; Boggon, T. J.; Dayaram, T.; Janne, P. A.; Kocher, O.; Meyerson, M.; Johnson, B. E.; Eck, M. J.; Tenen, D. G.; Halmos, B., EGFR mutation and resistance

of non-small-cell lung cancer to gefitinib. N Engl J Med 2005, 352, 786-792.

Kohn, D. B.; Dotti, G.; Brentjens, R.; Savoldo, B.; Jensen, M.; Cooper, L. J. N.; June, C. H.; Rosenberg, S.; Sadelain, M.; Heslop, H. E., CARs on Track in the Clinic: Workshop of the Blood and Marrow Transplant Clinical Trials Network Subcommittee on Cell and Gene Therapy Washington DC, 18 May 2010. Molecular Therapy 2011, 19, 432.

Kreibig, U.; Vollmer, M., Optical properties of metal clusters. Springer: Berlin ; New York, 1995.

Kumar, S.; Aaron, J.; Sokolov, K. V., Directional conjugation of antibodies to nanoparticles for synthesis of multiplexed optical contrast agents with both delivery and targeting moieties. Nature Protocols 2008, 3, 314-320.

Kumar, S.; Harrison, N.; Richards-Kortum, R.; Sokolov, K., Plasmonic Nanosensors for Imaging Intracellular Biomarkers in Live Cells. Nano Letters 2007, 7, 1338-1343.

Landazuri, N.; Tong, S.; Suo, J.; Joseph, G.; Weiss, D.; Sutcliffe, D. J.; Giddens, D. P.; Bao, G.; Taylor, W. R., Magnetic targeting of human mesenchymal stem cells with internalized superparamagnetic iron oxide nanoparticles. Small 2013, 9, 4017-4026.

Larson, T. A.; Bankson, J.; Aaron, J.; Sokolov, K., Hybrid plasmonic magnetic nanoparticles as molecular specific agents for MRI/optical imaging and photothermal therapy of cancer cells. Nanotechnology 2007, 18, 325101.

Lawrence, M. B.; Springer, T. A., Leukocytes roll on a selectin at physiologic flow rates: distinction from and prerequisite for adhesion through integrins. Cell 1991, 65, 859-873.

Laxman, B.; Morris, D. S.; Yu, J.; Siddiqui, J.; Cao, J.; Mehra, R.; Lonigro, R. J.; Tsodikov, A.; Wei, J. T.; Tomlins, S. A.; Chinnaiyan, A. M., A first-generation multiplex biomarker analysis of urine for the early detection of prostate cancer. Cancer Research 2008, 68, 645-649.

Lee, H.; Lee, E.; Kim do, K.; Jang, N. K.; Jeong, Y. Y.; Jon, S., Antibiofouling polymer-coated superparamagnetic iron oxide nanoparticles as potential magnetic resonance contrast agents for in vivo cancer imaging. Journal of the American Chemical Society 2006, 128, 7383-7389.

Lewinski, N.; Colvin, V.; Drezek, R., Cytotoxicity of nanoparticles. Small 2008, 4, 26-49.

Luhmann, T.; Rimann, M.; Bittermann, A. G.; Hall, H., Cellular uptake and intracellular pathways of PLL-g-PEG-DNA nanoparticles. Bioconjug Chem 2008, 19, 1907-1916.

Mallidi, S.; Larson, T.; Aaron, J.; Sokolov, K.; Emelianov, S., Molecular specific optoacoustic imaging with plasmonic nanoparticles. Opt Express 2007, 15, 6583-6588.

Malviya, G.; Nayak, T. K., PET imaging to monitor cancer therapy. Curr Pharm Biotechnol 2013, 14, 669-682.

Meng, S.; Tripathy, D.; Shete, S.; Ashfaq, R.; Saboorian, H.; Haley, B.; Frenkel, E.; Euhus, D.; Leitch, M.; Osborne, C.; Clifford, E.; Perkins, S.; Beitsch, P.; Khan, A.; Morrison, L.; Herlyn, D.; Terstappen, L. W.; Lane, N.; Wang, J.; Uhr, J., uPAR and HER-2 gene status in individual breast cancer cells from blood and tissues. Proceedings of the National Academy of Sciences of the United States of America 2006, 103, 17361-17365.

Metz, S.; Bonaterra, G.; Rudelius, M.; Settles, M.; Rummeny, E. J.; Daldrup-Link, H. E., Capacity of human monocytes to phagocytose approved iron oxide MR contrast agents in vitro. Eur Radiol 2004, 14, 1851-1858.

Mostert, B.; Kraan, J.; Bolt-de Vries, J.; van der Spoel, P.; Sieuwerts, A. M.; Schutte, M.; Timmermans, A. M.; Foekens, R.; Martens, J. W.; Gratama, J. W.; Foekens, J. A.; Sleijfer, S., Detection of circulating tumor cells in breast cancer may improve through enrichment with anti-CD146. Breast Cancer Research and Treatment 2011, 127, 33-41.

Murthy, A. K.; Stover, R. J.; Borwankar, A. U.; Nie, G. D.; Gourisankar, S.; Truskett, T. M.; Sokolov, K. V.; Johnston, K. P., Equilibrium gold nanoclusters quenched with biodegradable polymers. ACS Nano 2013, 7, 239-251.

Muthana, M.; Scott, S. D.; Farrow, N.; Morrow, F.; Murdoch, C.; Grubb, S.; Brown, N.; Dobson, J.; Lewis, C. E., A novel magnetic approach to enhance the efficacy of cell-based gene therapies. Gene Ther 2008, 15, 902-910.

Muul, L. M.; Spiess, P. J.; Director, E. P.; Rosenberg, S. A., Identification of specific

cytolytic immune responses against autologous tumor in humans bearing malignant melanoma. J Immunol 1987, 138, 989-995.

Nagrath, S.; Sequist, L. V.; Maheswaran, S.; Bell, D. W.; Irimia, D.; Ulkus, L.; Smith, M. R.; Kwak, E. L.; Digumarthy, S.; Muzikansky, A.; Ryan, P.; Balis, U. J.; Tompkins, R. G.; Haber, D. A.; Toner, M., Isolation of rare circulating tumour cells in cancer patients by microchip technology. Nature 2007, 450, 1235-1239.

O'Neal, D. P.; Hirsch, L. R.; Halas, N. J.; Payne, J. D.; West, J. L., Photo-thermal tumor ablation in mice using near infrared-absorbing nanoparticles. Cancer Lett 2004, 209, 171-176.

Ohlsson, B.; Stenram, U.; Tranberg, K. G., Resection of colorectal liver metastases: 25-year experience. World J Surg 1998, 22, 268-276; discussion 276-267.

Partridge, A. H.; Burstein, H. J.; Winer, E. P., Side effects of chemotherapy and combined chemohormonal therapy in women with early-stage breast cancer. J Natl Cancer Inst Monogr 2001, 135-142.

Peng, W.; Ye, Y.; Rabinovich, B. A.; Liu, C.; Lou, Y.; Zhang, M.; Whittington, M.; Yang, Y.; Overwijk, W. W.; Lizee, G.; Hwu, P., Transduction of tumor-specific T cells with CXCR2 chemokine receptor improves migration to tumor and antitumor immune responses. Clin Cancer Res 2010, 16, 5458-5468.

Peterson, A. C.; Harlin, H.; Gajewski, T. F., Immunization with Melan-A peptide-pulsed peripheral blood mononuclear cells plus recombinant human interleukin-12 induces clinical activity and T-cell responses in advanced melanoma. Journal of clinical oncology 2003, 21, 2342-2348.

Pittet, M. J.; Mempel, T. R., Regulation of T-cell migration and effector functions: insights from in vivo imaging studies. Immunol Rev 2008, 221, 107-129.

Pockaj, B. A.; Sherry, R. M.; Wei, J. P.; Yannelli, J. R.; Carter, C. S.; Leitman, S. F.; Carasquillo, J. A.; Steinberg, S. M.; Rosenberg, S. A.; Yang, J. C., Localization of 111indium-labeled tumor infiltrating lymphocytes to tumor in patients receiving adoptive immunotherapy. Augmentation with cyclophosphamide and correlation with response. Cancer 1994, 73, 1731-1737.

Porter, D. L.; Levine, B. L.; Kalos, M.; Bagg, A.; June, C. H., Chimeric antigen receptor–

modified T cells in chronic lymphoid leukemia. New England Journal of Medicine 2011, 365, 725-733.

Punnoose, E. A.; Atwal, S. K.; Spoerke, J. M.; Savage, H.; Pandita, A.; Yeh, R. F.; Pirzkall, A.; Fine, B. M.; Amler, L. C.; Chen, D. S.; Lackner, M. R., Molecular biomarker analyses using circulating tumor cells. PLoS One 2010, 5, e12517.

Qiao, R.; Yang, C.; Gao, M., Superparamagnetic iron oxide nanoparticles: from preparations to in vivo MRI applications. Journal of Materials Chemistry 2009, 19, 6274-6293.

Qiu, P.; Jensen, C.; Charity, N.; Towner, R.; Mao, C., Oil phase evaporation-induced self-assembly of hydrophobic nanoparticles into spherical clusters with controlled surface chemistry in an oil-in-water dispersion and comparison of behaviors of individual and clustered iron oxide nanoparticles. Journal of the American Chemical Society 2010, 132, 17724-17732.

Qu, M.; Mallidi, S.; Mehrmohammadi, M.; Truby, R.; Homan, K.; Joshi, P.; Chen, Y.-S.; Sokolov, K.; Emelianov, S., Magneto-photo-acoustic imaging. Biomedical optics express 2011, 2, 385-396.

Rae, J. M.; Scheys, J. O.; Clark, K. M.; Chadwick, R. B.; Kiefer, M. C.; Lippman, M. E., EGFR and EGFRvIII expression in primary breast cancer and cell lines. Breast Cancer Research and Treatment 2004, 87, 87-95.

Rath, A.; Glibowicka, M.; Nadeau, V. G.; Chen, G.; Deber, C. M., Detergent binding explains anomalous SDS-PAGE migration of membrane proteins. Proceedings of the National Academy of Sciences 2009, 106, 1760-1765.

Ricles, L. M.; Nam, S. Y.; Sokolov, K.; Emelianov, S. Y.; Suggs, L. J., Function of mesenchymal stem cells following loading of gold nanotracers. Int J Nanomedicine 2011, 6, 407-416.

Riethdorf, S.; Fritsche, H.; Muller, V.; Rau, T.; Schindlbeck, C.; Rack, B.; Janni, W.; Coith, C.; Beck, K.; Janicke, F.; Jackson, S.; Gornet, T.; Cristofanilli, M.; Pantel, K., Detection of circulating tumor cells in peripheral blood of patients with metastatic breast cancer: a validation study of the CellSearch system. Clinical Cancer Research 2007, 13, 920-928.

Riethdorf, S.; Wikman, H.; Pantel, K., Review: Biological relevance of disseminated tumor cells in cancer patients. Int J Cancer 2008, 123, 1991-2006.

Riggio, C.; Calatayud, M. P.; Hoskins, C.; Pinkernelle, J.; Sanz, B.; Torres, T. E.; Ibarra, M. R.; Wang, L.; Keilhoff, G.; Goya, G. F.; Raffa, V.; Cuschieri, A., Poly-l-lysine-coated magnetic nanoparticles as intracellular actuators for neural guidance. Int J Nanomedicine 2012, 7, 3155-3166.

Rosenberg, S. A.; Aebersold, P.; Cornetta, K.; Kasid, A.; Morgan, R. A.; Moen, R.; Karson, E. M.; Lotze, M. T.; Yang, J. C.; Topalian, S. L.; et al., Gene transfer into humans--immunotherapy of patients with advanced melanoma, using tumor-infiltrating lymphocytes modified by retroviral gene transduction. N Engl J Med 1990, 323, 570-578.

Rosenberg, S. A.; Dudley, M. E., Cancer regression in patients with metastatic melanoma after the transfer of autologous antitumor lymphocytes. Proc Natl Acad Sci U S A 2004, 101 Suppl 2, 14639-14645.

Rosenberg, S. A.; Dudley, M. E., Adoptive cell therapy for the treatment of patients with metastatic melanoma. Curr Opin Immunol 2009, 21, 233-240.

Rosenberg, S. A.; Restifo, N. P.; Yang, J. C.; Morgan, R. A.; Dudley, M. E., Adoptive cell transfer: a clinical path to effective cancer immunotherapy. Nat Rev Cancer 2008, 8, 299-308.

Rosenberg, S. A.; Sherry, R. M.; Morton, K. E.; Scharfman, W. J.; Yang, J. C.; Topalian, S. L.; Royal, R. E.; Kammula, U.; Restifo, N. P.; Hughes, M. S., Tumor progression can occur despite the induction of very high levels of self/tumor antigen-specific CD8+ T cells in patients with melanoma. The Journal of Immunology 2005, 175, 6169-6176.

Rosenberg, S. A.; Yang, J. C.; Restifo, N. P., Cancer immunotherapy: moving beyond current vaccines. Nat Med 2004, 10, 909-915.

Sachlos, E.; Risueno, R. M.; Laronde, S.; Shapovalova, Z.; Lee, J. H.; Russell, J.; Malig, M.; McNicol, J. D.; Fiebig-Comyn, A.; Graham, M.; Levadoux-Martin, M.; Lee, J. B.; Giacomelli, A. O.; Hassell, J. A.; Fischer-Russell, D.; Trus, M. R.; Foley, R.; Leber, B.; Xenocostas, A.; Brown, E. D.; Collins, T. J.; Bhatia, M., Identification of drugs including a dopamine receptor antagonist that selectively target cancer stem

cells. Cell 2012, 149, 1284-1297.

Satake, I.; Yang, J. T., Interaction of sodium decyl sulfate with poly(L-ornithine) and poly(L-lysine) in aqueous solution. Biopolymers 1976, 15, 2263-2275.

Schlorf, T.; Meincke, M.; Kossel, E.; Gluer, C. C.; Jansen, O.; Mentlein, R., Biological properties of iron oxide nanoparticles for cellular and molecular magnetic resonance imaging. Int J Mol Sci 2010, 12, 12-23.

Shimizu, K.; Ito, A.; Arinobe, M.; Murase, Y.; Iwata, Y.; Narita, Y.; Kagami, H.; Ueda, M.; Honda, H., Effective cell-seeding technique using magnetite nanoparticles and magnetic force onto decellularized blood vessels for vascular tissue engineering. J Biosci Bioeng 2007, 103, 472-478.

Shukla, R.; Bansal, V.; Chaudhary, M.; Basu, A.; Bhonde, R. R.; Sastry, M., Biocompatibility of gold nanoparticles and their endocytotic fate inside the cellular compartment: a microscopic overview. Langmuir 2005, 21, 10644-10654.

Siegel, R.; Naishadham, D.; Jemal, A., Cancer statistics, 2012. CA Cancer J Clin 2012, 62, 10-29.

Sieuwerts, A. M.; Kraan, J.; Bolt, J.; van der Spoel, P.; Elstrodt, F.; Schutte, M.; Martens, J. W.; Gratama, J. W.; Sleijfer, S.; Foekens, J. A., Anti-epithelial cell adhesion molecule antibodies and the detection of circulating normal-like breast tumor cells. Journal of the National Cancer Institute (1988) 2009, 101, 61-66.

Slamon, D. J.; Leyland-Jones, B.; Shak, S.; Fuchs, H.; Paton, V.; Bajamonde, A.; Fleming, T.; Eiermann, W.; Wolter, J.; Pegram, M.; Baselga, J.; Norton, L., Use of chemotherapy plus a monoclonal antibody against HER2 for metastatic breast cancer that overexpresses HER2. N Engl J Med 2001, 344, 783-792.

Sokolov, K.; Follen, M.; Aaron, J.; Pavlova, I.; Malpica, A.; Lotan, R.; Richards-Kortum, R., Real-time vital optical imaging of precancer using anti-epidermal growth factor receptor antibodies conjugated to gold nanoparticles. Cancer Res 2003, 63, 1999-2004.

Sokolov, K.; Galvan, J.; Myakov, A.; Lacy, A.; Lotan, R.; Richards-Kortum, R., Realistic three-dimensional epithelial tissue phantoms for biomedical optics. J Biomed Opt 2002, 7, 148-156.

Somerville, R. P.; Devillier, L.; Parkhurst, M. R.; Rosenberg, S. A.; Dudley, M. E., Clinical scale rapid expansion of lymphocytes for adoptive cell transfer therapy in the WAVE(R) bioreactor. J Transl Med 2012, 10, 69.

Song, D.-G.; Ye, Q.; Carpenito, C.; Poussin, M.; Wang, L.-P.; Ji, C.; Figini, M.; June, C. H.; Coukos, G.; Powell, D. J., In vivo persistence, tumor localization, and antitumor activity of CAR-engineered T cells is enhanced by costimulatory signaling through CD137 (4-1BB). Cancer research 2011, 71, 4617-4627.

Song, H.-M.; Wei, Q.; Ong, Q. K.; Wei, A., Plasmon-resonant nanoparticles and nanostars with magnetic cores: synthesis and magnetomotive imaging. ACS nano 2010, 4, 5163-5173.

Stone, J. D.; Kranz, D. M., Role of T cell receptor affinity in the efficacy and specificity of adoptive T cell therapies. Front Immunol 2013, 4, 244.

Su, C. H.; Sheu, H. S.; Lin, C. Y.; Huang, C. C.; Lo, Y. W.; Pu, Y. C.; Weng, J. C.; Shieh, D. B.; Chen, J. H.; Yeh, C. S., Nanoshell magnetic resonance imaging contrast agents. J Am Chem Soc 2007, 129, 2139-2146.

Sun, C.; Lee, J. S.; Zhang, M., Magnetic nanoparticles in MR imaging and drug delivery. Adv Drug Deliv Rev 2008, 60, 1252-1265.

Sun, J.; Zhou, S.; Hou, P.; Yang, Y.; Weng, J.; Li, X.; Li, M., Synthesis and characterization of biocompatible Fe3O4 nanoparticles. J Biomed Mater Res A 2007, 80, 333-341.

Sykova, E.; Jendelova, P.; Herynek, V., MR tracking of stem cells in living recipients. Methods Mol Biol 2009, 549, 197-215.

Tam, J. M.; Tam, J. O.; Murthy, A.; Ingram, D. R.; Ma, L. L.; Travis, K.; Johnston, K. P.; Sokolov, K. V., Controlled assembly of biodegradable plasmonic nanoclusters for near-infrared imaging and therapeutic applications. ACS nano 2010, 4, 2178-2184.

Tong, L.; Zhao, M.; Zhu, S.; Chen, J., Synthesis and application of superparamagnetic iron oxide nanoparticles in targeted therapy and imaging of cancer. Front Med 2011, 5, 379-387.

Truby, R. L.; Emelianov, S. Y.; Homan, K. A., Ligand-mediated self-assembly of hybrid plasmonic and superparamagnetic nanostructures. Langmuir 2013, 29, 2465-2470.

Wang, H.; Brandl, D. W.; Le, F.; Nordlander, P.; Halas, N. J., Nanorice: a hybrid plasmonic nanostructure. Nano Lett 2006, 6, 827-832.

Wang, J.; Boriskina, S. V.; Wang, H.; Reinhard, B. M., Illuminating Epidermal Growth Factor Receptor Densities on Filopodia through Plasmon Coupling. ACS Nano 2011, 5, 6619-6628.

Wang, J.; Yu, X.; Boriskina, S. V.; Reinhard, B. M., Quantification of Differential ErbB1 and ErbB2 Cell Surface Expression and Spatial Nanoclustering through Plasmon Coupling. Nano Letters 2012, 12, 3231-3237.

Wang, L.; Luo, J.; Fan, Q.; Suzuki, M.; Suzuki, I. S.; Engelhard, M. H.; Lin, Y.; Kim, N.; Wang, J. Q.; Zhong, C. J., Monodispersed core-shell Fe3O4@Au nanoparticles. J Phys Chem B 2005, 109, 21593-21601.

Wang, L.; Wang, L.; Luo, J.; Fan, Q.; Suzuki, M.; Suzuki, I. S.; Engelhard, M. H.; Lin, Y.; Kim, N.; Wang, J. Q., Monodispersed core-shell Fe3O4@ Au nanoparticles. The Journal of Physical Chemistry B 2005, 109, 21593-21601.

Wang, Y.; Wong, J. F.; Teng, X.; Lin, X. Z.; Yang, H., "Pulling" Nanoparticles into Water: Phase Transfer of Oleic Acid Stabilized Monodisperse Nanoparticles into Aqueous Solutions of α-Cyclodextrin. Nano Letters 2003, 3, 1555-1559.

Wei, Q.; Song, H.-M.; Leonov, A. P.; Hale, J. A.; Oh, D.; Ong, Q. K.; Ritchie, K.; Wei, A., Gyromagnetic Imaging: Dynamic Optical Contrast Using Gold Nanostars with Magnetic Cores. JACS 2009, 131, 9728-9734.

Wei, Q.; Wei, A., Optical imaging with dynamic contrast agents. Chemistry 2011, 17, 1080-1091.

Wilczewska, A. Z.; Niemirowicz, K.; Markiewicz, K. H.; Car, H., Nanoparticles as drug delivery systems. Pharmacol Rep 2012, 64, 1020-1037.

Wu, C.-H.; Huang, Y.-Y.; Chen, P.; Hoshino, K.; Liu, H.; Frenkel, E. P.; Zhang, J. X. J.; Sokolov, K. V., Versatile Immunomagnetic Nanocarrier Platform for Capturing Cancer Cells. ACS nano 2013, 7, 8816-8823.

Xu, Z.; Hou, Y.; Sun, S., Magnetic core/shell Fe3O4/Au and Fe3O4/Au/Ag nanoparticles with tunable plasmonic properties. Journal of the American Chemical Society 2007, 129, 8698-8699.

Yee, C., Adoptive T cell therapy: Addressing challenges in cancer immunotherapy. J Transl Med 2005, 3, 17.

Yoon, S. J.; Mallidi, S.; Tam, J. M.; Tam, J. O.; Murthy, A.; Johnston, K. P.; Sokolov, K. V.; Emelianov, S. Y., Utility of biodegradable plasmonic nanoclusters in photoacoustic imaging. Opt Lett 2010, 35, 3751-3753.

Yu, H.; Chen, M.; Rice, P. M.; Wang, S. X.; White, R. L.; Sun, S., Dumbbell-like bifunctional Au-Fe3O4 nanoparticles. Nano Lett 2005, 5, 379-382.

Zhang, L.; Dokouhaki, P., Recent Advances in T Cell Adoptive Immunotherapy of Cancer. Current Cancer Therapy Reviews 2008, 4, 1-13.

Zhang, L.; Farrell, J. J.; Zhou, H.; Elashoff, D.; Akin, D.; Park, N. H.; Chia, D.; Wong, D. T., Salivary Transcriptomic Biomarkers for Detection of Resectable Pancreatic Cancer. Gastroenterology 2010, 138, 949-957.

Zhang, L.; Riethdorf, S.; Wu, G.; Wang, T.; Yang, K.; Peng, G.; Liu, J.; Pantel, K., Meta-analysis of the prognostic value of circulating tumor cells in breast cancer. Clin Cancer Res 2012, 18, 5701-5710.

Zheng, S.; Shen, Y.; Song, Y.; Yuan, Y., How to detour Treg cells in T cell-based antitumor immune therapy. Onco Targets Ther 2013, 6, 1243-1247.

Zheng, X.; Cheung, L. S.; Schroeder, J. A.; Jiang, L.; Zohar, Y., A high-performance microsystem for isolating circulating tumor cells. Lab Chip 2011, 11, 3269-3276.

Zhou, C.; Long, M.; Qin, Y.; Sun, X.; Zheng, J., Luminescent gold nanoparticles with efficient renal clearance. Angewandte Chemie 2011, 123, 3226-3230.